R-07-26

Quantifying in situ stress magnitudes and orientations for Forsmark Forsmark stage 2.2

C. Derek Martin, University of Alberta

November 2007

Svensk Kärnbränslehantering AB
Swedish Nuclear Fuel
and Waste Management Co
Box 5864
SE-102 40 Stockholm Sweden
Tel 08-459 84 00
+46 8 459 84 00
Fax 08-661 57 19
+46 8 661 57 19

ISSN 1402-3091
SKB Rapport R-07-26

Quantifying in situ stress magnitudes and orientations for Forsmark Forsmark stage 2.2

C. Derek Martin, University of Alberta

November 2007

Keywords: In situ stress, Overcoring, Hydraulic fracturing, Mean stress, Stress ratios, Deformation modulus, Geology.

Abstract

/Stephansson et al. 1991/ summarised the state of stress in Fennoscandia using a Rock Stress Data Base containing about 500 entries from more than 100 sites in Finland, Norway and Sweden by 1987. /Stephansson et al. 1991/ concluded that in the Fennoscandia shield: (1) there is a large horizontal stress component in the uppermost 1,000 m of bedrock, and (2) the maximum and minimum horizontal stresses exceed the vertical stress assuming the vertical stress is estimated from the weight of the overburden.

Several stress campaigns involving both overcoring and hydraulic fracturing, including the hydraulic testing of pre-existing fractures (HTPF), have been carried out at Forsmark to establish the in situ stress state. The results from the initial campaigns were summarised by /Sjöberg et al. 2005/ which formed the bases for the stresses provided in the Site Descriptive Model version 1.2 /SKB 2005a/. Since then additional stress measurement campaigns have been completed. The results from these stress measurement campaigns support the conclusions from /Stephansson et al. 1991/. In addition to these in situ stress measurements the following additional studies were undertaken to aid in assessing the stress state at Forsmark.

1. A detailed televiewer survey of approximately 6,900 m of borehole walls to depths of 1,000 m was carried out to assess borehole wall damage, i.e. borehole breakouts.
2. Evaluation of nonlinear strains in laboratory samples to depths of approximately 800 m to assess if stress magnitudes were sufficient to create stress-induced microcracking.
3. Assessment of the magnitudes required to cause core disking and survey of core disking observed at Forsmark.

The magnitudes and orientations from the stress measurement campaigns were analysed to establish the most likely stress magnitudes and orientations for Design Step D2 within the Target Area of the Complete Site Investigations /SKB 2005b/. The recommended stress magnitudes (stress gradients) and orientations with depth are given in the table below.

Depth range (m)	σ_H (MPa)	Trend (°)	σ_h (MPa)	Trend (°)	σ_{vert} (MPa)
0–150	19 + 0.008z, ± 20%	145 ± 20	11 + 0.006z, ± 25%	055	0.0265z, ± 0.0005
150–400	9.1 + 0.074z, ± 15%	145 ± 15	6.8 + 0.034z, ± 25%	055	0.0265z, ± 0.0005
400–600	29.5 + 0.023z, ± 15%	145 ± 15	9.2 + 0.028z, ± 20%	055	0.0265z, ± 0.0005

In the table above the components for the stress tensor are given as horizontal and vertical stress components. The maximum and minimum horizontal stress components are essentially the same as the maximum and intermediate principal stresses, σ_1 and σ_2, respectively. The minimum principal stress (σ_3) is synonymous with the vertical stress. The most likely range in values to be used in the design is also shown. The magnitudes have been separated into three depth ranges: 0 to 150 m corresponding to fracture domain FFM02, and the two additional depth ranges occurring in fracture domain FFM01 (150 to 400 m, 400 to 600 m). The increase in the horizontal stress magnitudes from 150 to 400 m reflect the decreasing open fracture frequency with depth and general improvement in the rock mass quality. Below 400 m depth the rock mass is characterised as sparsely fractured and massive, and the stress gradients are expected to continue to greater depths. The findings from this work are considered adequate for Design Step D2 and consistent with the conclusions of /Stephansson et al. 1991/.

Sammanfattning

Spänningsförhållandena i den Skandinaviska urbergsskölden sammanfattades av /Stephansson m fl 1991/ med stöd av en bergspänningsdatabas som innehöll ca 500 mätvärden från mer än 100 platser i Finland, Norge och Sverige till och med 1987. /Stephansson m fl 1991/ konstaterade att den Skandinaviska urbergsskölden: (1) har en stor horisontell spänningskomponent i berggrundens övre 1,000 m, och (2) de största och minsta horisontalspänningarna är större än vertikalspänningskomposanten, om man antar att den är lika med vikten av ovanliggande berg.

Flera kampanjer med spänningsmätningar har utförts i Forsmark. De har omfattat både överborrningsmetoden, samt hydraulisk spräckning och hydraulisk test av naturliga sprickor (HTPF). Resultaten från den första kampanjen rapporterades av /Sjöberg m fl 2005/, vilket gav underlag till det spänningstillstånd som rapporterades i Platsbeskrivande Modell version 1.2 /SKB 2005/. Därefter har ytterligare mätkampanjer slutförts. Resultaten från dessa spänningsmätningskampanjer stödjer de slutsatser /Stephansson m fl 1991/ gjorde. Förutom kampanjer med spänningsmätningar har följande insatser gjorts för att stödja värderingen av spänningstillståndet i Forsmark:

1. En detaljerad studie av undersökningar med televiewer i ca 6,900 m borrhål för att studera skador i borrhålens väggar, s.k. borehole breakouts.
2. Värdering av graden av icke-elastiska töjningar baserat på laboratorieprovning av prover från max ca 800 m djup för att bedöma om spänningsnivån mot djupet är tillräcklig för att orsaka spänningsinducerad mikro-sprickbildning i borrkärnor.
3. Uppskattning av vilka spänningsnivåer som erfordras för att förorsaka spänningsinducerad uppsprickning tvärs borrkärna, så kallad core disking, samt undersökning av frekvensen core disking som dokumenterats i borrkärnor från Forsmark.

Magnituder och orienteringar enligt utförda spänningsmätningar har analyserats för att bedöma det mest troliga spänningstillståndet inom det prioriterade området för de kompletta platsundersökningarna /SKB 2005/.De rekommenderade spänningsmagnituderna (spänningsgradienterna) ges i tabellen nedan.

Depth range (m)	σ_H (MPa)	Trend (°)	σ_h (MPa)	Trend (°)	σ_{vert} (MPa)
0–150	19 + 0.008z, ± 20%	145 ± 20	11 + 0.006z, ± 25%	055	0.0265z, ± 0.0005
150–400	9.1 + 0.074z, ± 15%	145 ± 15	6.8 + 0.034z, ± 25%	055	0.0265z, ± 0.0005
400–600	29.5 + 0.023z, ± 15%	145 ± 15	9.2 + 0.028z, ± 20%	055	0.0265z, ± 0.0005

Spänningskomposanterna i tabellen ges som horisontal- och vertikalkomposanter. De största och minsta horisontalspänningarna är i stort sett lika med den största och mellersta huvudspänningen, σ_1 and σ_2. Den minsta huvudspänningen (σ_3) är lika med den vertikala spänningskomposanten. De mest troliga intervallen att användas för projektering framgår av tabellen. Spänningsmagnituderna har delats upp i tre djupintervall: 0–150 m ligger inom sprickdomän FFM2, och de andra två intervallen härrör till sprickdomän FFM01 (150–400 m och 400–600 m). Den ökande horisontalspänningsmagnituden från 150 till 400 m reflekterar den minskande frekvensen öppna sprickor med djupet, och en ökande bergkvalité. Under 400 m kan berget karaktäriseras som massivt och med låg sprickfrekvens, och spänningsgradienten under det djupet fortsätter troligen mot större djup. Resultaten av detta arbete bedöms ge tillräckligt underlag till projektering D2 och är konsistent med slutsatserna från /Stephansson m fl 1991/.

Contents

1	**Introduction**	7
2	**Geological framework for interpreting stress data**	11
2.1	Fault kinematics	11
2.2	Site geology	13
	2.2.1 Deformation zones	14
	2.2.2 Fracture Domains	14
	2.2.3 Lithology	19
2.3	Summary	20
3	**Current boundary conditions**	21
3.1	Plate tectonics	21
3.2	Glacial isostatic adjustment	22
3.3	Crustal stresses and seismic activity	23
3.4	Summary	25
4	**Indicators of the state of stress**	27
4.1	Experience from construction of Forsmark Nuclear Facilities	27
4.2	Core damage and stress	28
4.3	Core disking	30
4.4	Borehole breakouts from acoustic televiewer logging	31
	4.4.1 Types of breakouts and summary statistics	32
	4.4.2 Breakouts and structure	36
	4.4.3 Breakout time dependency	37
	4.4.4 Summary	39
5	**Stress measurement campaigns and limitations**	43
5.1	Hydraulic fracturing	43
5.2	Overcoring	45
	5.2.1 Microcracking and ring-core disking	46
	5.2.2 Thermal effects	51
5.3	Summary	54
6	**Interpretation of in situ stress data**	57
6.1	Vertical stress	57
6.2	Mean stress	58
6.3	Principal stress ratios	63
	6.3.1 Stress ratio σ_1/σ_2	64
	6.3.2 Stress ratio σ_1/σ_3	64
6.4	Comparison of σ_2 from overcoring and hydraulic fracturing	65
6.5	Stress orientations	68
6.6	Summary	70
7	**Estimation of Forsmark stress state**	71
7.1	Methodology	71
	7.1.1 Application of methodology to AECL URL 420 Level	71
7.2	Target Area stress magnitudes: 0 to 1,000 m	73
	7.2.1 FFM02: 0 to 150 m depth	73
	7.2.2 FFM01: 150 to 300 m depth	73
	7.2.3 FFM01: 300 to 400 m depth	73
	7.2.4 FFM01: 400 to > 500 m depth	74
7.3	Target Area stress gradients: 0 to 600 m	75
7.4	Stress modelling of deformation zones	75
7.5	Variability and uncertainty in recommended stress gradients	77

8 Discussions and conclusions 81

References 85

Appendix A Overcore test results 91

Appendix B Hydraulic fracturing data 93

1 Introduction

In SKB's Underground Design Premises /SKB 2004/ the objective in the early design phase is to estimate if there is sufficient space for the repository at a site. One of the factors that could limit the space available is stability of the underground openings, i.e. deposition tunnels and deposition boreholes. /Martin et al. 2001/ and /Andersson 2007/ established the stress magnitudes associated with stress-induced instability around circular openings in crystalline rock. The in situ principal stresses (orientations and magnitudes) at a site must be known with sufficient confidence to assess if stress-induced instability will occur. In addition, the orientation and magnitudes of the maximum horizontal stress must also be established because as noted by /Martin et al. 2001/ it can impact the layout, i.e. orientation and shape, of the deposition tunnels.

Since the pioneering work of /Hast 1973/ in the early 1960's the stress state in Sweden has been continually investigated and updated. /Stephansson et al. 1991/ presented results from the Fennoscandia Rock Stress Data Base containing about 500 entries from more than 100 sites in Finland, Norway and Sweden by 1987. They concluded from this stress database that in the Fennoscandia shield: (1) there is a large horizontal stress component in the uppermost 1,000 m of bedrock, and (2) the maximum and minimum horizontal stresses exceed the vertical stress assuming the vertical stress is estimated from the weight of the overburden. These findings are similar to the data reported by /Herget and Arjang 1990/ for the Canadian Precambrian shield conditions with relatively flat topography. Hence prior to the investigations at Forsmark, the in situ stress magnitudes and orientations were expected to be constrained by the findings of /Stephansson et al. 1991/.

As part of the Forsmark Complete Site Investigation Phase, stress measurement campaigns have been carried out in selected boreholes. The measurement methods used were overcoring, hydraulic fracturing, including hydraulic testing of pre-existing fractures, and televiewer surveys of the borehole wall to detect breakouts, an indicator of stress orientation. A list of the boreholes used in the campaigns is provided in Table 1-1 and the detailed results from those boreholes are provided in individual SKB reports and these are also listed in Table 1-1. While summaries of the results are provided for easy reference in the Appendices of this report, readers interested in individual borehole or test results should always consult the SKB primary data reports noted in Table 1-1.

In addition to the measurements used in individual boreholes, logging of the core recorded if and where core disking occurred, as core disking is considered an indicator for elevated stress magnitudes. Testing of selected core samples was also carried out to evaluate the amount of stress-induced microcracks, also an indirect indicator of elevated stress magnitudes. Each of these topics and an evaluation of the stress measurements are discussed in this report.

The execution of the measurement campaign was carried out under strict quality control using the International Society for Rock Mechanics Suggested Methods /Hudson et al. 2003, Sjöberg et al. 2003, Haimson and Cornet 2003, Christiansson and Hudson 2003/. Many of these Suggested Methods resulted directly from developing the procedures and methodologies prior to commencing the Complete Site Investigation Phase. To the author's knowledge no other site in the world has made such an extensive effort to measure the state of stress using small (76-mm) diameter surface drilled boreholes to depths of 1,000 m.

Despite the extensive efforts made during the Forsmark Complete Site Investigation Phase, measuring the state of stress in the Forsmark Target Area to depths of 1,000 m has been challenging. An initial evaluation of state of stress at the Forsmark site was given in /Sjöberg et al. 2005/ and those results provided the bases for the stress state given in the Site Descriptive Model (SDM) version 1.2 which was used in Design Step D1. Those findings confirmed the findings of /Stephansson et al. 1991/. The purpose of this report is to integrate the information

collected since SDM 1.2 and establish the most likely estimate for the stress magnitudes and orientations, for the Forsmark Target Area and more specifically the proposed depth of the repository (400–500 m), for Design Step D2. The conclusions in this report are not only based on the primary stress measurements but also integrates data from both direct and indirect measurements that were used to constrain the stress tensor. The flow chart in Figure 1-1 outlines the methodology and data used to establish the stress magnitudes and orientations. It should be noted that in Figure 1-1 at each stage of data integration there is a consistency check to ensure that data from one set of direct and/or indirect measurements is consistent with other data and findings. The data that was used to establish the most likely in situ stress magnitudes and orientations for design step D2 is the data set with the greatest consistency. As shown in Figure 1-1 the uncertainty associated with the stress magnitudes and orientations for Design Step D2 will be checked during the construction of the access facilities (shafts and ramps).

Table 1-1. List of the boreholes used in the stress measurement campaigns carried out during the Complete Site Investigation Phase and available historic data. The numbers, e.g. P-04-311, refer to SKB report numbers which are available from www.skb.se. See Figure 2-10 for the location of the boreholes.

Borehole name	Overcoring (OC)	Hydraulic fracturing (HF & HTPF)	Breakout survey (BS)
KFM01A		P-04-311	P-07-07
KFM01B	P-04-83	P-04-311	P-07-07
KFM02A		P-04-311	P-07-07
KFM02B		P-07-205	P-07-07
KFM04A		P-04-311	P-07-07
KFM05A			P-07-07
KFM06A			P-07-07
KFM07A		P-07-206	
KFM07C	P-07-130	P-07-206	P-07-07
KFM08A		P-07-206	P-07-166
KFM09A		P-07-206	
KFM09B		P-07-206	
Historic data – Data reviewed in P-05-35			
DBT1	P-03-119	TULEA 1984:30	
DBT3	P-03-119		

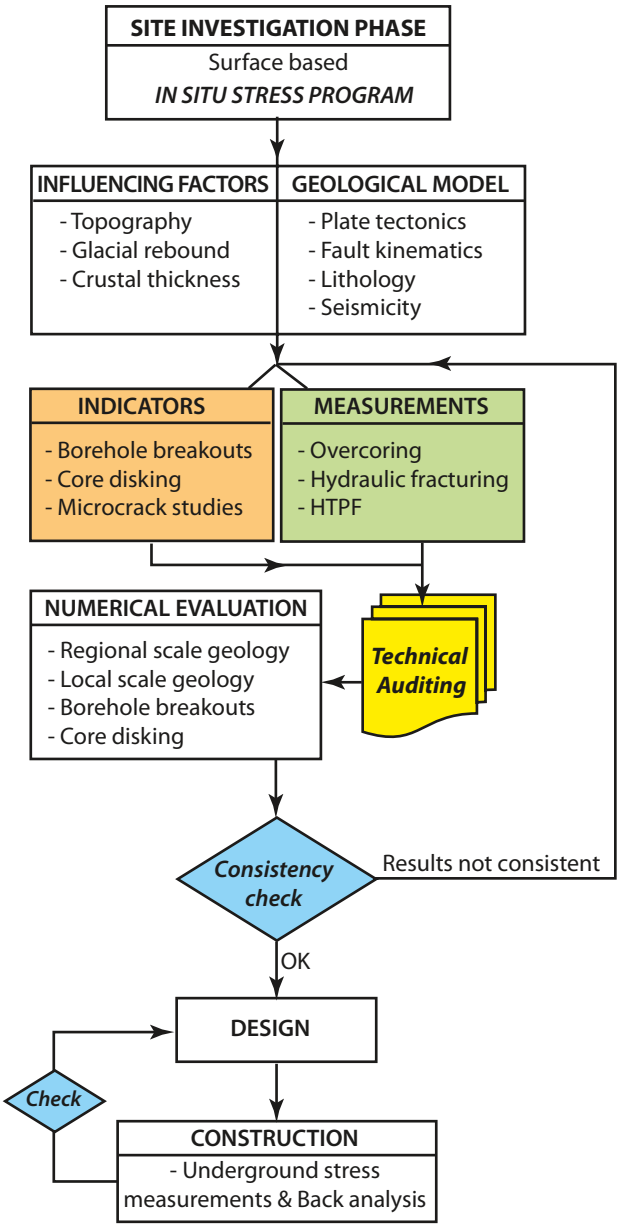

Figure 1-1. *Flow chart for the integration of data used to reduce uncertainty and establish consistency in the estimation of stress magnitudes and orientations for design step D2.*

2 Geological framework for interpreting stress data

The state of stress that exists in a rock mass today is a function of its geological history, rock mass properties and the boundary conditions that are currently being applied. Knowing this, it is apparent that predicting a stress state in a rock mass today is not practical given the complex geological history that ancients rocks have endured. Consequently in situ stresses must be measured. However, to interpret these measurements a geological framework that considers geological history, rock mass properties and boundary conditions is required. In the following sections the geological history and rock mass properties of the Forsmark site are discussed. Details of the site geology are given in the SKB's Site Descriptive Model for Forsmark, /SKB 2005a, 2006/

2.1 Fault kinematics

All rock masses contain faults at some scale. Hence it is important to understand the stress state that formed these faults. /Anderson 1951/ proposed a fault classification for thrust, strike-slip and normal faults, based on observations in areas of low topographic relief that related the horizontal stress magnitudes to the vertical stress magnitude (Figure 2-1). /Sibson 1974/ estimated the magnitude of the differential stress required to cause slip on these three types of faults. Sibson, assuming a coefficient of friction of 0.75, concluded that the ratios of the magnitudes of the differential stresses ($\sigma_1-\sigma_3$) necessary to initiate sliding on the thrust, strike-slip and normal faults was 4:1.6:1, respectively. In other words the differential stress ratio for thrust fault should be 4 times greater than the differential stress ratio for a normal fault, assuming that the strength of the fault is only controlled by frictional sliding. Sibson also showed that the distortional elastic strain energy corresponding to those stress ratios for the energy required for sliding on the three faults was 16:2.56:1. From these analyses Sibson noted that these stress and strain ratios were in general agreement with stresses and energy inferred from seismic analysis, i.e. seismic events associated with thrust and strike-slip faults release more energy than normal faults.

The simplified fault discussion presented above ignores the progressive nature of faulting and the rotation of stresses that can occur locally as faults develop. Detailed characterisation of the development of faults by /Riedel 1929/ and /Cloos 1955/ using clay-cake simple-shear experiments showed that the shear/fault zone is made up of series of discrete fractures forming at various angles to the direction of shearing. These fractures are today generally referred to as the

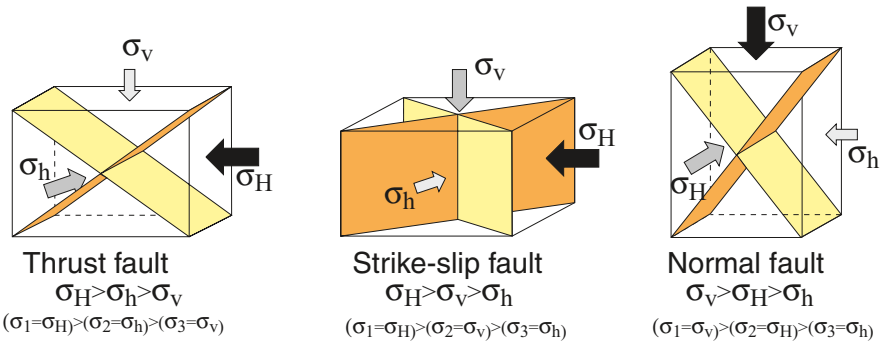

Figure 2–1. *Anderson's fault classification and the associated stresses. The orientation of the maximum principal stress is indicated by the large black arrow.*

R and *R′* Riedel shears (Figure 2-2a) with the *R* fractures forming at an angle of $\phi/2$ to the axis of shearing, where ϕ is the internal friction angle of the material (Figure 2-2a). /Morgenstern and Tchalenko 1967/ and /Tchalenko 1970/ using results from direct shear tests on clay also noted that the *R* fractures form first with *R′* fractures developing later at an angle $\pi/2-\phi/2$. / Skempton 1966/ using detailed field mapping of shear zones in clays, siltstones, and sandstones concluded that at large deformation the Riedel shears are linked by the principal displacement fracture (faults), i.e. the major plane of movement and that the final appearance of the shear zone was a function of the amount of displacement which often resulted in an undulating principal displacement fracture. /Tchalenko 1970/ showed that the fracture characteristics of these shear/fault zones was similar at all scales in nature. According to /Skempton 1966/, during the development of this deformation zone there is a rotation of the major principal stress towards the direction of shearing such that the minimum angle between the major principal stress and the principal displacement plane is $(45 - \phi°/2)$. This agrees with the well-known 'single plane of weakness' theory in rock mechanics where sliding preferentially occurs on a plane with its normal at $(45 + \phi/2)$ to the applied stress – which is the same as $(45 - \phi/2)$ between the stress direction and the plane.

Figure 2-2b shows a two dimensional plan view cartoon of the regional scale kinematics during the formation of the different sets of deformation zones at the Forsmark site. In this conceptual model it is assumed that all fractures formed in response to the same tectonic event during the latter part of the Svecokarelian orogeny, i.e. > 1,700 million years ago. Note the similarity between Figures 2-2a and 2-2b. As noted by /Tchalenko 1970/, this similarity occurs because the fractures form in response to the applied boundary conditions regardless of scale, however, the exact sequence of the fracture formation in Figure 2-2b do not necessarily have to concur with the sequence observed in the experiments. While the stresses that were necessary to form the deformation zones in Figure 2-2b 1,700 million years ago do not exist today, it is important to appreciate that the stresses that do exist today may be influenced by the geological structures that formed 1,700 million years ago, and therefore stress measurements at the Forsmark site must be interpreted in the context of its geological history, particulary the major discontinuous elements in the rock mass structure.

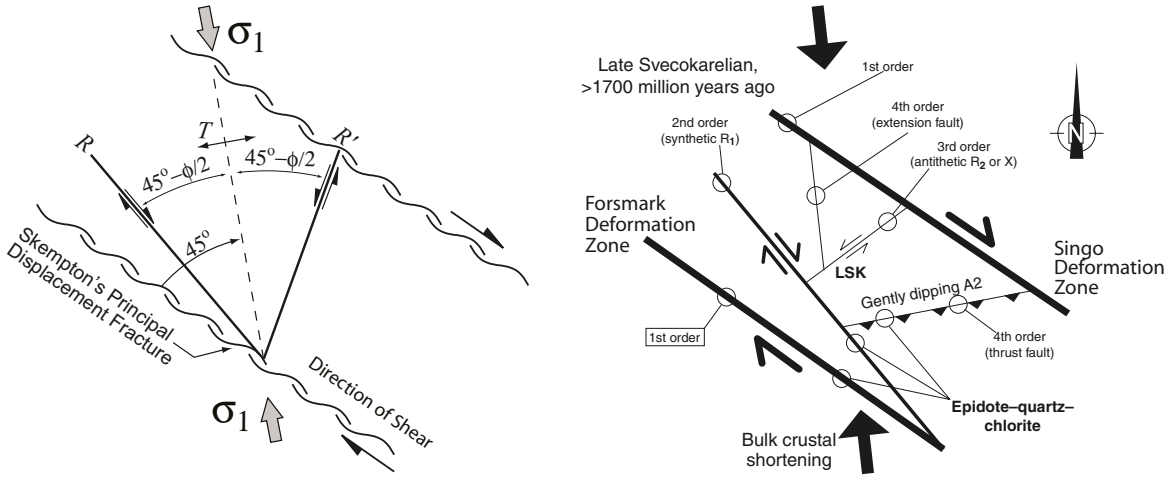

(a) Riedel shear fractures and Skempton's principal displacement fracture in clay experiments.

(b) Forsmark regional scale kinematics, from Figure 3-4 in /SKB 2006/.

Figure 2–2. *Comparison of the idealised Riedel shear fractures (R, and R') modified from /Bartlett et al. 1981/, and /Skempton 1966/'s principal displacement fracture connecting the Riedel shears, with the regional scale kinematic model for the Forsmark Site.*

2.2 Site geology

The geology of the Forsmark site is described in the Site Descriptive Model /SKB 2006, 2005a/ and only a brief summary is provided here. The Forsmark regional model area is situated within an ancient Precambrian crystalline terrain, referred to as the Fennoscandian Shield. Forsmark lies within the southernmost part of a complex structural domain with predominantly high-grade metamorphic rocks. In the regional structural context, the Target Area is located within a tectonic lens that developed more than 1,850 million years ago (Figure 2-3), when the rock units were situated at mid-crustal depths and were affected by penetrative but variable degrees of ductile deformation under amphibolite-facies metamorphic conditions. The bedrock inside the lens at the depths of the repository is relatively homogeneous whereas the lithology and deformation is more variable outside the lens.

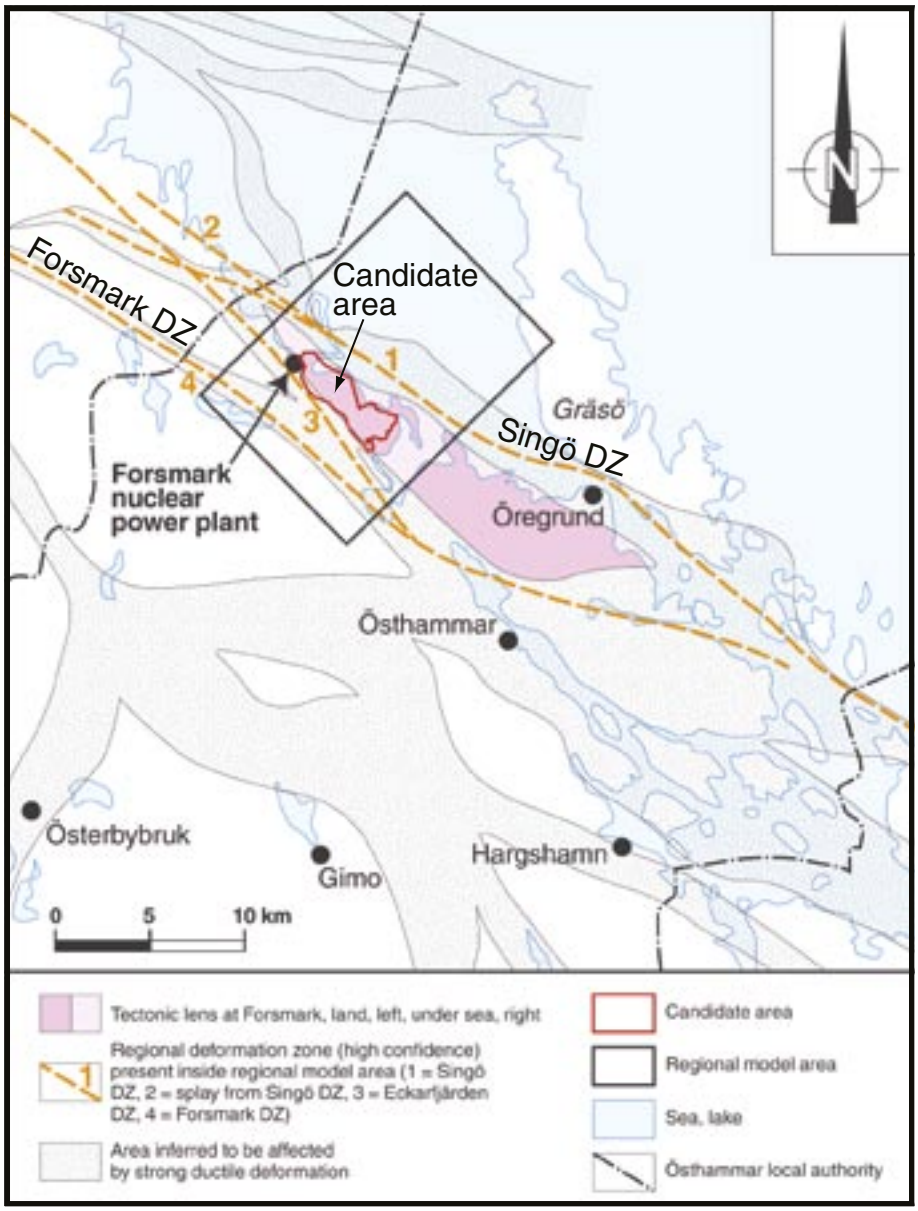

Figure 2-3. *Structural geological map of the Forsmark region showing the candidate area within the tectonic lens and the major deformation zones (DZ), adapted from Figure 3-1 in /SKB 2006/. The Target Area is the north western portion of the candidate area and is highlighted on Figure 2-10.*

2.2.1 Deformation zones

Three major sets of deformation zones have been recognised at the Forsmark site:

1. Vertical and steeply, SW-dipping zones with WNW and NW strike showing ductile and brittle deformation. The regional Forsmark and Singö deformation zones are both members of this set and form the boundary of the candidate volume.
2. Vertical and steeply-dipping, brittle deformation zones with NE strike (Figure 2-4). This set is strongly dominated by sealed fractures and sealed fracture networks. Deformation Zone ZFMNE0060 intersects the Target Area (see Figure 2-5) is a member of this set.
3. Gently SE-to S-dipping brittle deformation zones occur more frequently in the south-eastern part of the candidate volume. Relative to the other two sets, there is an increased frequency of open fractures along the gently dipping set. Deformation zone ZFMNE00A2 is one of these prominent gently dipping deformation zones in the Target Area (see Figure 2-5).

2.2.2 Fracture Domains

As stated previously, the state of stress that exists in a rock mass today is a function of its rock mass properties. It is well known that the fracture frequency in a rock mass influences the rock mass deformation modulus and as shown by /Cartwright 1997/ the deformation modulus can influence stress magnitudes. Hence it is important to establish the fracture frequency and inferred rock mass modulus in the rock mass.

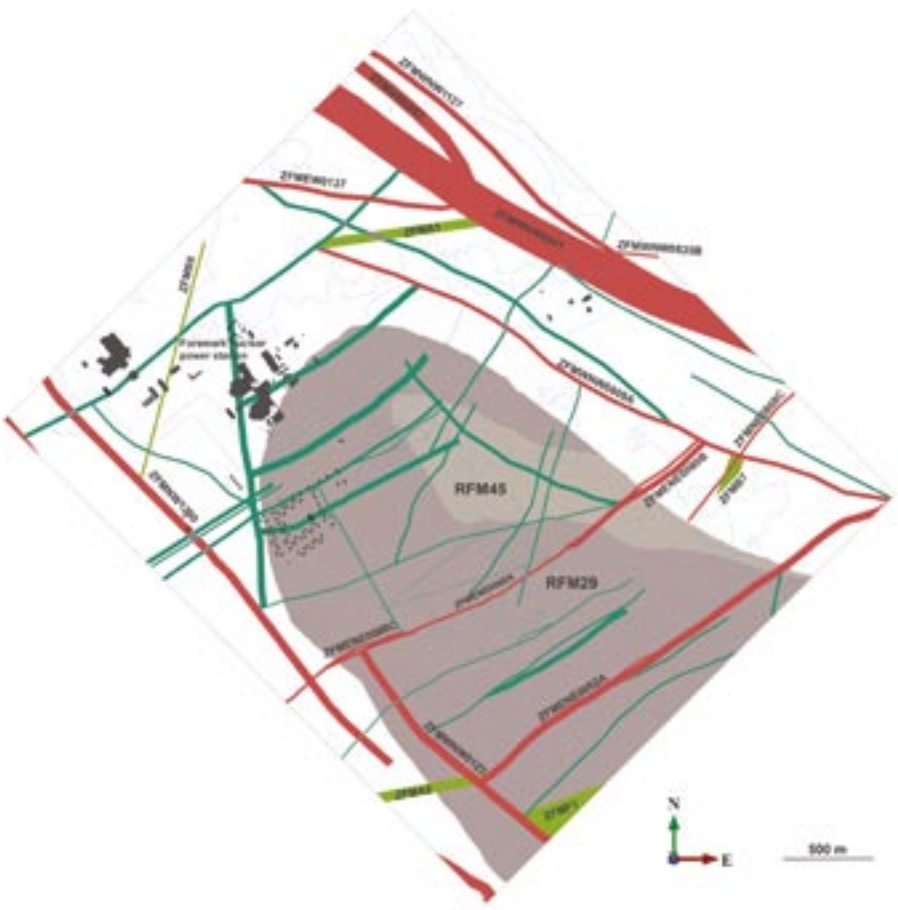

Figure 2-4. *Plan view of the deformation zones at the Forsmark site with a trace length greater than 1,000 m, on a surface at 500 m depth (figure from SKB R-07-45).*

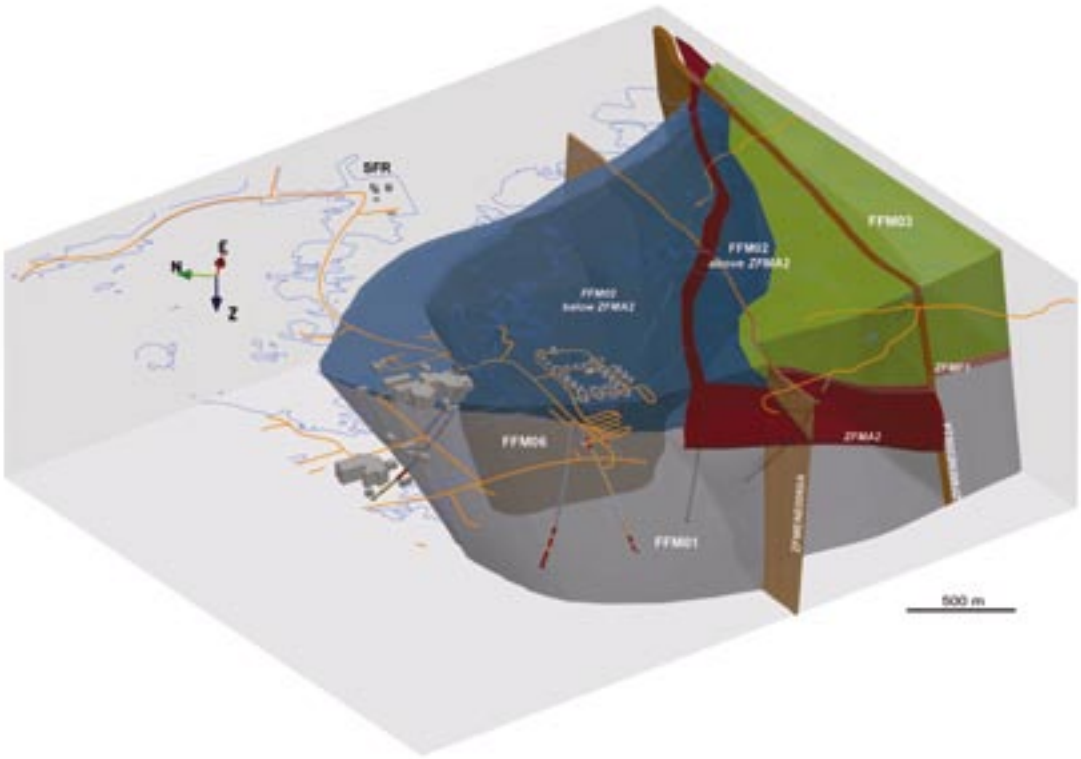

Figure 2-5. *Deformation zones ZFMNE00A2 and ZFMNE0060 encountered in the Target Area. Also shown are the fracture domains FFM01, FFM02 and FFM03. From /Olofsson et al. 2007/.*

Smaller zones and fractures, not covered by the deterministic deformation zone, are described as fracture domains. The descriptions are based on fracture observations in the boreholes, mapped fractures at outcrops and from interpretation of lineaments. Figure 2-6 shows the dominant fractures observed in outcrops. Note the dominant Northwest-Southeast and Northeast-Southwest fracture sets. These fracture sets combined with the gently dipping fractures forms the blocky rock characteristic of Fracture Domain FFM02 described below (Figure 2-7).

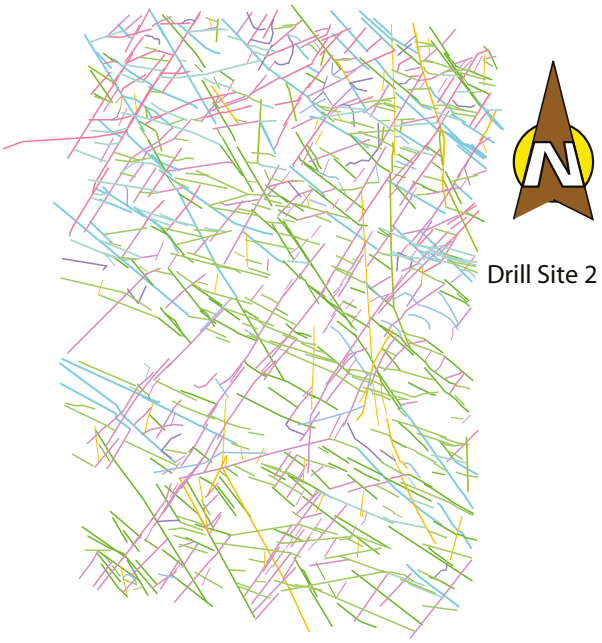

Figure 2-6. *Fracture trace maps with different fracture sets identified in outcrop shown in different colours. Note the dominant Northwest-Southeast and Northeast-Southwest fracture sets.*

Figure 2-7. *Observed near horizontal and subvertical fracturing along the Forsmark cooling water inlet channel.*

The fracture domain model captures both open and sealed fractures and many of the sealed fractures are hydrogeologically indistinguishable from the intact rock. In SDM 2.1 there were three fracture domains in the Target Area (see Figure 2-5 for the location).

Domain FFM01: The rock mass can be described as sparsely fractured, with steeply dipping minor deformation zones with sealed fractures and low fracture frequency between zones. The experience at the SFR Facility, suggests that within this domain, subhorizontal fractures may appear as localised occurrences of limited areal extent.

Domain FFM02: High frequency of subhorizontal fractures that occur in the upper 150 m. This fracture domain contains the open and hydraulically connected fractures and stress relief fractures. The vertical extension of FFM02 appears to increase towards SE and has its maximum depth at the location of boreholes KFM01A and KFM05A.

Domain FFM03: High frequency of gently dipping minor deformation zones that are open and show hydraulic connections over a large area.

Figure 2-8a shows the frequency with depth below ground surface of 10351 open fractures encountered in the Forsmark Site Characterisation boreholes and available from SICADA on 2007 April 23. These open fractures were classed in SICADA with confidence code 1 2 or 3 and noted as visible in the BIPS log. The 10351 open fractures in Figure 2-8a show a gradual decrease in frequency with depth. Figure 2-8b, contains only the gently dipping open fractures (< 20°) from the same data set. These fracture (3382) represent approximately 32% of the total open fractures. The gently dipping fractures in Figure 2-8b shows a more dramatic reduction in frequency below a depth of 200 m, with very few gently dipping open fractures occurring below 450 m depth. The open steeply-dipping (> 70°) fractures from the same data set are plotted

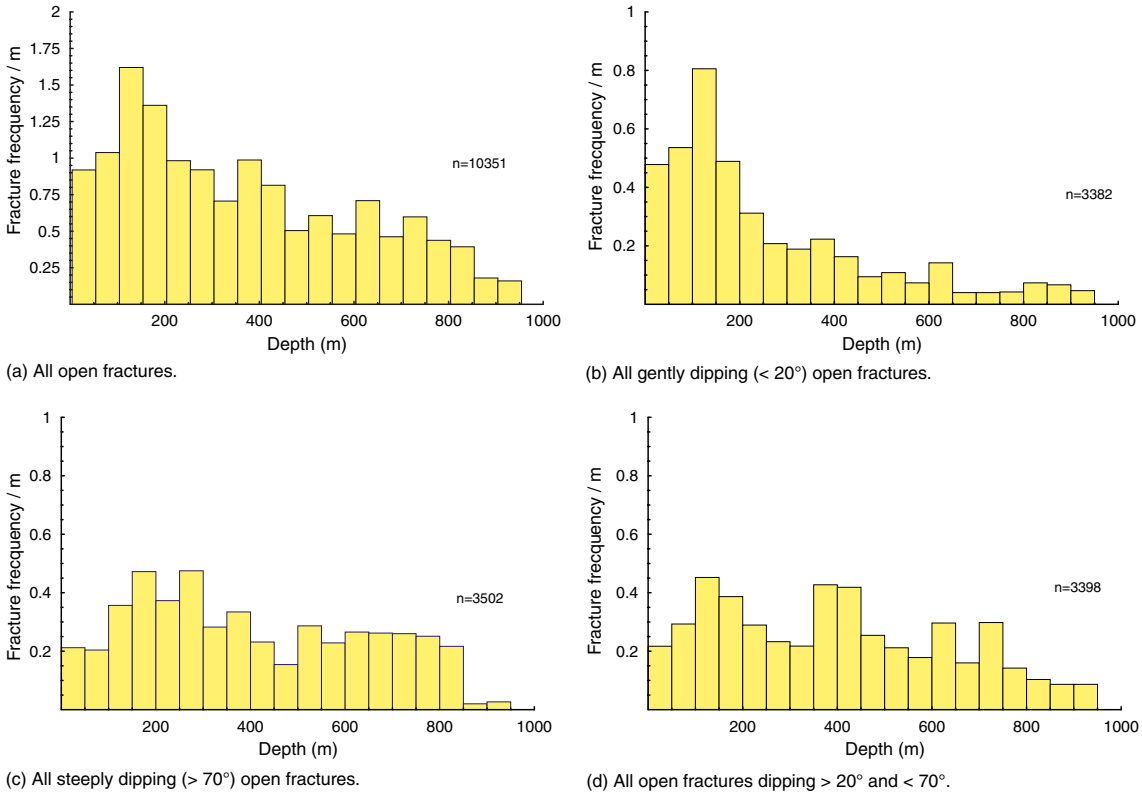

Figure 2–8. *All open fractures from Forsmark boreholes that are visible on the BIPS log. Data obtained from SICADA 2007 April 23.*

in Figure 2-8c. These steeply-dipping fractures (3502, 22%) appear to be more uniformly distributed with depth than the gently dipping fractures. Figure 2-8d shows (3398) the remaining open fractures, dipping between and 20 and 70°. There is a slight increase in the frequency of these fractures below a depth 400 m depth. In general, Figure 2-8 illustrates that the observed decrease in open fracture frequency with depth mainly occurs in the gently dipping fractures. The frequency of occurrence in all data sets between 800 m and 1,000 m is not likely to be statistically reliable because of the lack of boreholes penetrating this depth interval.

The fracture frequencies in Figure 2-8 clearly show a significant reduction in fracture frequency below a depth of 150 m. However, these fracture frequencies can only give a general indication of the rock mass quality with depth because of the difficulty of assigning trace lengths and large-scale properties to these fracture-borehole intersections. The contrast between fracture domains FFM01 and FFM02/FFM03 is supported by the fracture frequency distribution shown in Figure 2-8b. In addition, a regional seismic survey conducted as part of Forsmark Site Characterisation program also reported significantly lower P-wave velocities between 0 and 100 m depth (Figure 2-9). The velocity of seismic P-waves are sensitive to open fractures and hence provide an indirect measure of rock mass quality and stiffness. Note in Figure 2-9 that below approximately 400 m there is little increase in P-wave velocity and that the P-wave exceeds 6,000 m/s suggesting that the rock mass at depth is relatively massive and sparsely fractured. This is further supported by the low open hydraulically-connected fracture frequency in fracture domain FFM01, i.e. < 0.01 per m, /SKB 2006/.

About 16 km of high resolution seismic data were acquired along five separate profiles varying in length from 2 to 5 km. Nominal source and receiver spacing was 10 m with 100 active channels when recording data from a dynamite source (15–75 g). The profiles were located within a relatively undeformed lens of bedrock that trends in the NW-SE direction. The lens is surrounded by highly deformed rock on all sides. In conjunction with the reflection component of the study, all shots were also recorded on up to eleven 3-component fixed Orion seismographs. These recordings provided long offset data from which a velocity model of the uppermost 400 m of bedrock could be derived.

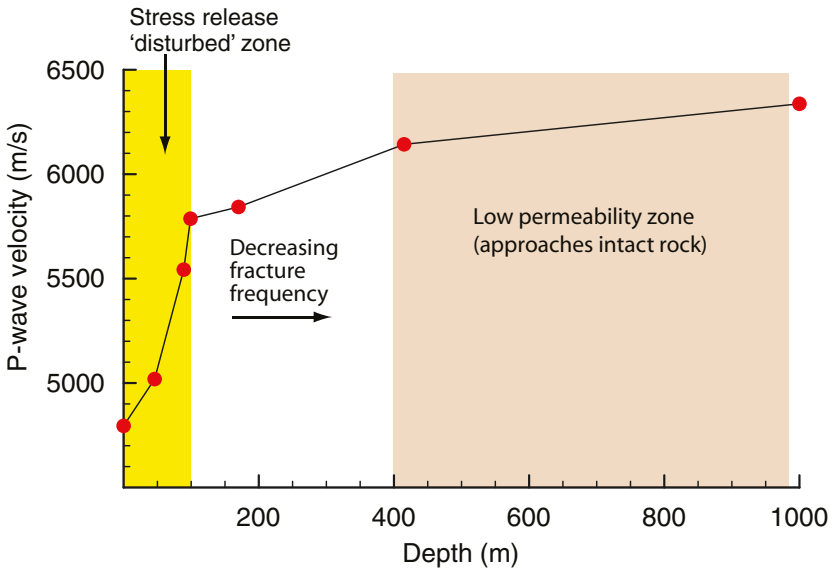

Figure 2–9. *Seismic P-wave velocities from a 16 km long, high resolution regional seismic survey, conducted within the candidate area in 2002, data from /Juhlin et al. 2002/.*

2.2.3 Lithology

The candidate area is located within the tectonic lens and, due to its internal homogeneity, most of the lens can be described as a single "rock domain" denoted RFM029 in the Site Descriptive model. Figures 2-10 and 2-11 shows the general rock types in the candidate area. Approximately 75% of RFM029 is medium-grained granite to granodiorite. Subordinate rock types are fine- to medium-grained metagranodiorite or metatonalite (5%), amphibolite (5%), pegmatitic granite or pegmatite (10%), and fine- to medium-grained granite (2%). The dominant rock type and the subordinate rock types, except for amphibolite, have high quartz content, i.e. 20 to 50%. A foliation within the metagranite is folded and both fold axis and mineral stretching lineation plunge towards the south-east. In the NE part of rock domain RFM029 is the minor domain RFM045 also included in the so called Target Area. This volume has been estimated to contain an altered (bleached) metamorphic and aplitic granite to 66% /SKB 2006/.

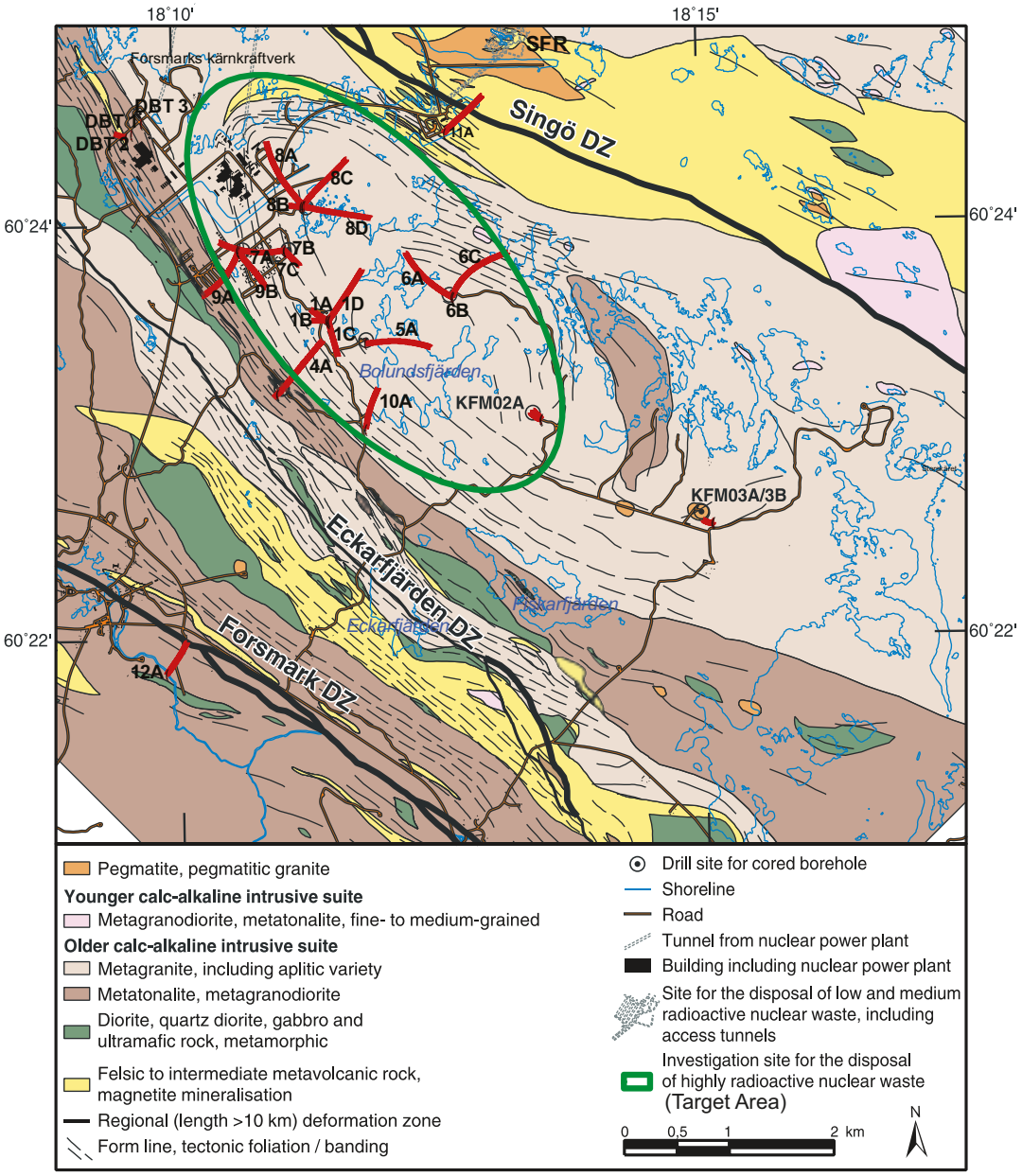

Figure 2–10. *Bedrock geological map of the Forsmark site. The Target Area is shown as the green ellipse shape. The locations of the cored boreholes including the holes used in the stress campaigns within the Target Area are also shown. Note that DBT1 and DBT3 (stress measurement boreholes) are located to the West of the Target Area. Modified from /Juhlin and Stephens 2006/.*

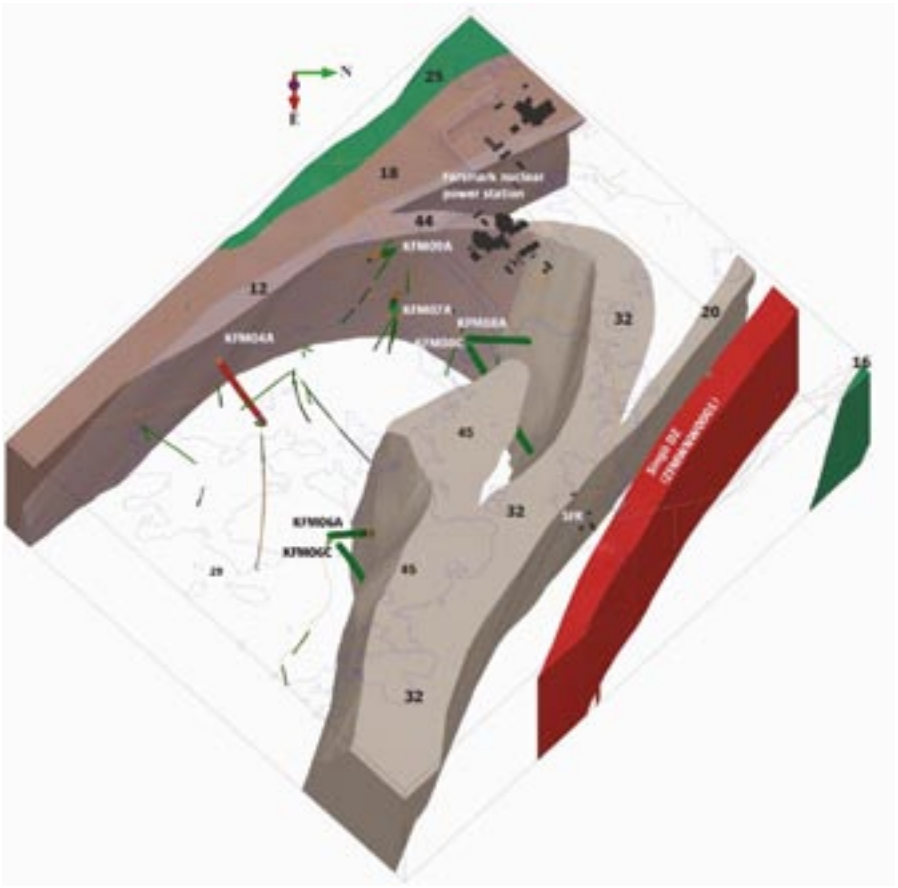

Figure 2–11. *Three dimensional view of the rock domain model, Figure 3-3 in Forsmark SDM version 2.1 /SKB 2006/. The colours indicate the dominant rock type in each domain.*

The lens is surrounded by various domains that strike north-west, dip steeply to the south-west and are dominated by tectonites containing both planar and linear ductile mineral fabrics. In general, the rocks in these domains show considerable ductile deformation relative to that observed inside the tectonic lens and the bedrock is heterogeneous and composed of various types of felsic to intermediate metavolcanic rocks and metagranitoids. The lithology gradually increases in foliation as the boundaries of the lens are approached and the lithological banding becomes more apparent reflecting the gradual change to the more gneissic lithology that surrounds the lens.

2.3 Summary

The geology at the Forsmark site can be summarised as a relatively homogeneous crystalline lens that has experienced relatively limited straining. Most of the strain appears to have been taken up by strike slip movement along the near vertical Northwest-Southeast trending Forsmark and Singö faults. The gently dipping deformation zones are interpreted to be fourth order events formed from thrust stress conditions created by straining along the Forsmark and Singö faults. The fracturing (i.e. jointing) that has occurred in the lens in the Target Area decreases significantly with depth and transmissive fractures are reported to be essentially non-existent below 400 m. Fracture Domain FFM02 which contains open mainly gently dipping fractures extending to depths between 100 to 200 m may be described as a “disturbed zone”. In this zone stress release has occurred by the formation of extensive, sub-horizontal exfoliation fractures (Figure 2-7) and by the opening of these and the majority of other fractures.

This notion of a stress released zone near the surface is also supported by the significant lower P-wave velocity between 0 and 100 m depth determined from a regional seismic survey (see Figure 2-9).

3 Current boundary conditions

In the previous section the rock mass conditions were described. In this section the regional boundary conditions that are acting on the rock mass are examined. In Fennoscandia two significant boundary conditions are inducing strains in the rock mass: (1) plate tectonics and (2) glacial rebound.

3.1 Plate tectonics

It is well known that the earth's crust is composed of thin plates that are moving relative to each other (Figure 3-1). As our understanding of plate tectonics has evolved it has become more apparent that the intraplate regions of the world are characterised by relatively uniformly oriented compression due to this plate movement. For example, /Müller et al. 1992/ showed using approximately 1,500 stress orientation determinations from across Europe, three distinct regional patterns of maximum compressive horizontal stress (σ_{Hmax}) orientation in Europe: a consistent NW to NNW σ_{Hmax} stress orientation in western Europe; a WNW-ESE σ_{Hmax} orientation in Scandinavia; and a consistent E-W σ_{Hmax} orientation and N-S extension in the Aegean Sea and western Anatolia (between the mainlands of Greece and Turkey respectively). They concluded that the different stress fields can be attributed to plate-driving forces acting on the boundaries of the Eurasian plate, locally modified by lithospheric properties in different regions. They also concluded that on average, the orientation of maximum stress in western Europe is subparallel to the direction of relative plate motion between Africa and Europe but is rotated approximately 17° clockwise from the direction of absolute plate motion. The relative plate motion between the European and American plates is WNW-ESE. Hence, in Scandinavia today a general WNW-ESE (approximate azimuth 130 to 150°) compression would be anticipated. This has been supported by stress measurements compiled by the World Stress Map Project (Figure 3-2).

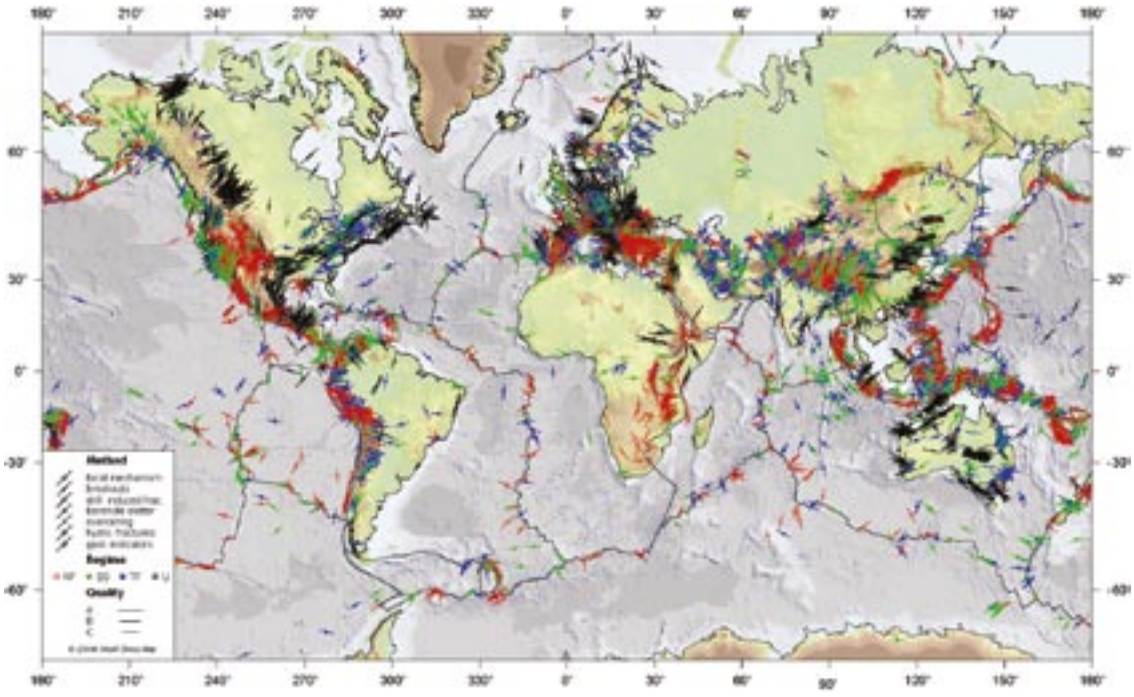

Figure 3–1. *Major plate boundaries and the orientation of the maximum horizontal stress, data from the World Stress Map, http://www-wsm.physik.uni-karlsruhe.de.*

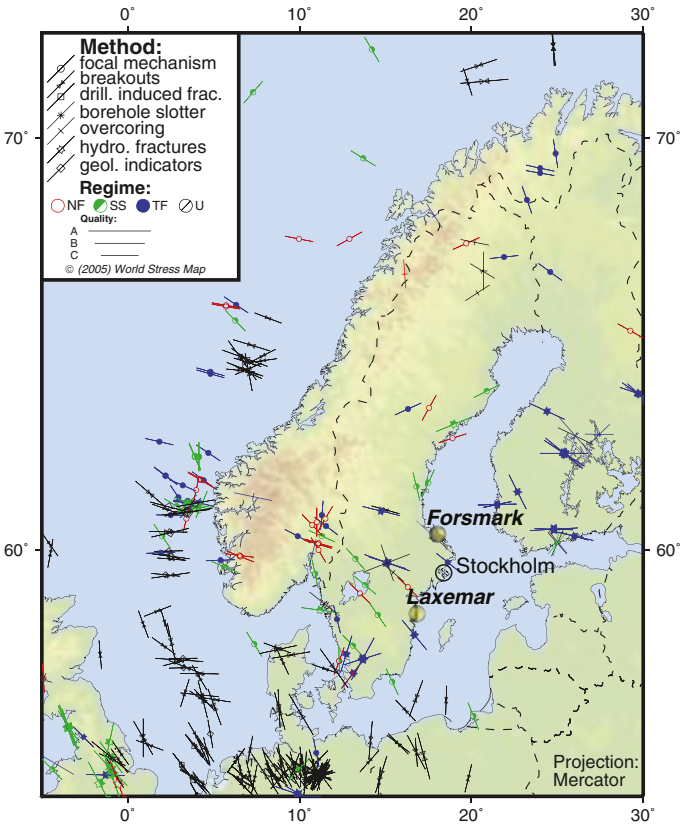

Figure 3–2. *Stress directions for Sweden, data from the World Stress Map Project, http://www-wsm.physik.uni-karlsruhe.de.*

/Marotta et al. 2004/ used a suite of spherical, thin sheet, finite element models to investigate the pattern of horizontal tectonic deformation in the Mediterranean and Fennoscandian region. The calculations incorporated the effects of Africa-Eurasia convergence, Atlantic Ridge push forces, and changes in the lithospheric strength of the East European and Mediterranean subdomains. Using plate velocities that ranged from 1 to 5 mm/year, they concluded that a best fit to the measured global positioning system (GPS) data was obtained by simultaneously considering the effects of plate tectonics plus glacial rebound.

3.2 Glacial isostatic adjustment

In Fennoscandia glacial isostatic adjustment (GIA) has been studied extensively over the past 20 years. The measurements were initially restricted to vertical displacements and referred to sea level or to an arbitrarily chosen reference point. Today global positioning systems (GPS) allows for estimating three dimensional surface deformations. The BIFROST permanent GPS network in Sweden and Finland provide three-dimensional maps of postglacial rebound over Fennoscandia such as that shown in Figure 3-3. Figure 3-3a indicates that the vertical velocities show an oblong-shaped uplift pattern with a maximum vertical rate of approximately 11 mm/yr several hundred kilometres north of Stockholm decreasing to essentially zero south of Sweden. Horizontal velocities, associated with these vertical deformations, show widespread extension with rates of the order of 1–2 mm/yr pointing away from the area of maximum uplift. /Carlsson and Olsson 1982/ suggested that this glacial isostatic rebound was a possible reason for elevated horizontal stress magnitudes in the Forsmark region. However, it is often not practical to differentiate stresses associated with plate tectonics from those associated with glacial isostatic adjustment because the local horizontal extension due to the GIA is approximately the same as the rate of compression due to plate motions.

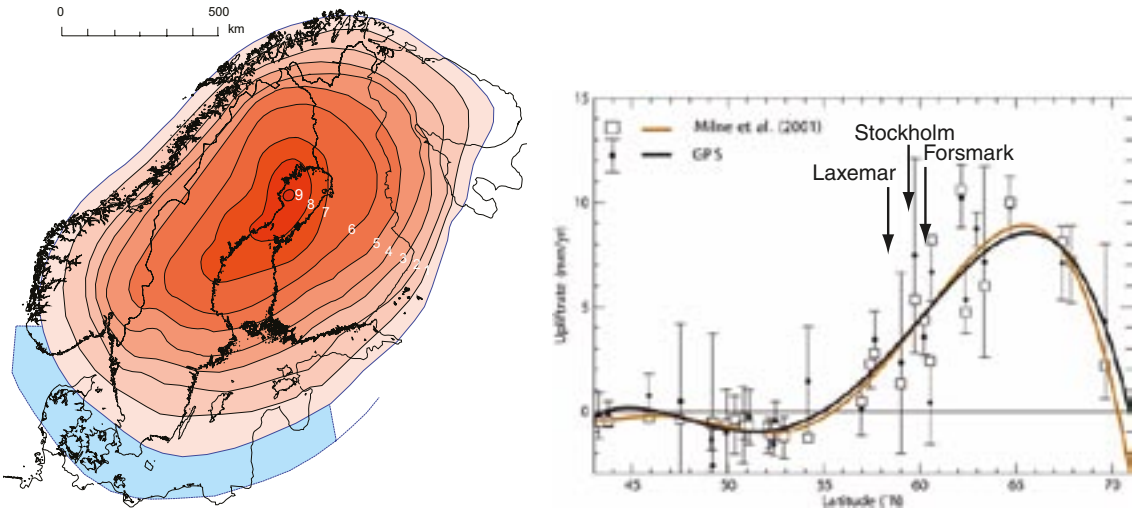

(a) Recent land uplift rate mm/yr in Fennoscandia, data from /Ojala et al. 2004/.

(b) Profile of vertical uplift rate as a function of latitude, data from /Nocquet et al. 2005/.

Figure 3-3. *Glacial uplift rates in Fennoscandia.*

3.3 Crustal stresses and seismic activity

Earthquakes are the most obvious indicator of bedrock deformation. As discussed above both plate tectonics and glacial isostatic adjustments contribute to the bedrock deformations in Fennoscandia. The earthquake records in Fennoscandia date back to 1375 and the current understanding is largely based on 25 years of seismic data collected with modern instrumentation /Ojala et al. 2004/. In Fennoscandia, the majority of the seismic activity is concentrated near the western coastline of Norway and southwestern Sweden (Figure 3-4).

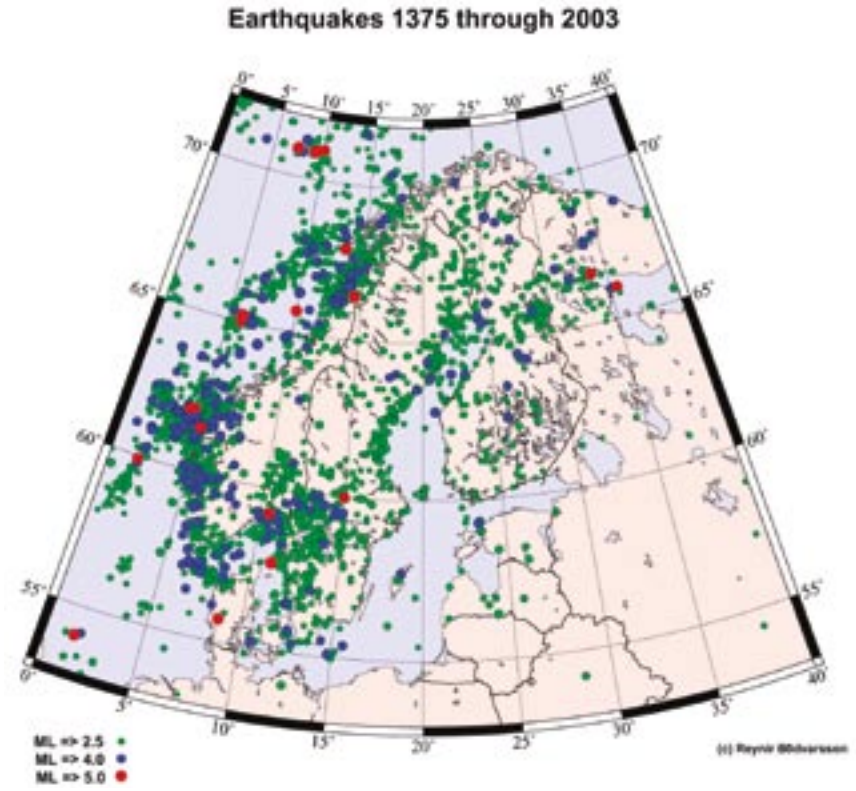

Figure 3–4. *Location of earthquakes in Fennoscandia, from /Ojala et al. 2004/.*

/Slunga 1991/ analysed approximately 200 seismic events collected from the Swedish Seismic Network. All the seismometers were placed on Precambrian bedrock and the seismic events had moment magnitudes between 0.6 to 4.5. /Slunga 1991/ identified three layers of seismic activity in the crust of southern Sweden: (1) the upper crust between 0 and 18 km had the highest earthquake frequencies, (2) the middle crust between 18 and 35 km, and (3) the seismically quiet lower crust. /Slunga 1991/ noted that the decrease in the earthquake frequency was 5 km shallower (13 km instead of 18 km) in northern Sweden. /Slunga 1991/ suggested that this seismicity boundary was due to a lithological boundary and that this boundary was more shallow in the older northern crust.

The seismic events analysed by /Slunga 1991/ clearly showed a clustering of events in Southwestern Sweden to the west of the Protogine zone, which separates the younger rocks in the southwest from the old Precambrian rocks to the East and North (Figure 3-5). /Slunga 1991/ noted that regardless of the location of the events there was a consistent horizontal direction for energy release and concluded that the regional direction of maximum horizontal compression was N60°W. /Hicks et al. 2000/ also found a similar horizontal compression direction from stress inversion of earthquake focal mechanism solutions from onshore and offshore Norway. /Slunga 1991/ concluded that the uniformity of the compression orientation in both southern and northern Sweden implied that the seismic fault movements were caused by the same systematic horizontal deformation of the crust and hence likely caused by plate tectonic processes rather than uplift processes.

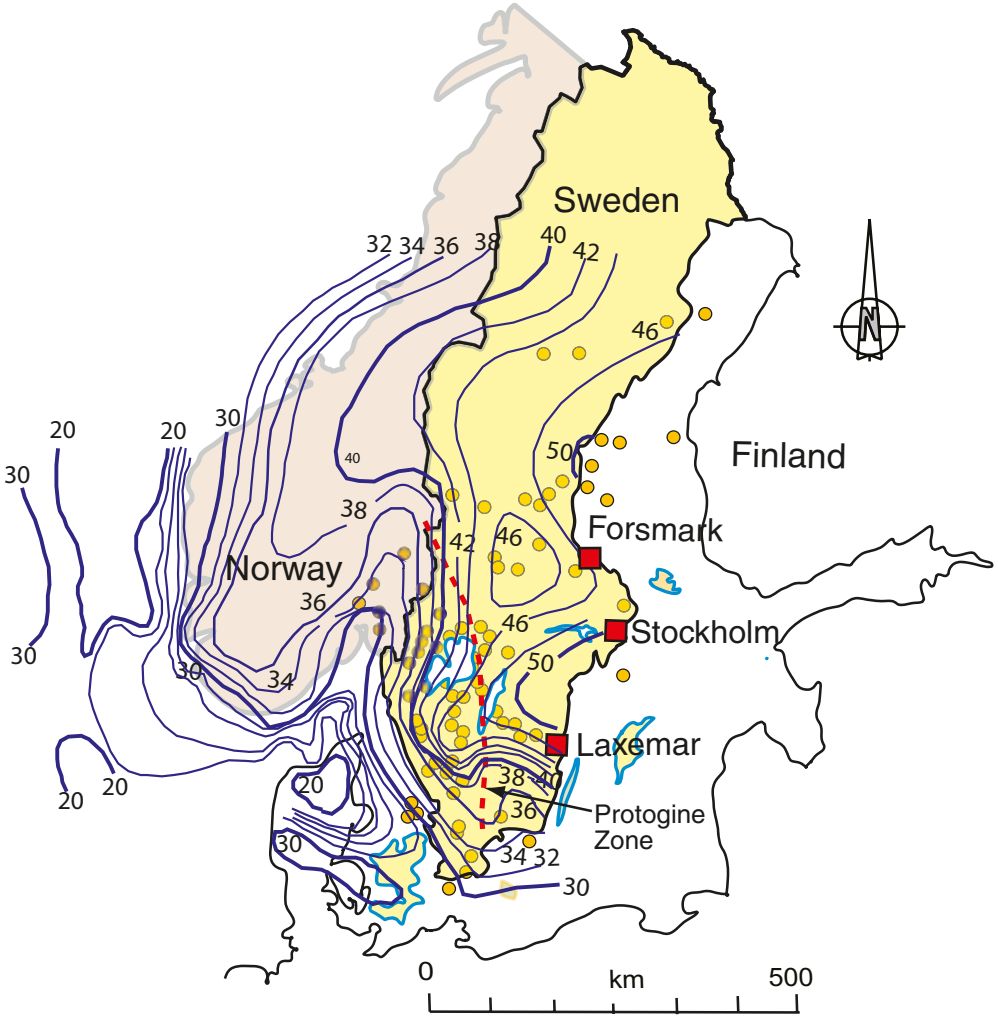

Figure 3–5. *Fennoscandia crustal thickness contours (in km), modified from /Kinck et al. 1993/. The yellow circles represent some of the seismic events analysed by /Slunga 1991/.*

/Slunga 1991/ concluded that the dominant type of faulting associated with the seismic events in Southwestern Sweden was strike-slip, while the seismic events in northern

Sweden indicated a thrust fault environment. /Slunga 1991/ attributed the change from strike-slip in southern Sweden to thrust regimes in northern Sweden to the Protogine zone (Figure 3-5). /Kinck et al. 1993/ used seismic profiling to establish crustal thickness contours for Fennoscandia (Figure 3-5). They found that the thinnest crust (approximately 20 km) was located to West of Protogine zone and while East-central Sweden had a very thick crust (approximately 50 km). /Kinck et al. 1993/ suggested that the seismic events concentrate where the change in thickness is greatest and that this differential thickness in the crust may be related to the different seismic signatures obtained by Slunga. /Lund et al. 2001/ also examined the change in crustal thickness in southeastern Sweden and concluded that the change in thickness from 52 to 36 km did not occur as a gradual change but was found to occur in steps, suggesting much more abrupt change in thickness. Comparing Figures 3-5 and 3-4, there is a strong correlation between the location of the seismic events and the change in crustal thickness.

3.4 Summary

In summary, the seismic record for Sweden shows that the regional horizontal stress is oriented N60°W. This orientation of the maximum horizontal stress is consistent throughout Sweden and most of Europe and reflects the overall direction of plate motion. Despite this consistency in horizontal stress orientation the source of the seismic events in southern Sweden are associated with strike-slip faults while towards the north the seismic events are dominated by a thrust fault. This implies, using the Anderson fault classification that the orientation of the principal stresses could be different in Southern Sweden compared to Northern Sweden, at least at the depths of seismic events.

4 Indicators of the state of stress

While the state of stress can only be quantified by measurements, indicators and observations can be used to infer the general trends of stress magnitudes and orientations. Descriptions of the various methods used to quantify the stress magnitudes and orientations are given by /Ljunggren et al. 2003/. In addition to these measurement techniques, the following methods can also be used to infer the state of stress:

- spalling around underground openings,
- core damage,
- core disking, and
- borehole breakouts.

These methods are discussed in the following sections. While it is not possible to determine the stress tensor using these indicators, they can be used to bound the horizontal stress magnitudes and the direction of the maximum horizontal stress.

4.1 Experience from construction of Forsmark Nuclear Facilities

It is well known that when the stress magnitudes on the boundary of an excavation in brittle hard rock reach the rock mass strength spalling is observed. /Andersson 2007/ showed that this response can be induced by excavation-induced stresses and/or thermal-induced stresses. /Hoek and Brown 1980/ compiled case histories from South Africa where the ratio of the maximum to minimum far-field stress in the plane of the excavation is equal to 2, and concluded that minor spalling occurs when $\sigma_1/\sigma_c > 0.2$, where σ_1 is the maximum far-field stress and σ_c is the uniaxial compressive strength). /Hoek and Brown 1980/ compiled additional South African observations from underground mining in massive brittle rocks and suggested the stability classification given in Figure 4-1. The stability classification in Figure 4-1 ranges from 0.1 through 0.5 and can be briefly described as follows: ($\sigma_1/\sigma_c \leq 0.1$) a stable unsupported opening, i.e. no damage;

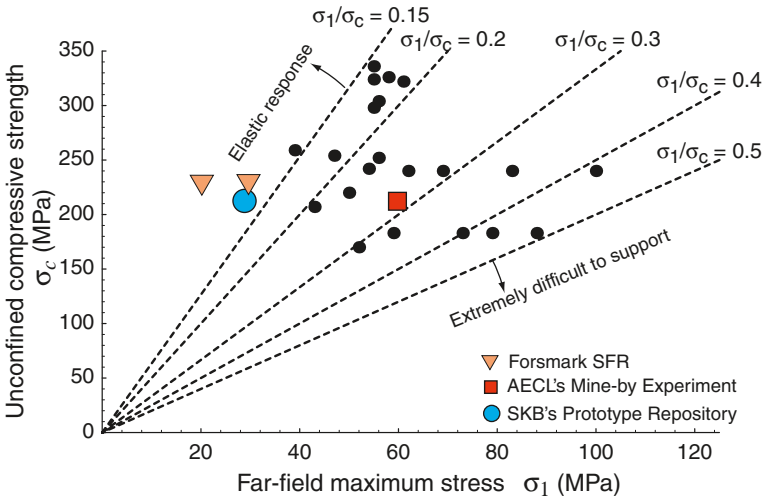

Figure 4–1. *Empirical stability classification developed for horizontal tunnels in South Africa where the maximum stress is vertical, modified from /Hoek and Brown 1980/. The far-field maximum stress in the figure refers to far field maximum stress in the plane normal to the tunnel being evaluated.*

($\sigma_1/\sigma_c = 0.2$) minor spalling can be observed, requiring light support; ($\sigma_1/\sigma_c = 0.3$) severe spalling, requiring moderate support; ($\sigma_1/\sigma_c = 0.4$) heavy support required to stabilise the opening; and ($\sigma_1/\sigma_c = 0.5$) stability of the opening may be very difficult to achieve, extreme support required. The results in Figure 4-1 were compiled for square openings in a mining environment. For comparison, the stress magnitudes for SKB's Protoype Repository where no spalling was reported, and AECL's Mine-by Experiment where significant spalling was reported, are also shown on Figure 4-1. It appears from Figure 4-1 that the stability classes suggested by /Hoek and Brown 1980/ provide a reasonable estimate of the maximum stress/strength magnitude if spalling is observed.

Construction of the nuclear power plant and the low and intermediate level waste repository (SFR Facility) at Forsmark required excavation to depths between 0 and 140 m /Carlsson and Christiansson 2007/. While the site investigations and the excavations took place northwest of the Target Area, the ground conditions may be indicative of the ground conditions within the Target Area. /Carlsson and Christiansson 1986/ described the elevated stress magnitudes measured during the site investigations for the Forsmark facilities. However, only limited occurrence of high stresses was encountered during the construction of the underground openings. /Carlsson and Christiansson 2007/ noted that stress-induced spalling in the roof of the tunnel from unit 3 was encountered when the rock cover over the tunnel was less than 50 m, indicating significant stress concentrations caused by the high horizontal stresses. Other than this one occurrence, no problems due to high stresses were reported during construction of the underground openings at the Forsmark facilities /Carlsson and Christiansson 2007/. Using a uniaxial compressive strength of approximately 225 MPa for the Forsmark Granite, Figure 4-1 would suggest that except for the one instance where localised spalling was reported, for the remainder of the excavations at Forsmark to depth of 140 m the maximum principal stress did not exceed 30 MPa. It should be noted that the SFR is located to the North of Singö fault and it is unknown if the stress magnitudes in the region of the SFR are the same as within the Target Area.

4.2 Core damage and stress

It is well known that extracting core samples at depth can lead to a significant increase in crack porosity /Chernis 1984, Martin and Stimpson 1994/. This crack porosity can occur from two sources: (1) new stress-induced microcracks associated with the coring process, and (2) naturally closed pores that open when the in situ stress magnitudes are released. In all cases the increase in crack porosity will lead to an increase in nonlinear stress-strain behaviour in unconfined compression tests. In the stress-strain curve during the compression loading of a rock cylinder, the specimen behaviour can be divided into four sections (Figure 4-2): (1) O-A: nonlinear microcrack and pore closure; (2) A-B: linear elastic behaviour; (3) B-C: stable fracture initiation and propagation; and (4) C-D: unstable fracture propagation. In the stage O-A, the nonlinear behaviour is a function of the pore space in the sample. If there was no porosity the stress-strain response would only be a function of the solid particles and their contact stiffness. In hard rocks this contact stiffness is essentially the same as the stiffness of the intact particles and hence the stress-strain response is linear. As the porosity increases, the stress-strain response is composed of two parts: (1) the stress-strain response of the volume of rock containing the pore and (2) the stress-strain response of solid rock volume. It is intuitive that as the volume of the porosity increases so should the nonlinearity of the stress-strain response.

/Martin and Stimpson 1994/ established for Lac du Bonnet granite that the amount of nonlinearity in the stress-strain curve was a function of the maximum principal stress relative to the uniaxial compressive strength. More recently /Lim et al. 2007/ developed a methodology for estimating the energy, referred to as crack closure energy, required to close the cracks i.e. Point A in Figure 4-2. They examined the the crack closure energy for samples taken from Forsmark granite (lithology domain RFM029) and AECL's Underground Research Laboratory (Lac du Bonnet granite). Figure 4-3 shows the comparison for both sites and the

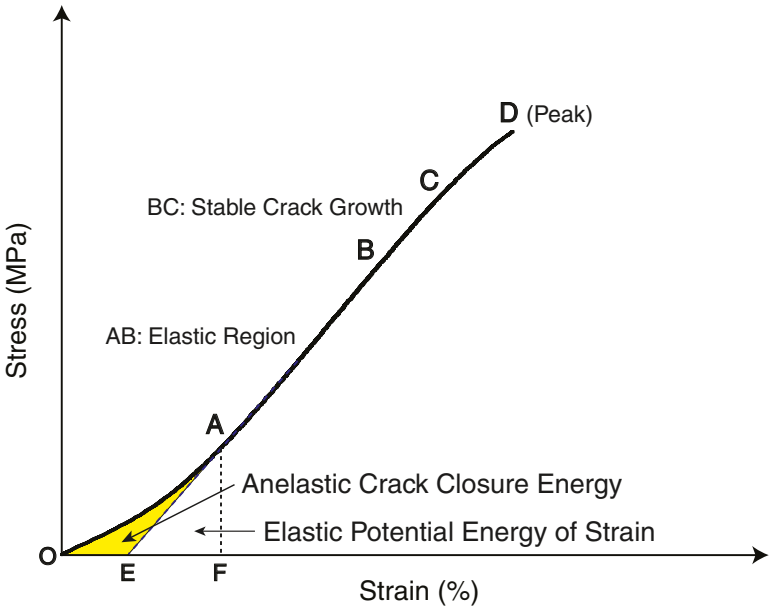

Figure 4-2. *Concept of crack closure energy used by /Lim et al. 2007/.*

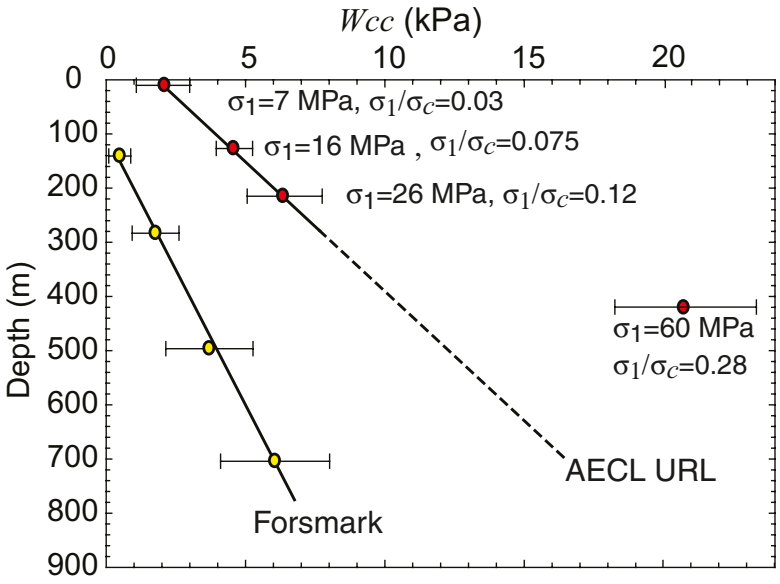

Figure 4-3. *Comparison of the Crack Closure Energy on core samples from Forsmark and AECL's Underground Research Laboratory (URL) data from /Lim et al. 2007/. Note the significant increase in crack closure energy at AECL URL at a depth of 420 m when the maximum principal stress is 60 MPa.*

stress magnitudes associated with the location of the samples for the Lac du Bonnet samples. The crack closure energy is linear with depth at both sites except at the 420 m depth at AECL URL where the maximum principal stress is approximately 60 MPa and the ratio of maximum principal stress to the uniaxial compressive strength is approximately 0.28. This ratio is similar to that established by /Hoek and Brown 1980/ and shown in Figure 4-1 for tunnels that display spalling. The methodology used by /Lim et al. 2007/ relied on uniaxial tests to quantify the crack closure energy. More recently /Jacobsson et al. 2007/ used hydrostatic compression tests with loading up to 50 MPa and 100 MPa on Forsmark granite specimens to establish the crack volume strain to depths of 700 m. They also concluded that the crack volume strain increased linearity with depth below 500 m suggesting there was no sudden increase in stress magnitudes at the Forsmark site that was sufficient to cause significant stress-induced cracking.

4.3 Core disking

Core disking is a phenomenon in which the drilled core disks with uniform spacing and shape due to the transient stress changes, and stress release during drilling. During the site investigation drilling at Forsmark, to depths of 1,000 m, localised core disking was encountered. /Sjöberg et al. 2005/ compiled core disking observations during the early phase of the Site investigations. The disking was observed in short (<1-m long) sections of solid core, and as ring-disking in overcore hollow cylinders. The majority of the disking observations at Forsmark occurred as ring-disking during overcoring. The overcoring system at Forsmark used a 76-mm hole diameter with a pilot hole diameter of 36 mm. Overcoring equipment includes a conventional Craelius T2-76 core barrel and coring bit, producing a nominal core diameter of 61.7 mm. Hence, the overcoring produced a thin hollow cylinder with a nominal thickness of 12 mm.

The investigation of the core disking mechanism and its application to estimate the far-field stress state was started in 1963 by Jaeger and Cook. They found an inverse relationship between the applied principal stress and disk thickness through laboratory experiments conducted with cylindrical cores. /Obert and Stephenson 1965/ suggested a criterion which provides the threshold of axial and lateral stress for inducing core disking by biaxial loading for various rock types. /Hakala 1999/ used three dimensional elastic numerical modelling to develop stress magnitudes related to solid core disk thickness. /Lim et al. 2006/ also used a three dimensional elastic model and a three dimensional linear elastic fracture mechanics model to examine the stress path experienced by the solid core disks and ring disks, the disk shape and thickness. /Lim et al. 2006/ showed that:

- ring disking will begin before solid core disking for the drill bit configuration used at Forsmark,
- the direct tension tensile strength determines when ring disking will occur, and
- a combination of direct tension and Brazilian tensile strength determines when solid core disking will occur.

/Lim et al. 2006/ found that the solid core disk thickness at Forsmark ranged between 10 and 15 mm in the Forsmark granite and that the disks were mainly planar. /Lim et al. 2006/ conducted a series of three dimension numerical models to establish the relationship between tensile stress and horizontal stress that would produce a disk thickness of 10 mm at a depth of 500 m (Figure 4-4). The mean Brazilian tensile strength for the Forsmark granite (FFM029) at a depth of 500 m is 14 MPa and direct tensile strength was found to be 0.68 of the Brazilian strength.

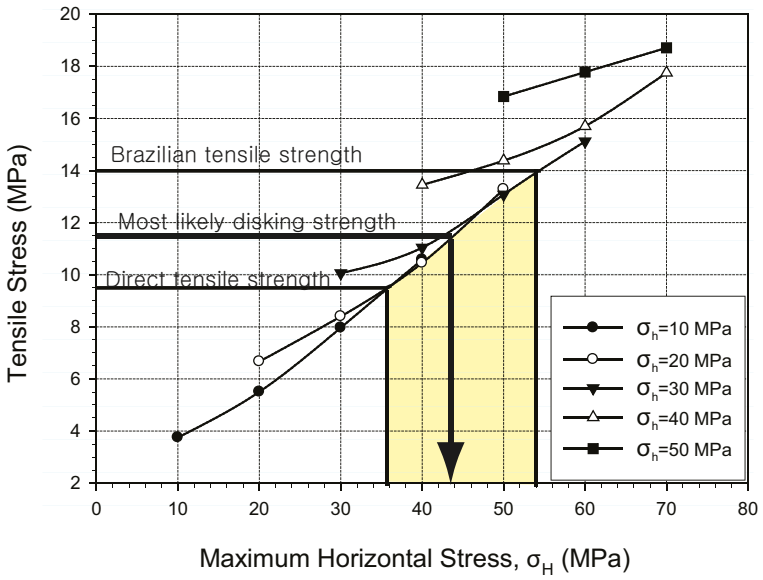

Figure 4-4. *Limits for core disking in terms of tensile stress and horizontal stress.*

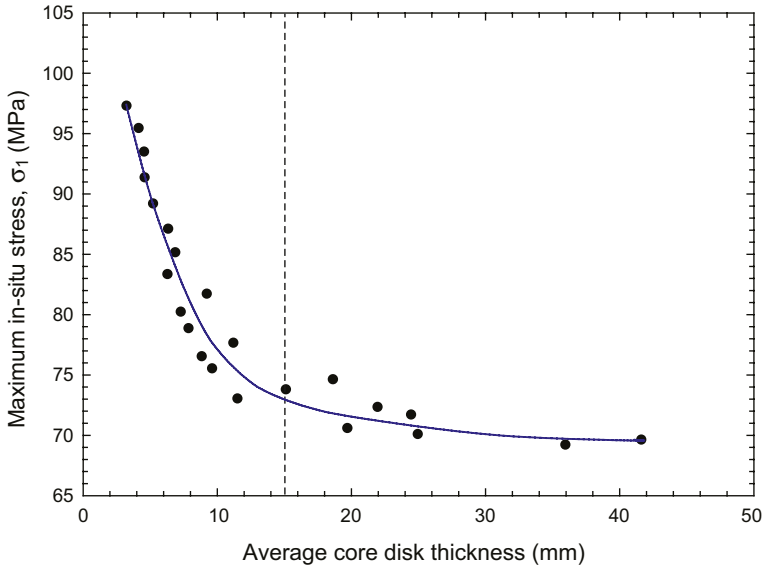

Figure 4-5. *Disk thickness measured at AECL's Underground Research Laboratory as a function of maximum principal stress, from Lim (In Progress).*

This would imply in Figure 4-4 that the maximum horizontal stress at 500 m depth could range between 35 and 55 MPa, while the minimum horizontal stress would range between 20 and 30 MPa. /Sjöberg et al. 2005/ arrived at similar conclusions based on the work of /Hakala 1999/. However, because the core disking process must reach components of both the direct tensile and Brazilian tensile strength, the maximum horizontal stress is expected to be about 44 MPa and the minimum horizontal stress is expected to be between 20 and 30 MPa. It should be noted that these horizontal stress magnitudes represent an upper limit as solid core disking is seldom seen. In addition, because core disking is also seldom seen at depths of 1,000 m, it would imply that the horizontal stress magnitudes do not significantly increase with depth.

4.4 Borehole breakouts from acoustic televiewer logging

Traditional borehole breakouts are an indicator of stress anisotropy and when stress magnitudes on the boundary of the excavation reach the rock strength. The "classical" definition of borehole breakout used by /Bell and Gough 1979/ is given in Figure 4-6.

/Martin et al. 1994/ carried out an extensive study of the stress magnitudes required to cause borehole breakouts in Lac du Bonnet granite using a series of vertical boreholes with diameters ranging from 75 to 1,250 mm, and a 75-mm-diameter borehole drilled along the centre of a 3.5-m-diameter test tunnel. /Martin et al. 1994/ concluded that the stress magnitudes required to form breakouts was similar in all openings regardless of size, particularly if the small diameter borehole was drilled in the same direction as the larger opening. Hence breakout observations in surface based 76-mm-diameter exploration boreholes can be used as an indicator to assess the potential for breakouts around underground openings.

The acoustic televiewer logs from boreholes KFM01A, KFM01B, KFM02A, KFM03A, KFM03B, KFM04A, KFM05A, KFM06A and KFM07C were analysed by Ramboll for breakouts (Table 4-1). A summary of their findings, as well as the details of the survey method and their analysis, is given by /Ringgaard 2007b/. /Ringgaard 2007b/ discusses the details of the data processing and issues associated with data quality. The interested reader should refer to that report for the detailed data from their analyses. In this report the data provided by Ramboll is analysed and interpreted relative to the geology provided in the site descriptive model /SKB 2005a, 2006/.

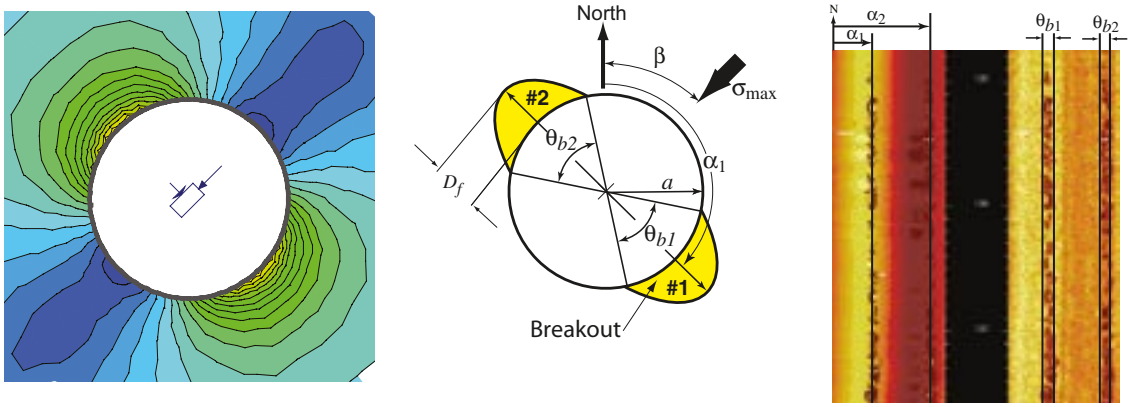

Stress concentrations around a borehole caused by anisotropic in-situ stresses

Borehole breakout resulting from the stress concentrations

Typical televiewer breakout observed in high stress environment in 75-mm-diameter borehole

Figure 4-6. *Definition of "classical" borehole breakout. The stress concentrations in the left figure must reach the rock strength to produce the breakout shown in the figure on the right.*

Table 4-1. Summary of the boreholes used in the Ramboll Survey /Ringgaard 2007b/.

Borehole name	Survey start (m)	Survey end (m)	Inclination (deg from hor)	Orientation (deg from GN)
KFM01A	102	1,001	–84.73	318.35
KFM01B	0	500	79.04	267.59
KFM02A	102	1,002	–85.38	275.76
KFM03A	100	1,001	–85.75	271.52
KFM03B	8	101	–85.30	264.49
KFM04A	107	1,001	–60.08	045.25
KFM05A	108	1,002	–59.80	080.90
KFM06A	101	1,000	–60.25	300.92
KFM07C	95	500	–85.40	098.39

In the Rambol survey the acoustic televiewer was used to determine the ovoid shape of the borehole with depth. Ramboll report that the radial resolution of the televiewer was 0.075 mm and therefore conclude "There has been found no ovality in the boreholes exceeding 0.1 mm, unless it is related to fallouts or breakouts." In other words Ramboll measured the ovality of the 76-mm-diameter boreholes to 0.1 mm resolution. As Ramboll note the confidence decreases if the tool is not centralised in the borehole and this is an issue when holes are inclined.

4.4.1 Types of breakouts and summary statistics

Traditionally, breakouts are considered to result from over-stressing of the borehole wall and hence the origin of these breakouts is assumed to be stress-induced, i.e. the in situ stress magnitudes interacting with the borehole results in stress concentrations on the borehole wall that are a function of the in situ stress magnitude and orientation. Ramboll have identified four types of breakouts (Figure 4-7):

1. Breakouts (BB): These are considered the "classical" breakout that are caused by over-stressing of the borehole wall resulting in yielding of the rock.
2. Micro-fallouts (MF): It is unclear as to the origin of this feature. As shown in Figure 4-7, micro-fallouts start and end abruptly suggesting that they may be associated and/or induced by drilling. Given that the televiewer resolves diameters to 0.1 mm, micro-fallouts may represent a roughened borehole wall.

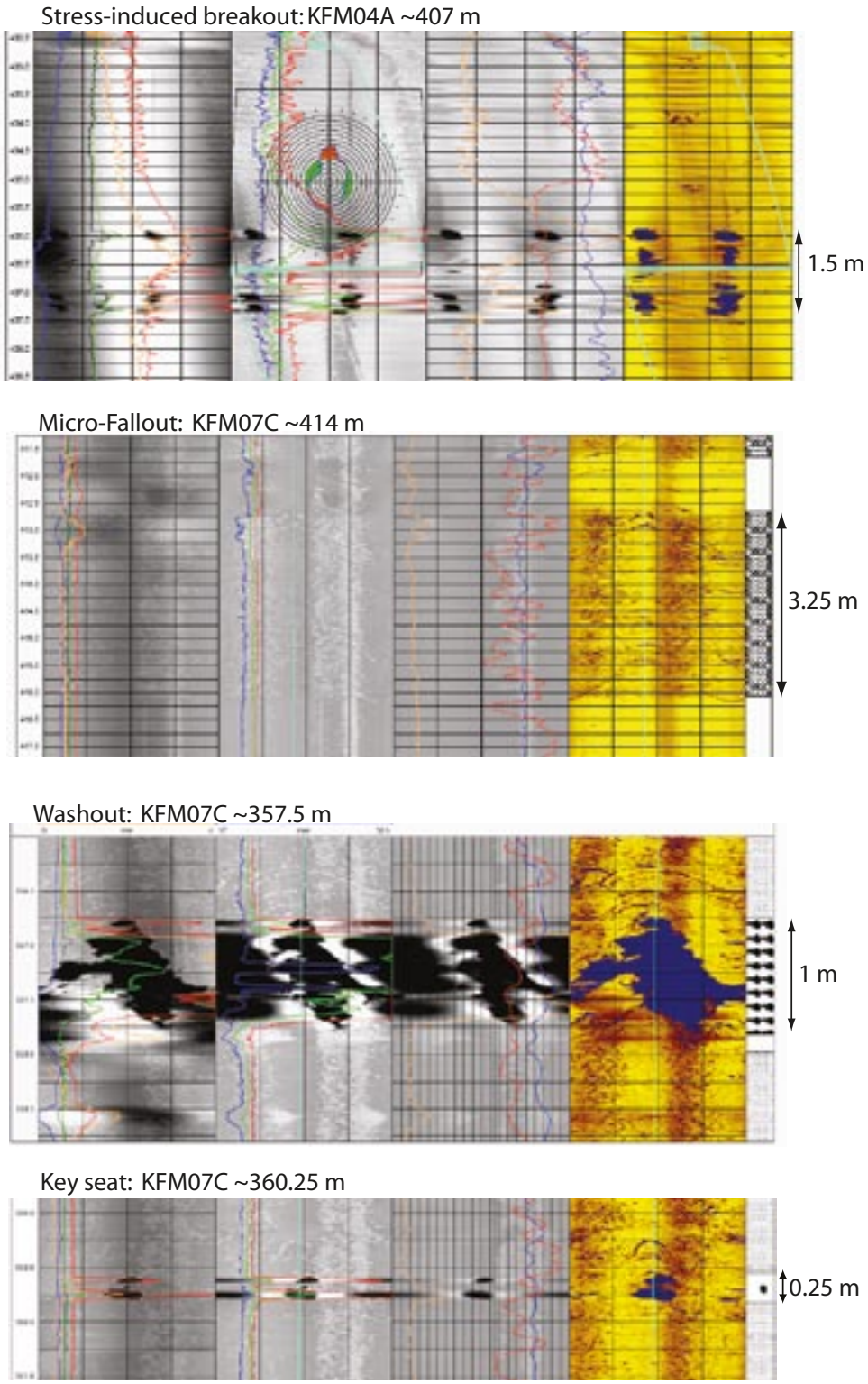

Figure 4-7. *Summary of breakout types identified and characterised by Ramboll.*

3. Washouts (WO): According to Ramboll "washouts are separated from breakouts, as there is fallout in the whole perimeter of the borehole, thus the minimum diameter is enlarged".
4. KeySeat (KS): According to Ramboll "The keyseat is recognised as fallout in only one direction at the relevant depth."

This terminology is defined in /Ringgaard 2007b/ and will be used in this report. A summary of Ramboll's data classified using the breakout types listed above is given in Table 4-2. From Table 4-2, 16% (1,096 m) of the 6,939 m showed some type of breakout and that the majority (786 m, 11%) was classed as Micro-fallout and only 206 m (3%) was classed as a Breakout. Also shown in Table 4-3 is the mean azimuth of the breakouts (all types) associated with each borehole. If the mean breakout azimuth is 64 degrees, and these breakouts are caused or related to in situ stress, the mean trend of the maximum horizontal stress is 64+90=154 degree from True North (see Figure 4-6 for explanation).

Figure 4-8 gives the occurrence of breakouts by borehole as a function of borehole depth. Each breakout type as well as the length encountered in the borehole is shown on the figure. It is more convenient to consider the depth below surface when comparing data from boreholes at various orientations and dip. Figure 4-9 shows the frequency or occurrence of all breakout types as a function of depth below surface. Figure 4-10 shows the the length of all breakouts per 50 m

Table 4-2. Summary of the breakout length by breakout class. Data taken from /Ringgaard 2007b/. The surveyed length in this table is taken as the end of the data in the individual PDF files for each borehole and listed in /Ringgaard 2007b/.

Borehole name	Survey length (m)	Ramboll description (m) Breakouts	Micro-Fallout	Washout	Keyseat	Total (m)
KFM01A	1,000	18.4	278.1	4.8	0.8	302
KFM01B	480	23.5	0.0	0.8	70.7	95
KFM02A	979	55.2	91.7	4.4	2.5	154
KFM03A	989	21.2	81.6	1.0	0.2	104
KFM03B	83	0.2	30.7	1.2	0.0	32
KFM04A	984	30.8	70.6	1.0	2.4	105
KFM05A	990	23.0	47.8	7.8	1.0	80
KFM06A	933	6.7	8.2	1.0	0.8	17
KFM07C	512	26.5	178.0	2.9	0.3	208
(m)	6,939	205.6	786.7	24.9	78.5	1,096
% of surveyed length		3	11.3	0.4	1.1	16%

Table 4-3. Summary of the breakout azimuth by breakout class. Data taken from /Ringgaard 2007b/. The surveyed length in this table is taken as the end of the data in the individual PDF files for each borehole and listed in /Ringgaard 2007b/.

Borehole name	Survey length (m)	Ramboll azimuth (MN) Breakouts	Micro-Fallout	Washout	Keyseat	Mean Azimuth
KFM01A	1,000	69	45	57	50	67
KFM01B	480	53	–	64	50	56
KFM02A	979	78	81	115	102	86
KFM03A	989	47	66	61	32	55
KFM03B	83	77	22	–	–	43
KFM04A	984	59	56	41	98	65
KFM05A	990	78	93	–	v85	84
KFM06A	933	56	35	56	100	61
KFM07C	512	59	56	44	–	59
	Mean	64	57	63	74	64

depth interval. Note that the frequency or distribution of breakouts with depth is not uniformly distributed, nor does it increase with depth as one might suspect, if the breakouts are a functions of stress magnitudes that increase with depth. Also note that in all cases there is an increase in breakout occurrence at a depth of approximately 400 m.

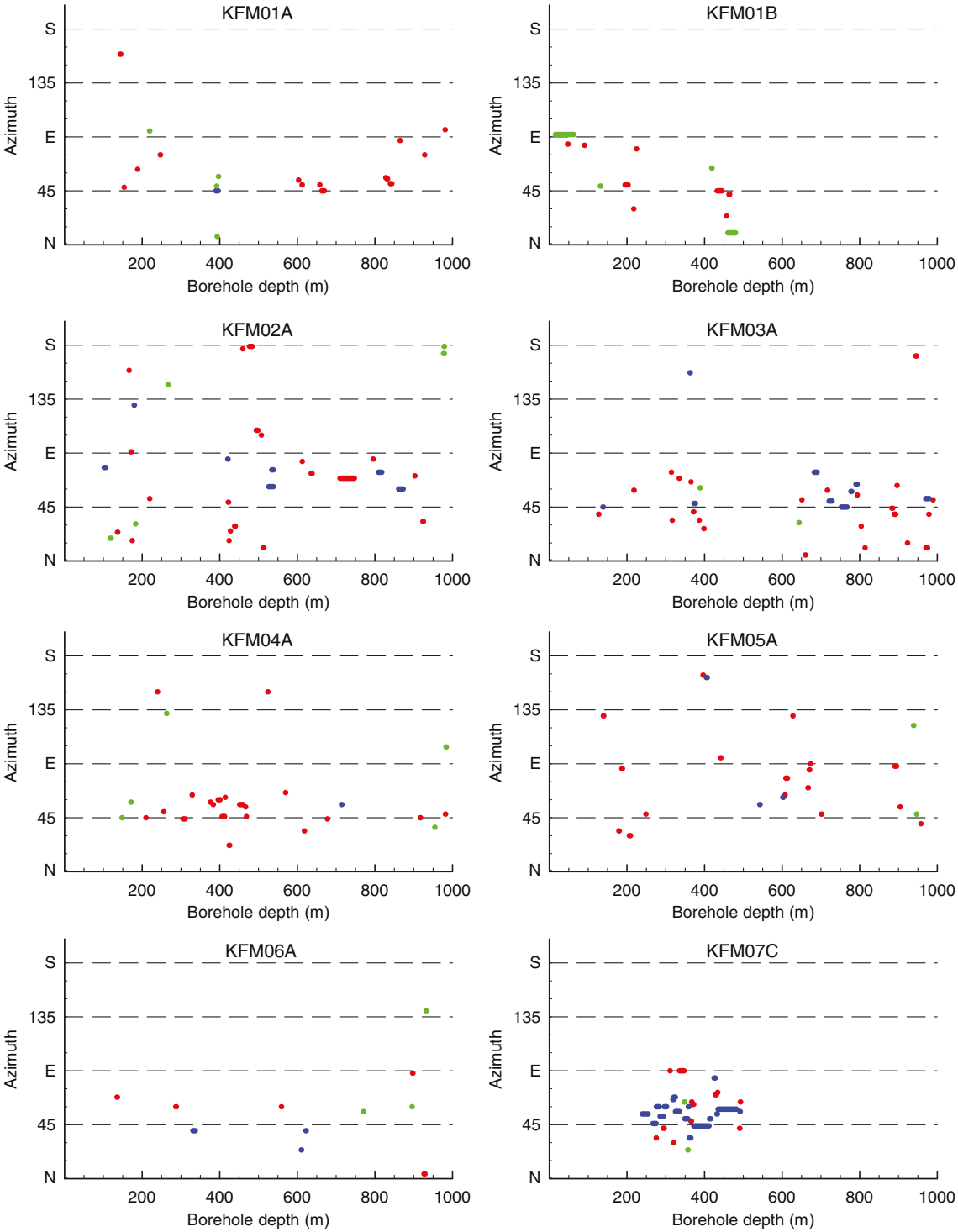

Figure 4-8. *Summary of Ramboll breakouts by borehole showing the azimuth of the breakouts as a function of borehole depth (length). Symbols: Red=BB, Blue=MF,Green=WO, Brown=KS.*

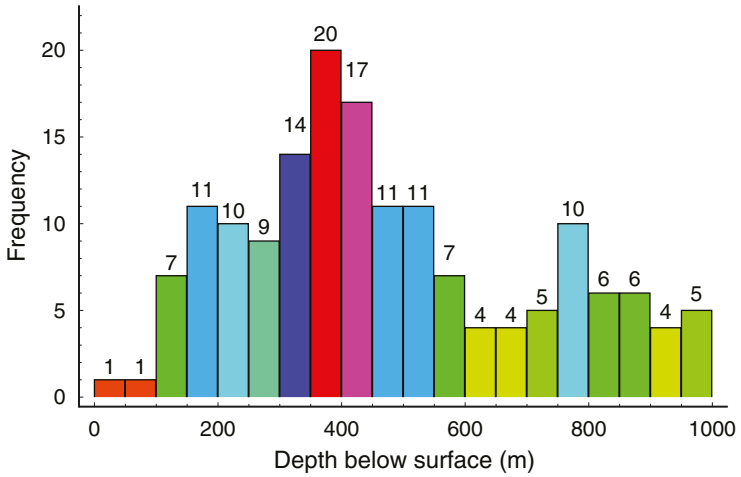

Figure 4-9. *Distribution of breakout frequency with vertical depth below surface. For this plot all Ramboll breakout types are included in a bin size of 50 m. Note that breakouts are observed close to the ground surface and there is a concentration in the frequency of breakouts around 400 m depth. See Table 4-1 for the borehole survey lengths.*

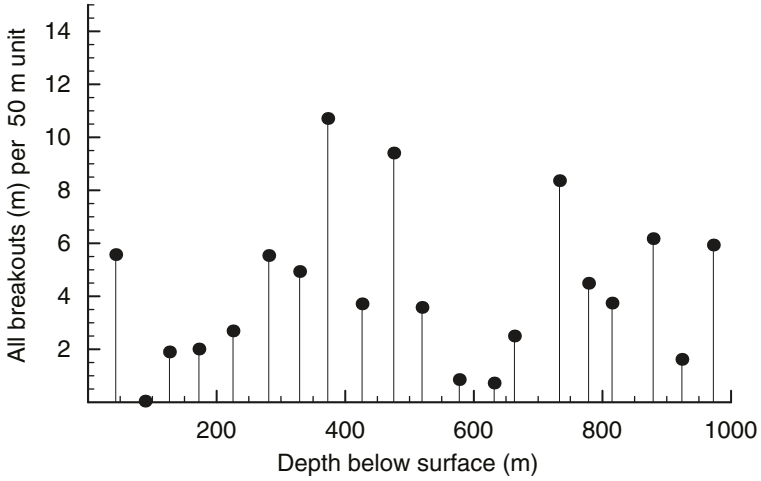

Figure 4-10. *Total length of all breakouts per 50 m segment identified by Ramboll in all boreholes.*

4.4.2 Breakouts and structure

Ramboll noted if the breakouts identified correlated with structure observed in the Televiewer Logs. The structure could be a single fracture or a local group of fractures and Figure 4-11 shows a typical example observed in KFM07C. Figure 4-12 shows the percentage of each breakout type associated with structure. These breakouts have been extracted from the database and plotted along with the Deformation Zones from the Single Hole Interpretation data in /SKB 2006/ (Figure 4-13). In essentially all holes there appears to be a reduction in the scatter of the breakout Azimuth below a depth of 400 m. This is highlighted in KFM02A in Figure 4-13 where there is a clear reduction in Azimuth scatter below the Deformation Zone A2. This reduction in scatter is probably associated with the reduction in open fracture frequency that occurs in fracture domain FFM01.

/Carlsson and Christiansson 2007/ reported, based on the constructions experience from the Forsmark facilities that the rock mass encountered, outside the major deformation zones, was blocky with two major vertical joint/fracture sets: one trending NW-SE and the other trending NE-SW. A sub-horizontal set was also identified. The fractures within the dominant three sets often occur in clusters, forming minor deformation zones. Figure 4-14a shows the azimuth of

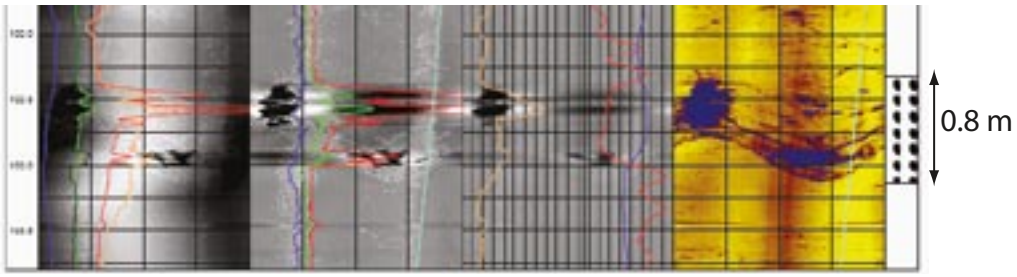

Figure 4-11. *Example of a breakout associated with structure in KFM07C.*

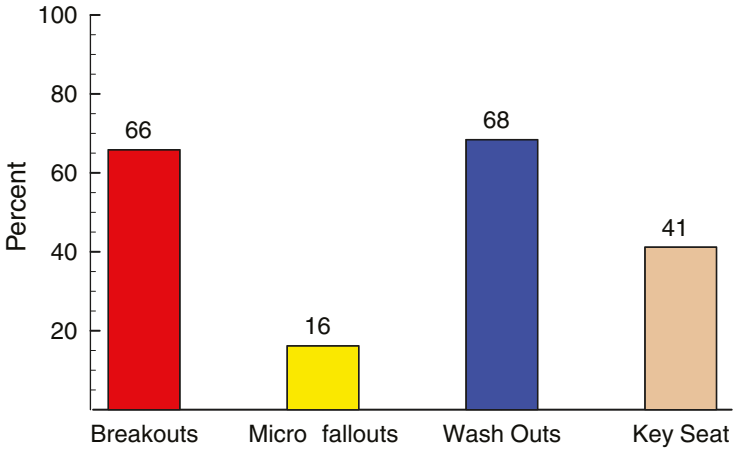

Figure 4-12. *Percentage of each breakout type identified by Ramboll as associated with structure.*

all the breakouts identified by Ramboll as being associated with structure. Figure 4-14b shows the same data but processed using a moving average of 6 data points and the orientation of the a lower hemisphere stereonet of the joints reported by /Carlsson and Christiansson 2007/. Note that the breakout orientations varies between an azimuth of 140 and 200 deg above 500 m depth. Between 500 m and 800 m depth the breakout azimuth shows less variation and suggests an average breakout azimuth of approximately 144 deg.

4.4.3 Breakout time dependency

If the breakouts recorded in the Forsmark boreholes were stress induced it would imply that the edges of the existing breakouts and possibly other sections of the boreholes were marginally stable. Given the progressive nature of stress-induced brittle failure one would expect that the size (width and length) of the breakouts would increase with time. To assess the potential time-dependency of the breakouts at Forsmark borehole KFM08A was surveyed twice with the acoustic televiewer. The first survey of KFM08A was carried out in 2005-04-28, 4 weeks after the drilling was completed. The second survey was carried out in March 2007, i.e. approximately 2 years later. The hole was logged between approximately 100 m and 900 m (borehole depth). The results from both surveys were reported /Ringgaard 2007a/

The first survey was carried out using a logging tool with 2.7 × 8 mm pixel-size, while the 2007 logging was carried out with logging tool that had a pixel size of 2 × 2 mm. The 2005 survey identified 12.1 m of the 901 m surveyed, i.e. 1.3%, with features that resembled breakouts. /Ringgaard 2007a/ noted that with the 2005 low resolution survey the identification of some borehole breakouts, particularly the recognition of Micro-fallouts, was challenging. /Ringgaard 2007a/ manually compared the images to provide the best possible comparison between the two surveys. /Ringgaard 2007a/ concluded that there was no evidence of any change in the original breakouts over the two year time period.

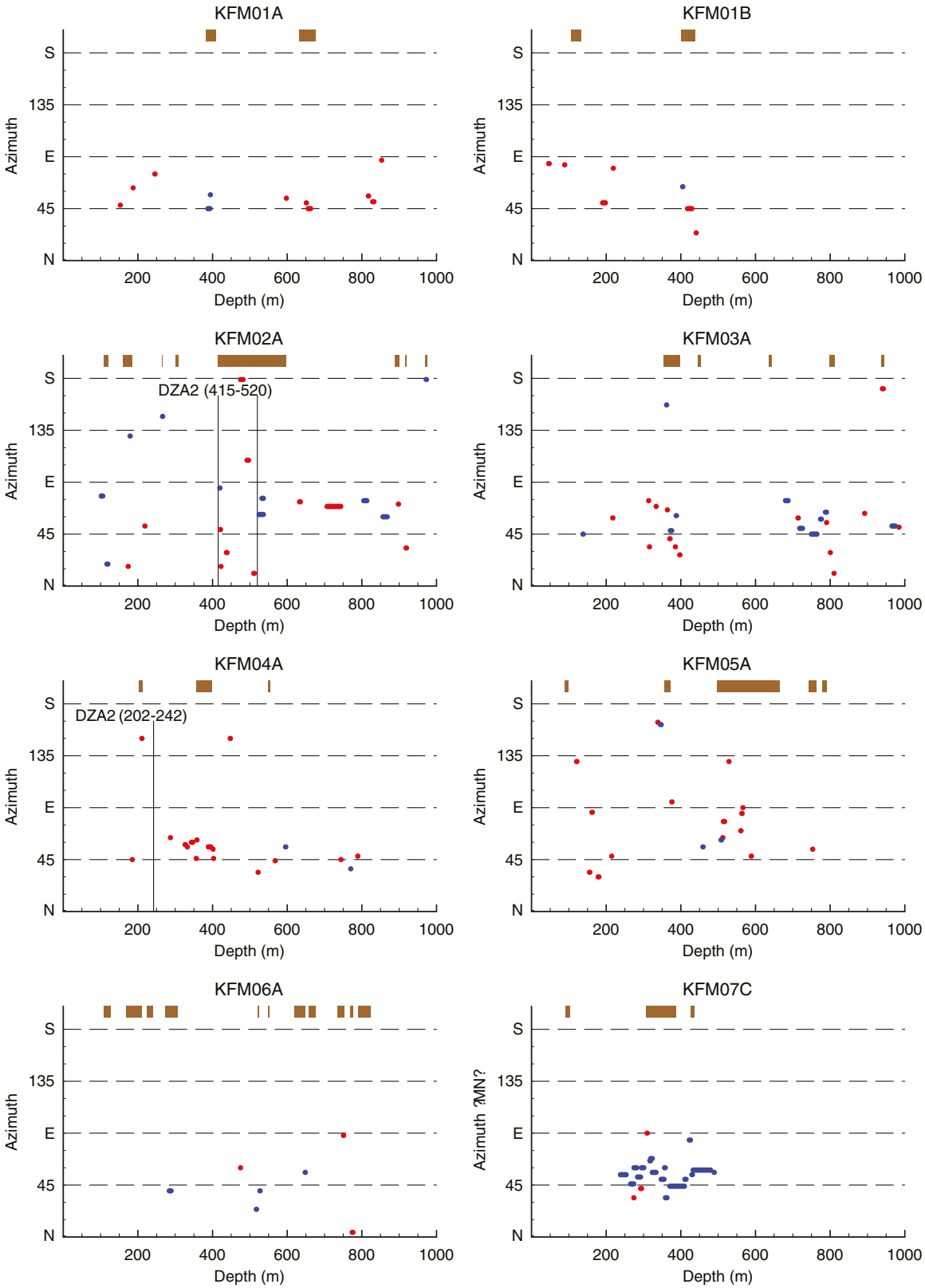

Figure 4-13. *Plots showing the Ramboll Breakouts (Red=BB) and Micro-fallouts (Blue=MF) correlated with the deformation zones identified from Single Hole Interpretation provided in /SKB 2006/. The location of the deformation zones are shown as solid dark brown rectangles near the top of each plot.*

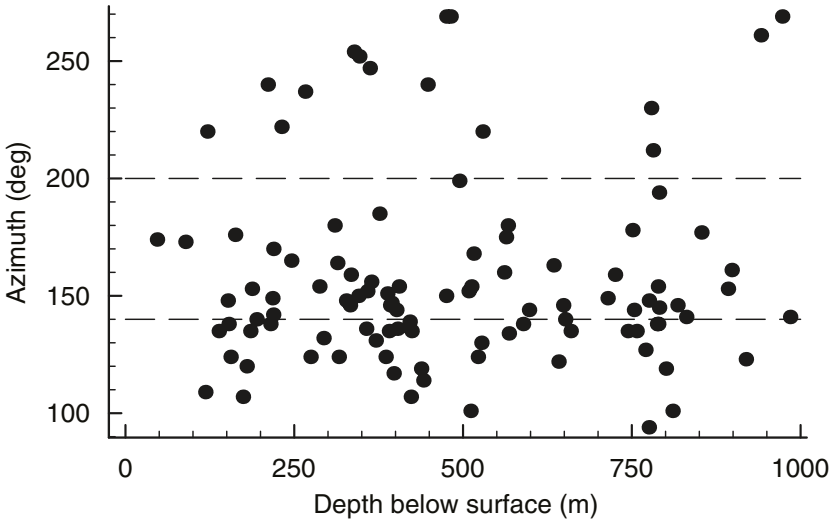

(a) Azimuth of Ramboll breakouts associated with structure.

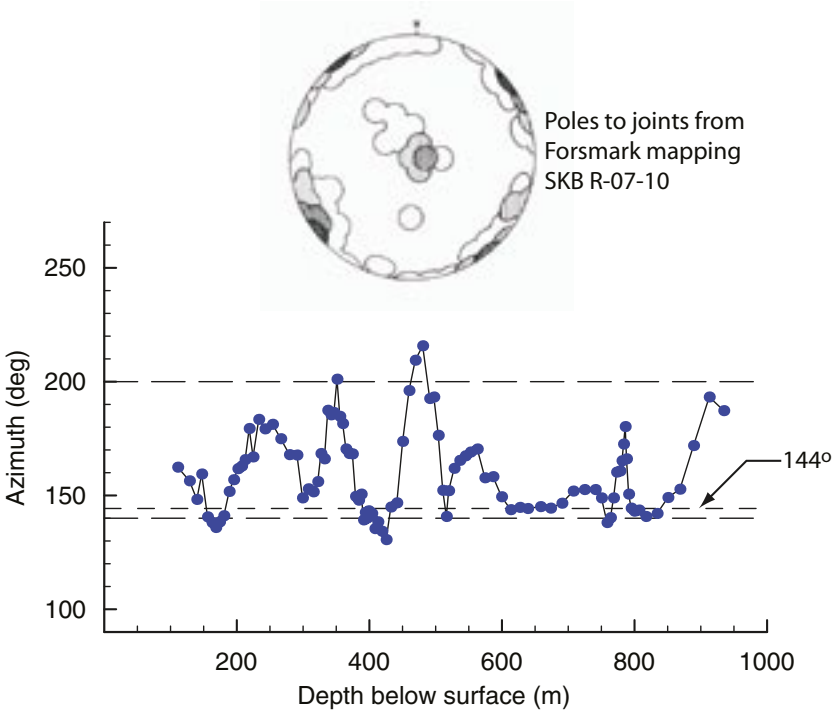

(b) Moving average Azimuth of breakout structure and stereonet of joints encountered during Forsmark construction.

Figure 4-14. *Comparison of the azimuth of Ramboll breakouts associated with structure with the joint mapping at Forsmark, mapping data from /Carlsson and Christiansson 2007/.*

4.4.4 Summary

The analysis of breakout survey conducted by Ramboll can be summarised as follow:

- 1,096 m (16%) of the borehole lengths surveyed (6,939 m) contained some form of breakout (breakout, micro-fallout, washout, key-seat). Of this breakout length 786.7 m (72%) is associated with micro-fallouts. The cause of this feature is unclear. Only 205.6 m (3%) of the survey length has features which can be classed as "classical" breakouts and as shown in Figure 4-12 66% of those are associated with structure. The "washout" and "key-seat" features were only 0.4% and 1.1% of the survey length.

- A distribution of the Azimuth of the all breakouts, regardless of type is given in Figure 4-15. The results in Figure 4-15 are divided above and below a depth of 450 m. Below 450 m depth the frequency of open fractures is significantly reduced. The average Azimuth of all the breakouts above 450 m depth would imply a maximum horizontal stress oriented at Azimuth 157 deg, assuming that the breakouts are formed by over-stressing of the borehole wall. Below 450 m depth the maximum horizontal stress, inferred from all the breakout results, has an Azimuth of 153 deg.
- The distribution of the Azimuths associated with only the "classical" breakouts is shown in Figure 4-16. The Azimuth of the maximum stress required to cause these breakouts would be approximately 135–315 deg.
- Breakouts are encountered at very shallow depths (<200 m) suggesting that the either the stress magnitudes are significantly elevated in the Forsmark region, or the breakouts reported are not the "classical" breakouts induced by over-stressing. Experience has shown that if stress-induced breakouts are observed in boreholes, stress-induced problems are also observed in underground excavations at similar depths. At Forsmark, stress-related problems were not reported for the underground excavations to a depth of 140 m.
- The distribution of breakouts with depth shows a concentration of breakouts at a depth of approximately 400 m.
- There is no noticeable increase in the frequency or extent of breakouts with depth. This is not consistent with the author's experience from other projects. Once the depth is reached where stress-induced breakouts occur going deeper in the same rock type produces more extensive breakouts. This has not been observed at Forsmark.

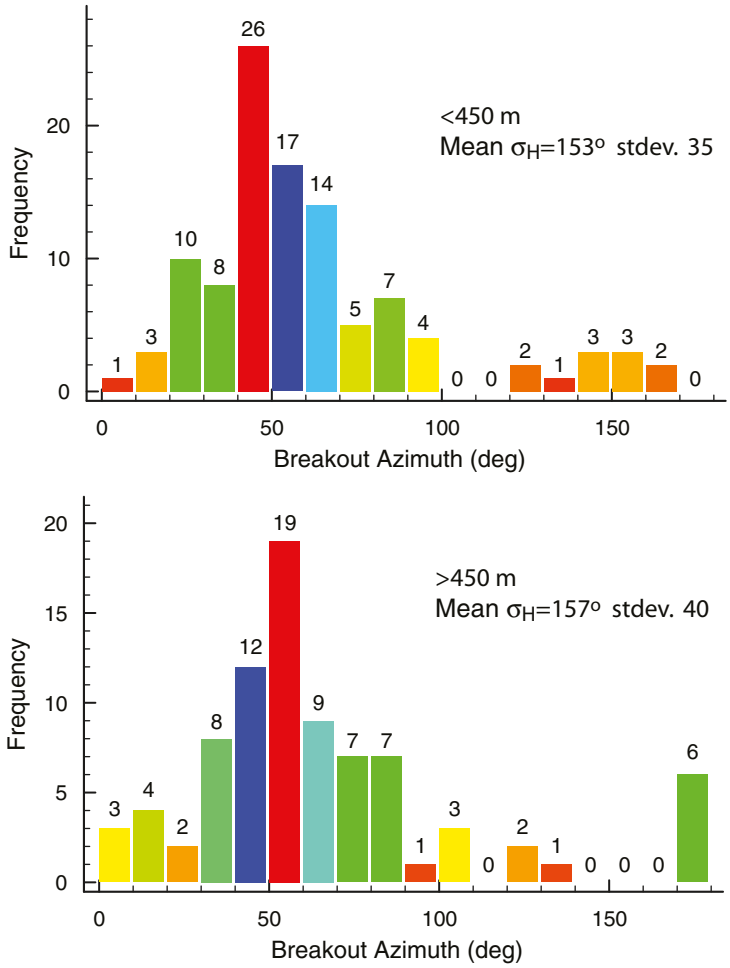

Figure 4-15. *Summary of the Ramboll breakout Azimuths identified above 450 m and below 450 m.*

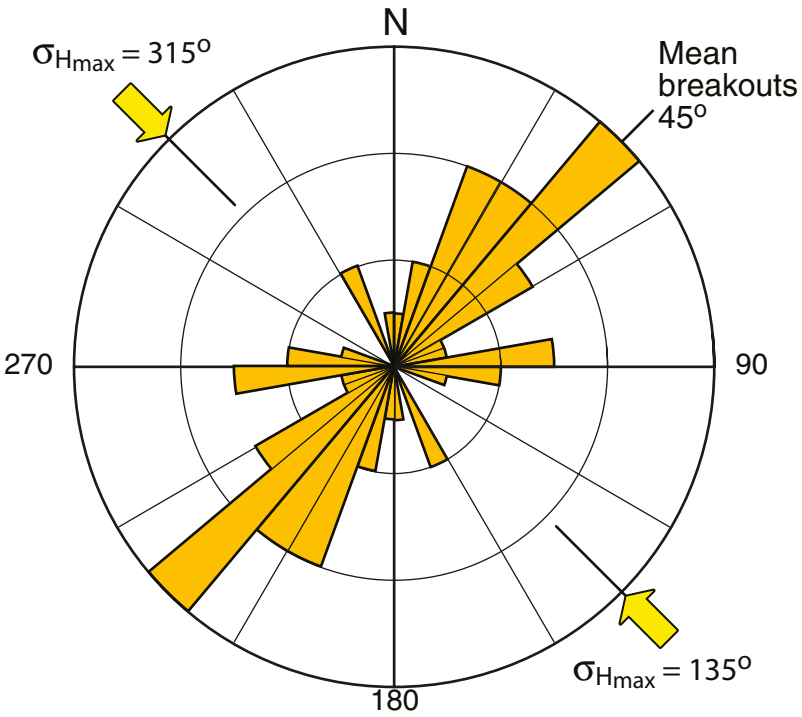

(a) Rose diagram showing the orientation of the "classical" breakouts not associated with structure.

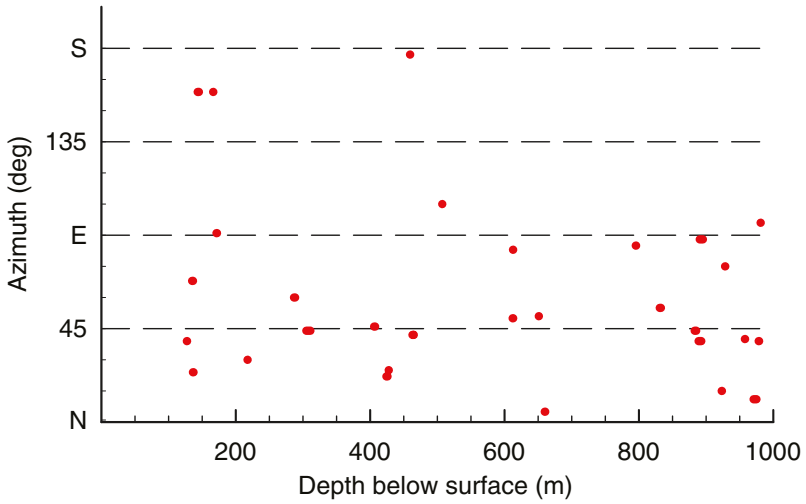

(b) Distribution with depth.

Figure 4-16. *Azimuth of Ramboll "classical" breakouts with depth at Forsmark.*

- Regardless of the origin of the breakouts identified by Ramboll, there is a relatively consistent orientation associated with the breakouts. This orientation is likely more influenced by the interaction of the geological structure with the in situ stress, i.e. the stress concentrations produce minor slip on the geological structure and/or minor fallouts on the structure.
- A comparison of a breakout survey in 2005 with a repeat survey in 2007 showed that there was no change in the distribution or size of the breakouts, suggesting that the formation of the breakouts was not time-dependent.

5 Stress measurement campaigns and limitations

In situ stress measurements were carried out using the Borre probe and hydraulic fracturing, including hydraulic testing of pre-existing fractures (HTPF). The stress campaigns were carried out in a number of boreholes in the Target Area in an attempt to establish stress variability across the site and the stress gradients with depth (see Table 1-1). The detailed results from these campaigns, including an assessment of the data quality associated with each test method are given in the SKB data reports listed in Table 1-1. /Sjöberg et al. 2005/ reviewed and summarised the stress data from the initial measurement campaigns as well as the the historic stress data from the Forsmark area. A summary of the individual measurements from the overcore and hydraulic fracturing campaigns is provided in Appendix A and Appendix B, respectively.

As noted by /Doe et al. 2006/ not all stress measurement methods carried out in deep boreholes will work in all geological environments. They note that in over-stressed rock, e.g. rock masses where the horizontal stresses significantly exceed the weight of the overburden (a thrust regime) none of the stress measurement techniques work particularly well. Because the hydraulically fracturing method produces a fracture normal to the minimum stress, hydraulic fracturing in such a stress regime tends to produce horizontal fractures and hence measures the weight of the overburden /Evans and Engelder 1989/. The over-coring method relies on elastic theory and in such a stress regime micro-cracking may occur inducing a non-linear stress-strain response which makes it difficult to interpret the results /Martin and Christiansson 1991a/.

While it may be difficult to measure the in situ stress state directly using traditional overcoring and and hydraulic fracturing methods in some in situ stress regimes (geological environments), the results from such measurement campaigns, nonetheless, contribute significantly to understanding the in situ stress state at a site, as illustrated in Figure 1-1. In the following sections the limitations of the overcoring and hydraulic fracturing campaigns experienced at Forsmark are discussed in detail. The results from the overcoring and hydraulic fracturing campaigns are used to establish the in situ stress trends discussed in Section 6.

5.1 Hydraulic fracturing

Hydraulic fracturing and the HTPF method provides the stress normal to the induced fracture and existing fracture, respectively. In the small-diameter boreholes used in the SKB investigations only the orientation of the fracture at the injection-borehole wall can be determined. It is assumed that the fracture orientation measured where it intersects the injection borehole is the same as the fracture orientation at the end of the test. This has always been a major shortcoming of the current technology for small diameter boreholes.

Two hydraulic fracturing campaigns were conducted. The first campaign consisted of traditional hydraulic fracturing in the subvertical boreholes KFM01A, KFM01B, KFM02A, KFM04A, and the results are reported /Rummel and Weber 2004/. Opening of pre-existing fractures was also attempted. The first campaign used hydraulic fracturing

methodology where the volume of water is not a limiting factor in the injection procedure. Figure 5-1a shows the stress results obtained from the first campaign normalised to the calculated vertical stress (minimum stress in a geological thrust regime). Note that many of the test results are approximately equal to the calculated vertical stress and it was assumed that the subvertical fractures measured in the injection boreholes had rotated to a near horizontal orientation during propagation.

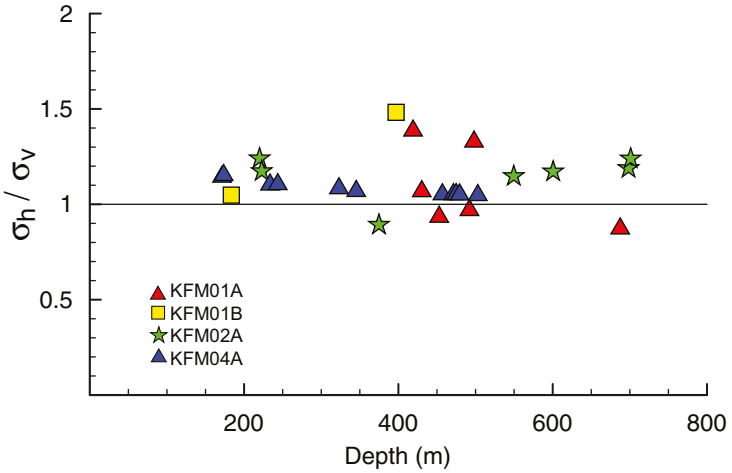

(a) Summary of the minimum stress magnitudes from the subvertical boreholes in the first hydraulic fracturing campaign.

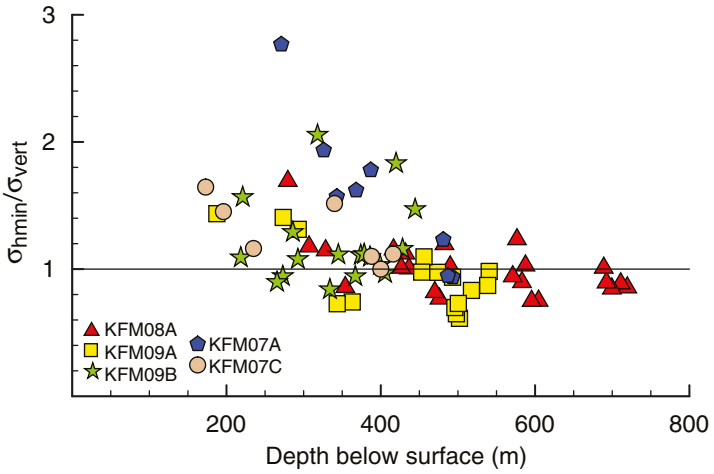

(b) Summary of the minimum stress magnitudes from the second hydraulic fracturing campaign. Includes both hydraulic fracturing and HTPF methods.

Figure 5-1. *Summary of the minimum stress magnitudes from the hydraulic fracturing campaigns normalised to the calculated vertical stress. Includes both hydraulic fracturing and HTPF methods. A minimum horizontal stress magnitude less than the weight of the overburden implies a strike-slip fault regime.*

After reviewing the results from the first hydraulic fracturing campaign the testing procedure was revised in an attempt to control the direction of fracture propagation, i.e. keep the fracture vertical in a vertical borehole, regardless of orientation of the minimum stress. This was attempted by restricting the volume of water injected to 2 to 5 litres during the first injection phase. In addition significant effort was made to measure the stress using existing open fractures as described in the HTPF method /Haimson and Cornet 2003/. Electrical images of these existing fractures and the induced hydraulic fractures were used to determine the orientation and dip of the fractures. This imaging technology is a major improvement over the traditional impression packer. Figure 5-1b shows the results from the second hydraulic fracturing campaign carried out in boreholes KFM07A, KFM07C, KFM08A, KFM09A and KFM09B.

The data in Figure 5-1b suggests a large number of tests gave the measured stress to be significantly less than the calculated vertical stress. This is not as evident in Figure 5-1a and may be related to the differences in test procedure. Regardless of the reasons, a measured stress less than the vertical stress suggests a possible strike-slip geological stress-regime if the measured stress represents approximately the minimum horizontal stress which is not consistent with the current geological thrust regime for the Forsmark region. The HTPF method relies

on the opening of existing fractures. According to ? most of the open hydraulically connected fractures in fracture domain FFM01 are either gently dipping or subhorizontal and at depth these gently dipping open fractures are connected via widely spaced subvertical fractures. Hence, hydraulically induced or existing fractures that appear vertical in the borehole may be connected to these gently dipping or subhorizontal fractures. It is possible that the HTPF results are influenced by these gently dipping fractures since these fractures play a significant role in controlling the hydrogeology at the Forsmark site ?.

5.2 Overcoring

Overcoring was first carried out in the Forsmark area in the late 1970's and early 1980's in conjunction with the construction of the Forsmark nuclear power plant and the SFR facilities. The boreholes (DBT1 and DBT3) used for that overcoring campaign are located to the west of the current Target Area and stress measurements were obtained to depths of approximately 500 m /Carlsson and Christiansson 1986/. At that time the strain measurements could only be made before and after the overcoring, i.e, there was no downhole data logger, and hence quality control was limited. The current Borre Probe is very similar to the original triaxial strain cell used in these early investigations but data is now collected using a downhole data logger /Sjöberg and Klasson 2003/. While the technology and quality control procedures have improved significantly the overcore results still depend on the original assumption that the rock during the overcoring process behaves as a continuous, homogeneous, isotropic and linear elastic material.

The overcoring in the Target Area was carried out in KFM01B and KFM07C (see Table 1-1). Figure 5-2 shows the distribution of successful overcore tests in the Target Area, including DBT1 and DBT3. The majority of the tests were successful between 150 and 250 m depth, and very few tests were successful below 250 m depth. Despite the improvement in technology considerable difficulties occurred that reduced the number of successful tests. The three most common difficulties reported were:

1. microcracking and ring-core disking during the overcoring process,
2. anomalous transient strains that make interpretation of the results difficult, and
3. unstable strains during biaxial testing.

Previous work by /Lindfors et al. 2005/ examined microcracks in ring-disks in KFM01B using thin-sections. /Lindfors et al. 2005/ concluded that long circumferential cracks were present in the ring-disks samples and that these cracks intersected the ring-disks. To assess if this was a wide-spread effect or only a associated with ring-disking, an extensive investigation into the

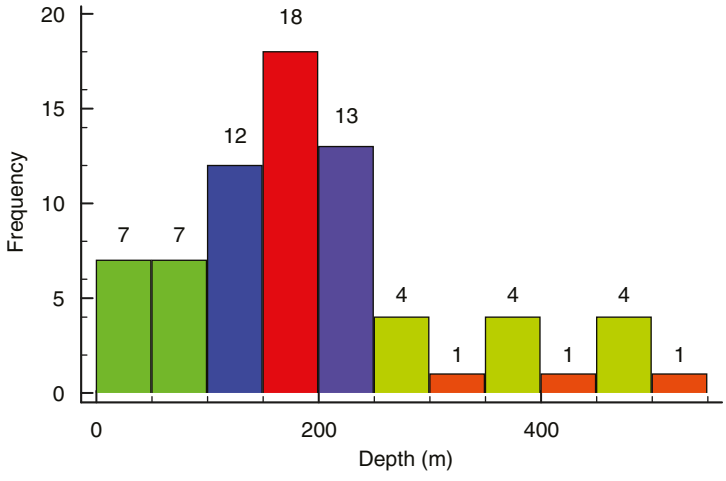

Figure 5-2. *Distribution of successful overcore tests with depth below ground surface. See Appendix A for location of individual tests.*

potential effect of microcracking on the overcore results was carried out using overcore tests in borehole KFM07C. Figure 5-3 shows the location of the overcore attempts with depth and rated using the 'a', 'b' and 'c' ratings with 'a' being the tests with the highest quality. Notice that the majority of the tests are rated 'b'(14) and 'c'(22), while only three tests were rated 'a'. There were 22 successful biaxial tests and 12 cases of ring-disking during the overcore attempts. The investigations that were carried out as part of this study and their findings are discussed in the following section.

5.2.1 Microcracking and ring-core disking

The effects of microcracking on overcoring results were documented in an extensive study by /Martin and Christiansson 1991b/. They concluded that microcracking in the overcored hollow-cylinder reduced the Young's modulus and Poisson's ratio obtained from biaxial testing. They also noted that if microcracking had occurred in overcored hollow-cylinders the stress-strain response from the biaxial test was nonlinear. Figure 5-4 shows a typical biaxial test result from the 420-m Level of AECL's Underground Research Laboratory (URL) and the nonlinear strains are readily observed. Figure 5-4 also shows that microcracking simply softens the material but that the strains are fully recovered, i.e. the stress-strain response is approximately nonlinear elastic. /Martin and Christiansson 1991b/ showed that if the properties of the hollow cylinder can be properly described it is possible to correct for this nonlinear behaviour and correct for the effect of microcracking. /Martin and Christiansson 1991b/ conducted their research on the 240-m Level of AECL's Underground Research Laboratory where the effect of microcracking was relatively minor. /Martin 1990/ showed that when the amount of microcracking in the biaxial tests, such as that shown in Figure 5-4, was too severe and the correction used by /Martin and Christiansson 1991b/ was not applicable.

The effect of microcracking on the deformation properties determined from biaxial testing of the hollow-cored cylinders at various depths at AECL's URL can be readily observed in Figure 5-5. The hollow-cored cylinders were obtained from overcoring of AECL's Modified Triaxial Strain Cell mainly in near horizontal boreholes drilled from the main access shaft which went from the ground surface to the 420-m level. Also shown in Figure 5-5 are the biaxial results from hollow cylinders obtained from overcoring the Swedish State Power Board (SSPB) triaxial strain cell. The SSPB cell which is nearly identical to the Borre Probe was drilled in a subvertical borehole and in the approximate location of the shaft (the borehole was drilled prior to shaft construction). Figure 5-5a shows that both the CSIR and SSPB biaxial tests gave similar Young's modulus values and that there was a significant reduction in the Young's modulus with depth. In other words the microcracking process was affecting the deformation properties of hollow-core cylinders. Also note in Figure 5-5b that the Poisson's ratio also decreased with depth.

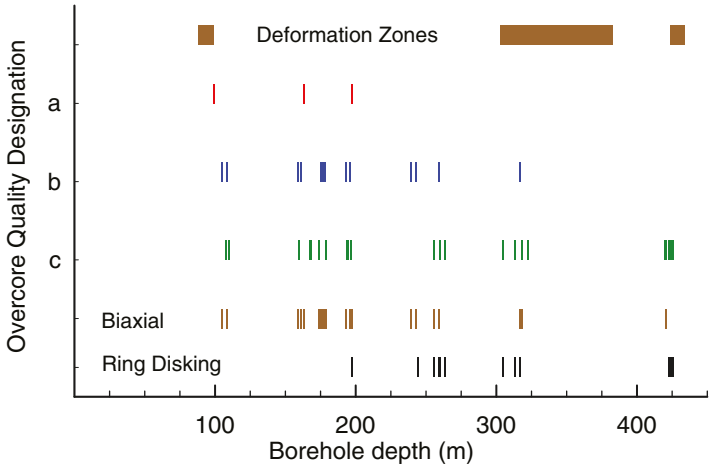

Figure 5-3. *Distribution of overcore attempts using the QA rating 'a', 'b' and 'c', location of successful biaxial tests and the location of ring-disking. The location of the major deformation zone from the single hole interpretation test is also shown.*

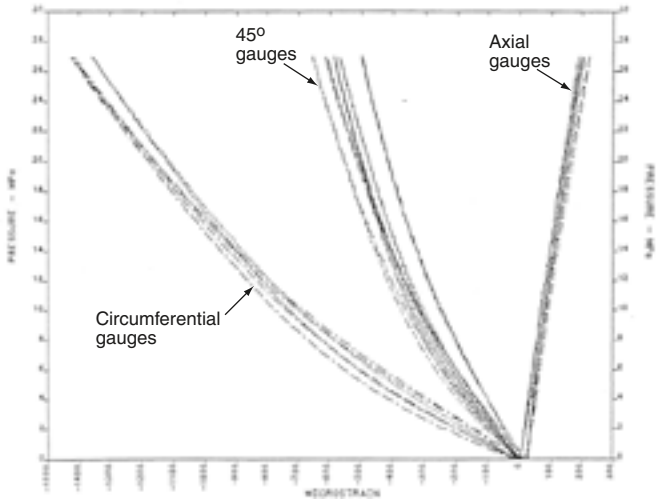

Figure 5-4. *Example of the effect of microcracking on the biaxial tests for a CSIR overcore at the 420-m level of AECL's URL.*

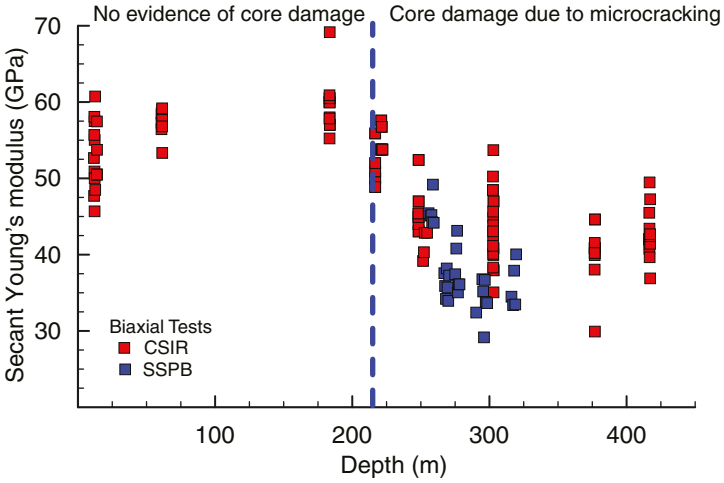

(a) Young's modulus from biaxial tests.

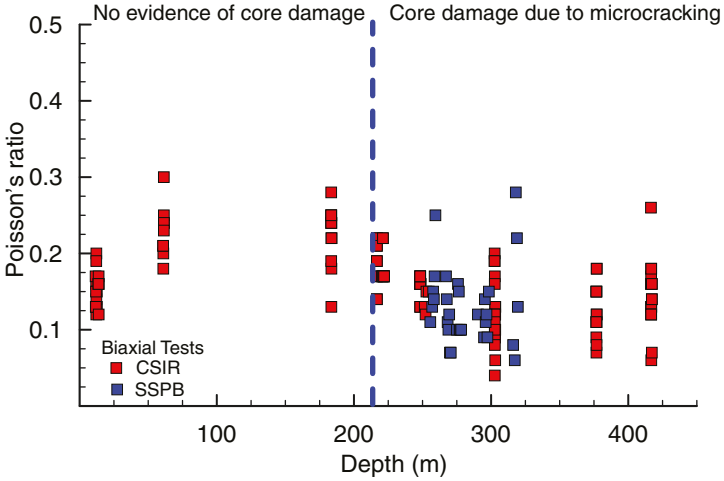

(b) Poisson's ratio from biaxial tests

Figure 5-5. *Summary of the Young's modulus and Poisson's ratio determined from Biaxial testing of hollow cylinders produced from overcoring of AECL's Modified CSIR Triaxial strain cell and the Swedish State Power Board (SSPB) triaxial strain cell.*

/Martin and Stimpson 1994/ carried out an extensive study of the effect of microcracking on the laboratory properties of solid core cylinders with depth at AECL's URL. Their findings supported the previous work using the hollow-cored cylinders and clearly showed that the greater the volume of microcracks the greater the nonlinear stress-strain response and the lower the laboratory deformation and strength properties of the solid cores. They showed that this microcracking was related to the in situ stress magnitudes and increased with depth as the stress magnitudes increased. At AECL's URL this increase was most noticeable between 200-m and 420-m depth. They also showed by comparing P-wave velocities and permeability measurements of the cores with in situ measurements that the microcracking only occurred in the cored samples and was not a characteristic of the in situ rock mass.

An indication that the biaxial results from the overcored hollow-cylinders from KFM07C do not always respond in a linear elastic manner is shown in Figure 5-6. As shown in Figure 5-6b the biaxial tests can show considerable hysteresis in the stress-strain response, and in many cases the biaxial results cannot be used. In KFM07C /Lindfors et al. 2007/ reported that 9 of the 22 biaxial test showed unstable strain readings. The stress-strain response when the strain reading are unstable typically display the hysteresis shown in Figure 5-6. Because this phenomena has been observed in all overcored boreholes drilled as part of the site investigations the glue bon-

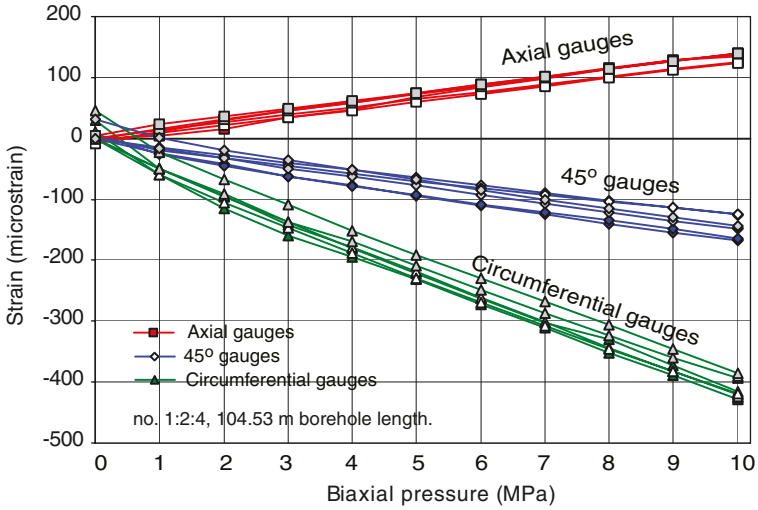

(a) Good quality biaxial test from KFM07C at a borehole depth of 104.53 m.

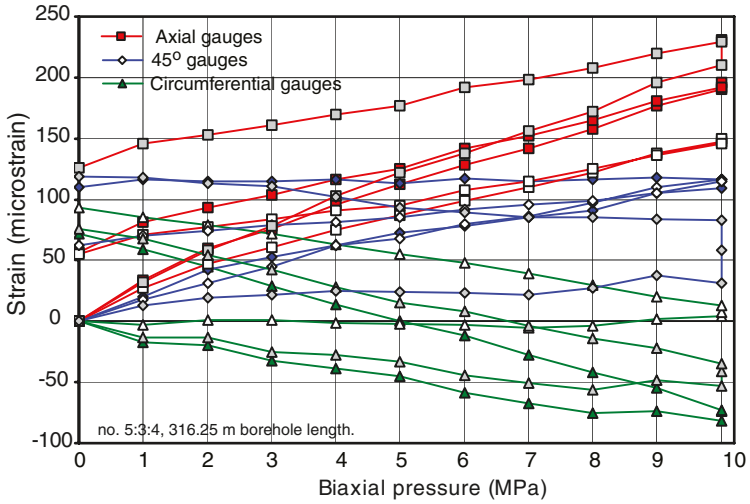

(b) Poor quality biaxial test from KFM07C at a borehole depth of 316.25 m

Figure 5-6. *Example of good and poor quality biaxial tests from KFM07C. Nearly all tests showed some evidence of hysteresis in the stress-strain response.*

ding the strain gauges has been carefully tested and inspected on individual tests. Even in cases where the Borre Probe triaxial strain cell appeared well bonded to the rock this hysteresis had been observed. In several cases the strain gauges were replaced and the biaxial tests repeated with acceptable results, suggesting the glue characteristics after overcoring may be related to the hysteresis phenomena observed. The investigation into this hysteresis phenomena observed in the biaxial test results, prior to KFM07C, had concluded that microcracking was the likely cause of the observed hysteresis phenomena. However, if microcracking is the cause for the hysteresis in Figure 5-6b it is difficult to explain why hysteresis was not observed in Figure 5-4 where microcracking was extensive.

Additional testing was carried out as part of the investigations into the effect of microcracking on the overcore results from KFM07C, and particularly the biaxial response /Lindfors et al. 2007/. Samples of the pilot core were selected and the secant Young's modulus and Poisson's ratio were determined on the pilot core samples. These samples had a diameter (d) of about 22 mm, and so a height (h) of 55 mm was selected, such that $h/d \approx 2.5$. Three samples were taken from each pilot core to represent each corresponding biaxial test. One sample was taken 30 mm above the exact position of the strain gauges for the corresponding test. A second sample was taken at the exact location of the strain gauge, and the third sample was taken 30 mm below the position of the strain gauges on the overcore sample. Figure 5-7 compares the secant Young's modulus and Poisson's ratio obtained from the hollow-cylinder biaxial tests and from

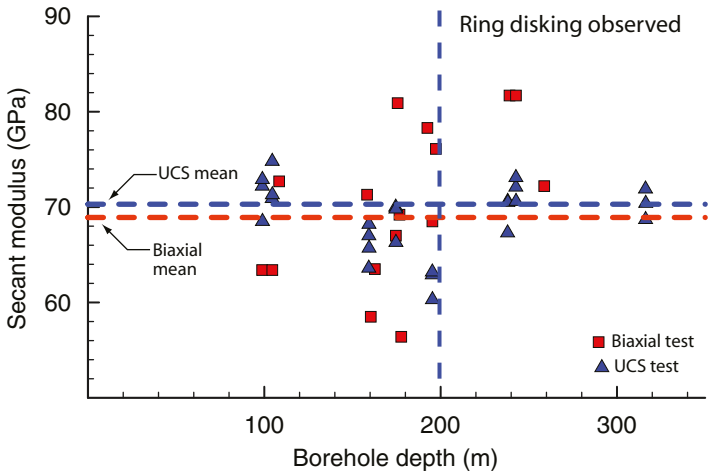

(a) Young's modulus

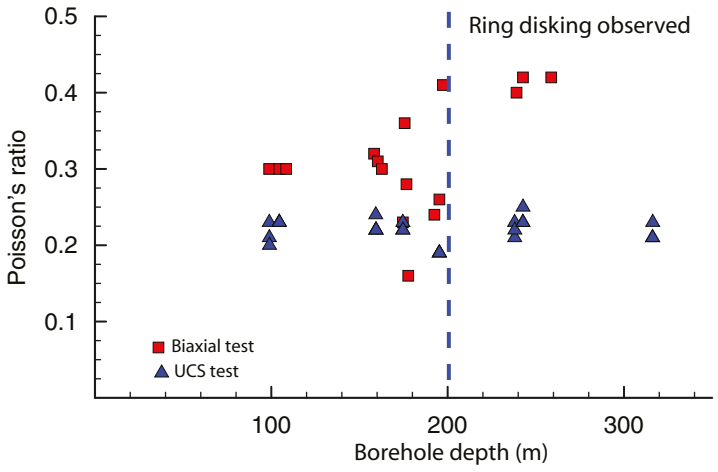

(b) Poisson's ratio

Figure 5-7. *Example of good and poor quality biaxial tests from KFM07C. Nearly all tests showed some evidence of hysteresis in the stress-strain response.*

the corresponding uniaxial tests. Despite the relatively small-scale, the uniaxial results gave consistent deformation properties with depth and the mean for the Young's modulus is very similar to the Young's modulus obtained from the biaxial test. Based on these Young's modulus results there does not appear to be a significant microcrack-effect in these cores despite the occurrence of ring-disking below 200 m depth. /Lindfors et al. 2007/ also determined the tangent Young's modulus for the uniaxial tests. A comparison of the tangent and secant Young's modulus can be an indicator of microcracking in the core samples. The mean ratio of secant to tangent Young's modulus for the uniaxial samples was 0.95 and showed no decrease with depth, again suggesting that the effect of microcracking, if any, must be very minor.

Another observation that suggests the biaxial response in KFM07C is not caused by microcracking can be seen in the Poisson's ratio shown in Figure 5-7b. When microcracks that have large aspect ratios, (length»>thickness) are introduced into a hollow cylinder and the hollow cylinder is loaded using a biaxial pressure the calculated Poisson's ratio can be less than the intact rock. This is not intuitive as microcracking tends to make the samples more compliant in the axial direction, i.e, less stiff. /Rothenburg et al. 1991/ showed that the Poisson's ratio in cracked material is a function of the ratio of the tangential stiffness (K_t) to normal stiffness (K_n) of the cracks. If $K_t \gg K_n$, such as stress-induced microcracks, Poisson's ratio can be much less than the Poisson's ratio for intact rock and in extreme cases Poisson's ratio can be negative. /Corkum and Martin 2007/ showed that extremely low and negative Poisson's ratio occurred in mudstones during the early stages of loading because of the structure of the clay platelets. Hence, when a biaxial test is carried out the Poisson's ratio determined from a sample that is microcracked tends to be less than the Poisson's ratio obtained from a sample that has fewer or no microcracks. This can be readily observed in Figure 5-5b. Yet the Poisson's ratio obtained from the biaxial tests from KFM07C show a general increase with depth from values of 0.3 at approximately 100 m depth to values of 0.42 at approximately 250 m depth (see Figure 5-7b). The Poisson ratios for the uniaxial tests show consistent values with depth and a mean value of 0.22. A Poisson's ratio of 0.4 in stiff rock such as granite is difficult to explain.

/Lindfors et al. 2007/ conducted P-wave velocity measurements on the overcore samples in the vicinity of the strain gauges. /Martin and Stimpson 1994/ had shown that P-wave velocities were sensitive to microcrack damage and that P-wave velocities in damaged samples could decrease up to approximately 50% depending on the amount of microcrack damage. Samples for P-wave measurements were collected between about 100 and 420 m borehole depth. The testing strategy was to measure the P-wave velocity from one to two tests at each measurement depth where overcoring and biaxial testing had been conducted. In total, P-wave velocity was measured on 39 samples from 12 test depths in borehole KFM07C. /Lindfors et al. 2007/ showed that the P-wave velocity decreased from about 5,600 m/s at approximately 100 m depth to approximately 5,000 m/s at about 200 m depth.

Below this depth there was a gradual increase in P-wave velocity to an average value 5,800 m/s at about 420 m depth. The trend in the P-wave velocity data is very similar to the trend in the biaxial Young's Modulus shown in Figure 5-7a, and hence whether the changes in P-wave reflect changes in microcrack density or minor lithological variations is unknown.

When stress-induced microcracking occurs during overcoring there is an expansion of the overcore sample in the axial direction /Martin and Christiansson 1991b/. The consequences of this nonlinear expansion of the core is that when the stress tensor is determined, the orientation of the maximum principal stress tends to align with the direction of overcoring. /Martin and Christiansson 1991b/ showed that this rotation could be corrected using an anisotropic modulus for the stress-tensor calculations when the amount of microcracking was relatively minor. However, once the microcracking became significant, periodically causing ring disking, the true orientation of the maximum principal stress could not be determined. If the orientation of the stress tensor is rotated by nonelastic microcracking during overcoring, the magnitude of the calculated vertical stress can be overestimated because the orientation of the minor principal stress is no longer vertical but plunging (assuming a stress regime for thrust faulting). The more significant the microcracking the greater the vertical stress will be overestimated. As will be shown later the mean stress tensors determined from the overcoring results give the minimum

principal stress as plunging essentially vertically regardless of depth, also suggesting that micro-cracking is likely not a significant issue for the overcoring program conducted at Forsmark. Nonetheless, the low success rate for high quality overcore tests and the hysteresis in the biaxial results suggests that the overcoring process is affected by a phenomena that occurs during the overcoring process at Forsmark. This phenomena is suggested in the next section.

5.2.2 Thermal effects

Overcoring using the Borre Probe produces a thin-wall overcore cylinder, i.e. the thickness of the overcore cylinder is 12.8 mm. In the overcoring process it is important that the temperature at the strain gauges be kept relatively constant /Martin and Christiansson 1991a/. As explained by /Thompson et al. 1986/ this was the main reason why a separate overcore cooling water supply system was installed for all the overcore stress measurements carried out as part of AECL's stress measurement program. It should be noted that monitoring of the strain temperatures while drilling is only practical when the stress measurements are carried out from underground openings where the data-logger can be connected to the drill-rig. When a remote data-logger is used, only a history of the temperatures can be recorded. The Borre Probe uses a remote data-logger, and the sensor that monitors the temperature is located in the data-logger not at the location of the strain cells. As a result a 3 degree increase in temperature of the data logger, which was commonly recorded at Forsmark, may imply a higher increase in the temperature at the location of the strain gauges. If the temperatures at the location of the strain gauge increased, it would locally increase the stresses during the overcoring process. The evidence for a possible thermal effect can be seen in the rapid decrease in strains once the cell was overcored, referred to as the 'ski-hill effect' (see Figure 5-8).

Transient strain analyses were introduced by /Hakala et al. 2003/ as a quality control check for overcoring stress measurement data. A computer program is used to simulate the transient strains and stresses during the overcoring process. The measured strains can be compared to the calculated strains to check whether the measured transient behaviour is consistent with the interpreted in situ state of stress. Transient strain analyses were conducted as part of the detailed investigations into the factors that could be affecting the overcore results in KFM07C discussed in the previous section. Transient analysis were carried out for all overcore tests with

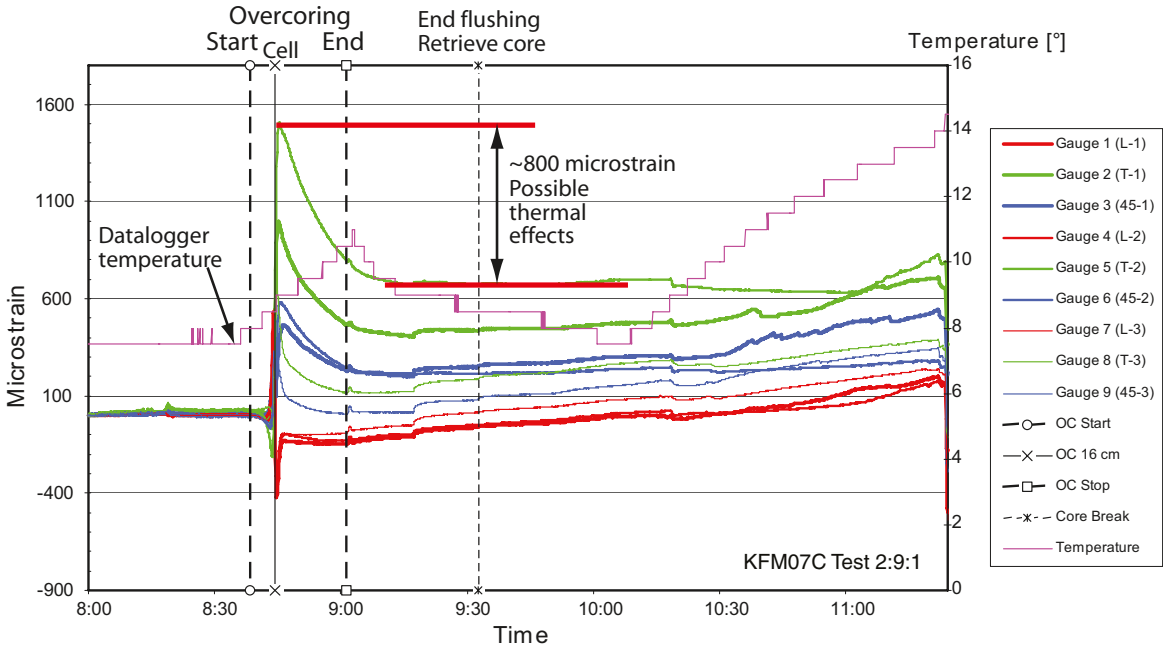

Figure 5-8. *Example of the strains recorded during overcore test no. 2:9:1, at a borehole length of 175.62 m in KFM07C. The nonlinear reduction in strains after the overcore bit passes the strain cell is presently thought to be related to thermally-induced strains and is referred to as the 'ski-hill' strains.*

a rating of either ‘a’ or ‘b’ from borehole depths of approximately 100, 160, 194, 240 and 315 m in KFM07C /Lindfors et al. 2007/. The transient strain analyses predicts the final overcore strains based on the strains obtained in the early stages of overcoring before stress-induced microcracking occurs, i.e. the transient strain calculations assumes the overcore sample is continuous, homogeneous, isotropic and linear elastic /Hakala et al. 2003/. The calculated strains were compared to the predicted strains for the overcore tests at each depth. /Lindfors et al. 2007/ concluded that the amount of ‘unexplained strains’ was found to be high (> 20%) for all depths. Only at one overcore location (borehole depth 98.76 m) in KFM07C was the amount of unexplain strain considered by /Lindfors et al. 2007/ to be low (5%). Interestingly this overcore test had very minor ‘ski-hill’ strains (approximately 25 microstrains) and had been rated as an ‘a’ quality test. Such evidence suggests that the ‘ski-hill’ strains may be the source of the low number of good quality overcore tests at Forsmark.

All the overcore tests in KFM07C had measurable ‘ski-hill’ strains and these ranged between 25 and 750 microstrains with an average of about 350 microstrain. Figure 5-9 shows the ratio of ‘ski-hill‘ strain to the maximum circumferential strain for each overcore test. The data in Figure 5-9 suggests that this ratio is increasing with depth. Why this ratio should increase with depth is not clear but may be related to the drilling. If the ‘ski-hill’ strains are thermally induced by the drilling and flushing, intuitively these strains should increase with depth. However, if these strains were a constant value, and the in situ horizontal stress magnitudes were increasing with depth, then this ratio should decrease with depth. The data in Figure 5-9 is preliminary and needs further work. It may be more illustrative, for example, to calculate the volumetric strain ($\varepsilon_1 + \varepsilon_2 + \varepsilon_3$) at peak strain and at the strain plateau after overcoring, to try and capture the complete volume strain response. These issues are currently under investigation.

Thermally-induced stress is a function of the temperature increase (ΔT), coefficient of thermal expansion (α) and the stiffness of the rock (E) and according to /Jaeger and Cook 1979/, for one dimension, is given as:

$$\Delta\sigma = \Delta T\, \alpha\, \frac{E}{1-\nu} \qquad (1)$$

In Figure 5-8 the possible thermally-induced strains is approximately 800 microstrain, representing nearly 50% of the total recorded strains. Most of the overcore tests did not display such large values but many tests gave values that ranged between from 14% to 64% of the maximum circumferential strain. Using α = 7.710−6/°C, E = 75,000 MPa, ν = 0.25 and assuming that the 300 microstrains are caused by ΔT , Equation 1 would suggest that a temperature increase of approximately 29°C was needed to cause the thermal effect. This equates to an increase in stress ($\Delta\sigma$) of approximately 22.5 MPa. Hence for the rock properties at Forsmark a 1°C increase in

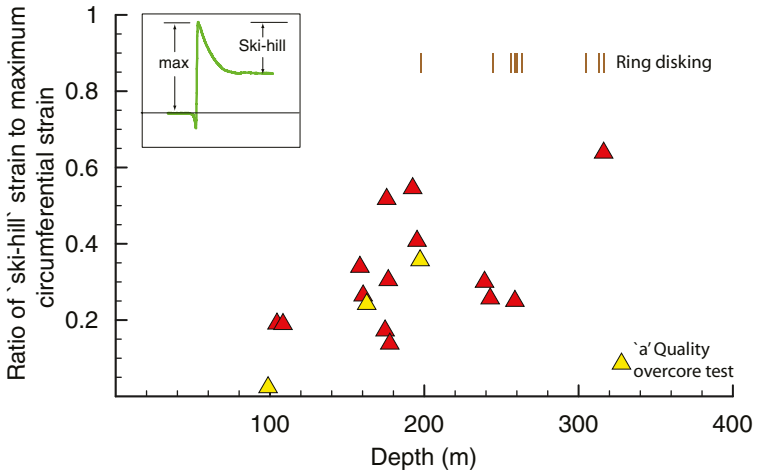

Figure 5-9. *Ratio of the strains related to the ‘ski-hill‘ to the maximum circumferential strain versus depth. The three high quality (‘a’) overcore tests are also shown as well as the location of ring-disking.*

temperature equates to approximately a 0.8 MPa increase in stress. While this simple example cannot be used to estimated the effect of a temperature increase on the stress tensor it does illustrate that a temperature increase may have a significant effect on the stress magnitudes and that interpretation of the overcore results cannot ignore this effect.

During the overcoring advance the coring bit would provide the heat source while the flushing water would provide the cooling mechanism. The actual heating process that would induce the thermal stains is likely a very complex transient process. A series of preliminary FLAC3D thermal analyses were carried out to assess the characteristics of the thermally-induced strains. Three thermal models were evaluated: (1) constant, (2) step and (3) peak (see Figure 5-10). A FLAC3D model of a typical overcore test was created and the temperature boundary conditions applied. The overcore was advanced in 10 mm steps and the thermally induced strains for each thermal model were monitored.

The thermally induced strains from each of the three models were then added to the mechanical strains to assess the total strain response. The shape of the thermally-induce strain response was visually compared to the actual overcore strain response to assess the applicability of the model. The constant thermal model did not appear applicable as the strains behind the strain cell were significantly increased which was not observed in the actual tests (to the left of the cell in Figure 5-8). This implied that the overcoring advance did not significantly affect the overcore strain gauges until the coring bit was in close proximity to cell. The step-model appeared to provide the strain response that was similar to the measured response. Figure 5-11 shows the result for the circumferential strain from the FLAC3D model with the step-thermal boundary conditions.

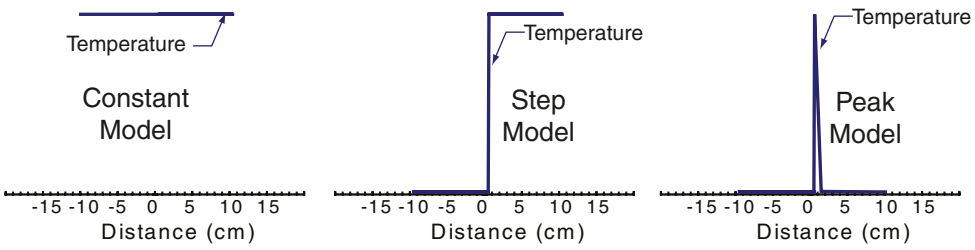

Figure 5-10. *The three thermal models used to evaluate the characteristics of the thermally induced strains. The distance of 0 cm equates to the location of the overcore strain cell.*

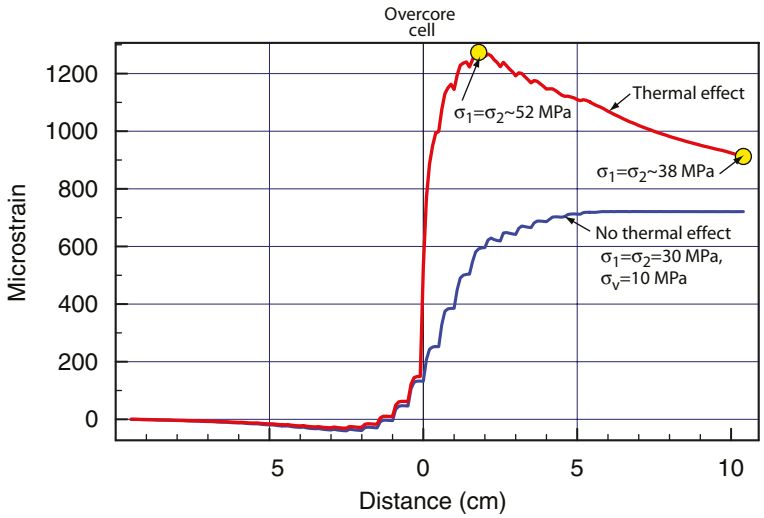

Figure 5-11. *Circumferential strain from a simulated overcore test in Flac3D. The in situ stress boundary conditions were $\sigma_1 = \sigma_2 = 30$ MPa and $\sigma_{vert} = 10$ MPa and the overcoring was carried out in the vertical stress direction. The combined thermal and mechanical stress magnitudes calculated at two different locations are shown for comparison to the mechanical stresses.*

For the example in Figure 5-11 the far-field stress state was $\sigma_1 = \sigma_2 = 30$ MPa with a vertical stress of 10 MPa which is similar to the stress magnitudes at Forsmark. The borehole was advanced in the vertical direction. The mechanical circumferential strains from this stress state would be approximately 700 microstrain for the 30 MPa horizontal stress. The combined thermal and mechanical horizontal stress determined at two positions ranged from 38 to 52 MPa, which is significantly higher then the in situ horizontal stress of 30 MPa. Figure 5-12 shows the overcore strains in Figure 5-8 plotted as a function of drill-bit advance. The results in Figure 5-11 are preliminary but are encouraging and suggest that the "ski-hill" strains observed in Figure 5-12 are likely caused by thermal effect. The step thermal model was also used to simulate the thermal strains in Figure 5-11. The results from the peak model were not consistent with observations. The thermal model that best simulates the overcoring process is likely a combined step and peak model. This combined model is presently under evaluation.

5.3 Summary

Several extensive hydraulic fracturing and overcoring stress measurement campaigns were conducted in the Forsmark Target Area. Analysis of the results from those campaigns have identified several issues that impact on the interpretation of the test results:

Hydraulic fracturing and HTPF campaigns

1. Many of the hydraulic fracturing tests produced test results that were approximately equivalent to the calculated weight of the overburden. The important issue is to establish if the results are a consequence of the test methodology in this geological thrust regime.
2. The uncertainty associated with the orientation of the hydraulic fracture once it leaves the injection borehole remains a serious limitation of this technology. This limitation also applies to the HTPF method, particularly where the majority of open transmissive fractures are gently dipping or subhorizontal.
3. There appears to be little benefit of controlling the rate or amount of fluid injection in an attempt to control the orientation of the propagating fracture. It appears the fracture will always propagate normal to the minimum stress regardless of injection rate and volume.

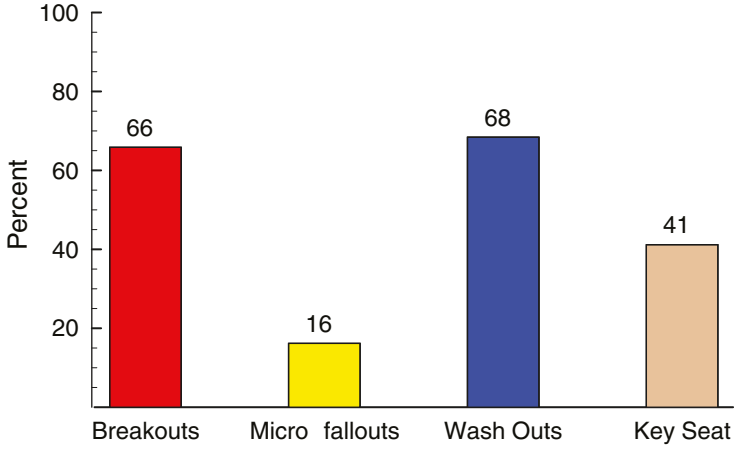

Figure 5-12. *Plot of overcore strain in Figure 5-8 as a function of bit advance. Note the similarity in strain response compared to Figure 5-11.*

Overcoring campaigns

1. The success rate for achieving 'a' quality overcore tests was very low. Nearly all overcore tests showed an unusual rapid reduction in strains once the overcore was passed. Unstable strain readings during biaxial testing resulted in many low quality biaxial test results.
2. An extensive investigation into the effect of microcracking on the overcore results from KFM07C showed that the effect of microcracking is very minor and and cannot be used to explain the unusual strain response during overcoring and biaxial testing. The unusually large Poisson's ratio of 0.4 from the biaxial tests cannot be explained by microcracking and is unusual for stiff rocks such as granite.
3. Nearly all the overcore tests in KFM07C including the high quality tests show 'ski-hill' strains which appear to be thermally induced by the drilling. The proportion of the 'ski-hill' strains to the total circumferential strain appears to increase with depth. If the 'ski-hill' strains were caused by a constant drilling effect, the ratio of 'ski-hill' strains to maximum circumferential strain should decrease with depth, assuming the horizontal stress magnitudes were increasing with depth.
4. The calculated stress magnitudes from the overcore results may be influenced by the heat generated during the overcoring process. The unusually large scatter in the overcore results may be related to this issue. The heat generated during the overcoring may affect the glue that bonds the strain gauges.
5. If the 'ski-hill' strains are thermally induced, these strains may create local stress magnitudes sufficient to cause ring-disking. This may explain why ring-disking is commonly observed below 200 m depth yet solid core disking is seldom observed even at depths of 1,000 m.
6. The thin (nominal 12-mm thick) overcore cylinder used for overcore testing with the Borre Probe may be the major reason for the problems described above.

At the time of this report the effect of the thermally-induced strains on the overcore results, particularly the stress magnitudes have not been quantified and the investigations into these effects are on-going. Thermally-induced stresses in an isotropic rock block would simply increase the mean stress and would have no effect on the deviatoric stress, i.e. the stress ratios (σ_1/σ_2, σ_2/σ_3, σ_1/σ_3) would remain unchanged. However, because of the overcoring boundary conditions this is not likely to be the case. Nonetheless because the stress ratios and mean stress may be less sensitive to these thermally-induced strains in the next section the stress ratios from the overcore results are also examined to help establish the stress state at Forsmark. /Ask et al. 2006/ noted that the high quartz content (20–45%) of dominant rocks at Forsmark resulted in up to 30% higher drill-feed force and approximately 30% lower drilling rate (9–13 cm/min) compared to drilling conditions at Oskarshamn Site at comparable depths. Hence, the geological environment at Forsmark may make the drilling conditions and the resulting thermal response somewhat unique. However, if the drilling technology at Forsmark produced relatively large thermally-induced strains sufficient to cause ring-disking during overcoring than similar thermally-induced strains may be responsible for the random solid core disking observed at Forsmark and the micro-fall outs observed in the borehole breakout study (see Figure 4-7). It is doubtful if these issues can be fully resolved.

6 Interpretation of in situ stress data

In this section the data from the stress campaigns are analysed to establish the best estimate of the stress magnitudes and orientations within the Target Area and at the proposed repository depth. In situ stress data are normally presented in terms of the magnitude and directions of the three principal stresses (σ_1, σ_2, σ_3). In areas of low relief, σ_1 and σ_2 are generally found to be near horizontal or gently dipping and hence in the literature these principal stresses are often replaced with horizontal stresses referred to as σ_H and σ_h. Because the horizontal stresses in many regions of the world are greater than the vertical stress, the ratio of average horizonal stress $(\sigma_H + \sigma_h)/2$ to vertical stress is often used to establish trends in data sets. However, while this is useful for establishing regional trends in data, at project sites it is important to establish the ratios between all three principal stresses and to know the orientation of the stresses, as the orientation of the underground openings, relative to the stress orientation, is usually an important factor in design. In this report, in addition to the principal stresses, the mean stress expressed as $(\sigma_1 + \sigma_2 + \sigma_3)/3$ and the stress ratios (σ_1/σ_2, σ_2/σ_3, σ_1/σ_3) are also used in establishing trends in the data set and for estimating the stress state in the Target Area. The individual test results data for the data set, discussed in the following sections, are given in Appendix A.

To establish trends in the data, the data was analysed using a moving-median data smoothing technique. This technique is less influenced by outliers in the data compared to a moving average technique. For all moving-medians results six data points were used to establish the median. When applying the moving-median technique to the stress data, the rules for 2nd order tensors were followed. In the figures in this section showing the trends with depth the boundary between fracture domain FFM02 and FFM01 is shown for reference at a depth of 150 m. In many boreholes the actual depth is less. Also shown in the trend figures is a dashed line at 400 m depth. Below 400 m depth the plots are noted ‘Low K’ which simply highlights the beginning of the very low permeability rock mass at Forsmark.

6.1 Vertical stress

The vertical stress in an area of relatively flat topography such as Forsmark can be estimated by the weight of the overlying rocks. Section 5.1 discussed the hydraulic fracturing campaigns and /Klee and Rummel 2004/ used suitably oriented fractures to determine the vertical stress using this technique. /Klee and Rummel 2004/ used the opening pressure of existing gently dipping fractures (dipping less than 20°from the horizontal) in KFM01A/B and KFM02A, to determine the weight of the overburden. /Sjöberg et al. 2005/ concluded that for these near vertical boreholes the measured vertical stresses to a depth of 800 m was in close agreement with the vertical stress calculated using a vertical stress gradient of 0.0265 MPa/m, i.e. an average rock density of 2,700 kg/m3.

Figure 6-1a shows the vertical stress measured in the overcore tests in the Target Area compared to the calculated stress (depth × 0.026 MPa/m). The vertical stress in Figure 6-1a is obtained from the stress tensor and is not the value of σ_3 unless σ_3 has a vertical plunge. Clearly the data shows a significant scatter suggesting that the vertical stress may be influenced by factors other than topography and the density of the overlying rocks. Figure 6-1b shows the same vertical stress data but analysed using a moving-median data smoothing technique. Also plotted on Figure 6-1b is the calculated vertical stress. Figure 6-1b suggests that the trend of the increase in measured vertical stress is similar to the increase in the calculated vertical stress to depths of approximately 300 m. Below 400 m depth there is a significant increase in the measured vertical stress. /Martin and Chandler 1993/ showed that geological structure, particularly major sub-horizontal fault zones containing extensive fault gouge and major asperities, could significantly affect stress heterogeneity including the vertical stress. However, in the Target Area

no major sub-horizontal deformation zones have been identified at the depths where the increase in vertical stress shown in Figure 6-1 occurs. Hence other factors appear to be influencing the vertical stress magnitudes. /Carlsson and Christiansson 1987/ suggested that in the Forsmark area the open gently dipping fractures may be responsible for the anonymously high vertical stresses at shallow depths.

6.2 Mean stress

The in situ stress state at AECL's Underground Research (URL) has been investigated since the late 1980's. /Martin 1990/ showed that three stress domains could be defined and these could be correlated to the rock mass quality. In the fractured granite the stress magnitudes were relatively low (Stress Domain I) while in the massive unfractured granite the stress magnitudes were relatively high (Stress Domain III). Stress Domain II was the transition between Stress Domains I and III (Figure 6-2a). The mean stress from the CSIR overcore measurements (obtained from underground excavations) used by /Martin 1990/ to characterise the stress state at the URL are shown in Figure 6-2a. Examination of Figure 6-2a shows that at depths below 200 m the scatter in the overcore measurements increases significantly. As noted by /Martin 1990/ and /Martin and Christiansson 1991b/ this scatted was caused by stress-induced microcracking

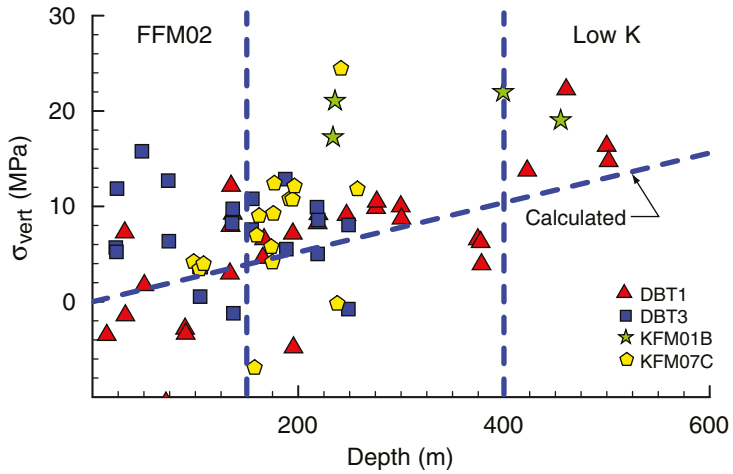

(a) Vertical stress measured in overcore tests compared to the calculated stress due to the weight of the overburden

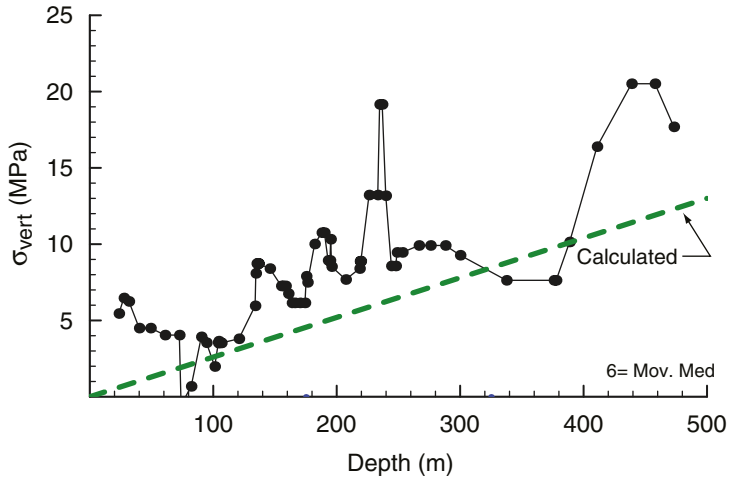

(b) Vertical stress using a moving-median data smoothing technique

Figure 6-1. *Summary of vertical stress from the overcoring campaigns. The data suggests that the vertical stress is influenced by factors not related to density of the overlying rocks and/or topography.*

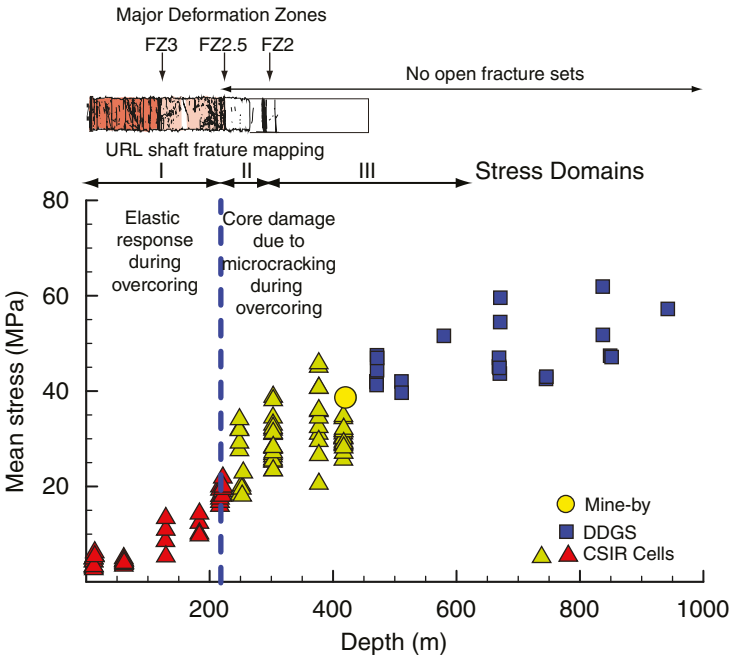

(a) Mean stress data

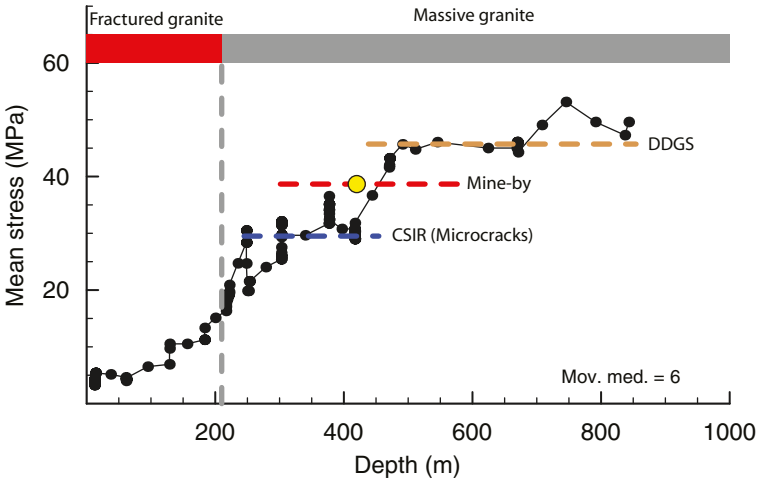

(b) Mean stress using a moving-median data smoothing technique

Figure 6-2. *Summary of mean stress magnitudes with depth for AECL's Underground Research Laboratory. Fracture shaft mapping from /Everitt and Lajtai 2004/ and stress data from /Martin 1990, Thompson and Chandler 2004/.*

during the overcoring process which made the stress magnitudes from these tests unreliable. /Read 1994/ conducted an extensive back-analysis of the Mine-by experiment and showed that the in situ stress state at the 420 m Level of the URL was underestimated by the CSIR overcore tests (see Figure 6-2a). In an attempt to overcome the effect of stress-induced microcracking during overcoring /Thompson and Chandler 2004/ used a modified Deep Doorstopper Gauge System (DDGS) to measure the stress state at the URL between 500 and 1,000-m depth. The results from those measurements are also shown in Figure 6-2a. Despite the efforts to reduce the microcracking using the DDGS, according to /Thompson and Chandler 2004/ the microcracks remained a problem for interpreting the DDGS results. As shown in Figure 6-2a the mean stress from DDGS results (the vertical stress was assumed to calculate the mean stress) is consistently greater than the Mine-by results. /Christiansson and Janson 2002/ also found that the DDGS overcore test results gave higher stress magnitudes than those obtained from triaxial overcoring and hydraulic fracturing, both of which were in relative agreement.

Figure 6-2b shows the mean in situ stress at the URL using the moving median data smoothing technique (Figure 6-2b). The data suggests that the change in mean stress is related to changes in the fracture frequency and that in the unfractured granite the mean stress is relatively constant. The value of the mean stress at 420 m depth ranges from 32 MPa from the CSIR results to 46 MPa from the DDGS results. The best estimate from the Mine-by back analysis was 38.6 MPa. Hence while the trends in mean stress magnitude can be related to changes in rock mass quality estimating the correct mean stress magnitude is difficult because additional factors can affect the stress measurement technique, i.e. microcracking in the case of the CSIR data.

It is known from laboratory tests that increasing the mean stress applied to cylindrical samples causes the open pores and microcracks to close resulting in a stiffer rock. /Jacobsson et al. 2007/ used that technique to estimate the crack volume in Forsmark samples. Similarly a reduction in mean stress results in closed-fractures opening. In a rock mass the open fractures would be expected near the ground surface where the mean stress is relatively low while at depth the frequency of open fractures should be reduced and the overall rock mass stiffness should be greater than that observed at shallow depths. Table 6-1 lists case studies in crystalline rock where the in situ stress has been measured and the rock mass deformation modulus (ED) has been back-calculated from deformation measurements. Figure 6-3 shows a plot of the mean in situ stress normalised to the laboratory uniaxial compressive strength versus the back-calculated deformation modulus normalised to the laboratory Young's modulus for the data in Table 6-1. The correlation in Figure 6-3 between mean stress and deformation modulus supports the trend seen in Figure 6-2b that the increase in mean stress with depth at AECL's URL is likely related to the measured decrease in fracture frequency, i.e. an increase in rock mass deformation modulus. This is not surprising as increases in stiffness in sedimentary basins have been correlated with increases in horizontal stress magnitudes /Cartwright 1997/.

The change in mean stress $(\sigma_1 + \sigma_2 + \sigma_3)/3$ with depth from the overcore data within the Forsmark site is summarised in Figure 6-4a and the trend obtained using a moving-median data smoothing technique is shown in Figure 6-4b. Also shown in Figure 6-4b is a trend line that appears to fit the data between a depth of 125 and 300 m. Above 100 m the mean stress initially decreases but remains relatively constant between 75 to 125 m. At 125 m the mean stress starts to increase. The near surface rock mass is part of Fracture Domain FFM02. As indicated in Section 2.2.2 FFM02 is dominated by gently dipping open fractures and Northeast-Southwest and Northwest-Southeast subvertical open fracture sets. The boundary between Fracture Domain FFM02 and FFM01, the sparsely fracture rock mass, is between 100 and 150 m in the Site Description Model 2.1 /SKB 2006/. Hence, the lack of significant change in the mean stress between 0 and 100 m may indicate the rock mass modulus is relatively unchanged. The gradual increase in mean in situ stress below 125 m could suggest the rock mass quality is gradually improving with depth.

Table 6-1. Case studies in crystalline rock used to establish the relationship between measured mean in situ stress and back calculated deformation modulus plotted in Figure 6-3.

Project	σ1 (MPa)	σ2 (MPa)	σ3 (MPa)	E_D (GPa)	E_i (GPa)	Depth (m)	Reference
Mine-by	60	45	11	60	68	420	/Read 1994/
APSE	30	15	10	55	76	450	/Andersson 2007/
Hockey Cavern	4.3	3.4	1.8	40	?	70	/Barton et al. 1994/
SNO	95	66	51	79	79	2070	/Castro 1996/
Quarry	18	9	0.26	50	65	10	/Martin et al. 2003/
Upper Shaft	15	12	6	47	68	185	/Barton /1988
CLAB	6.8	5.3	3.7	40	76	40	/Fredriksson et al. 2001/

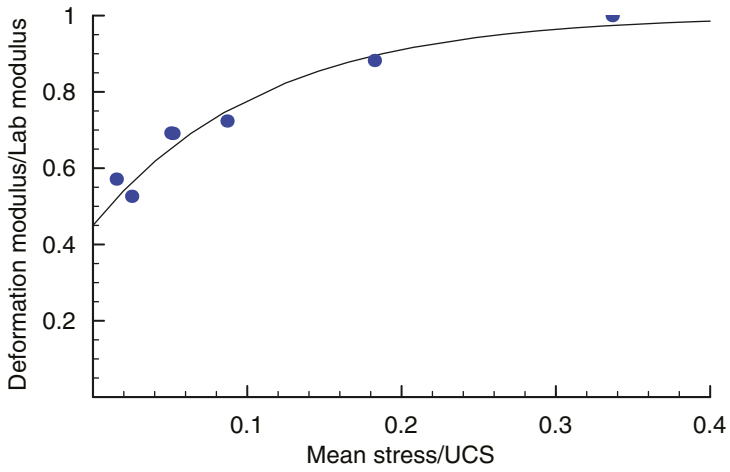

Figure 6-3. *Relationship between mean in situ stress determined from overcore measurements normalised to the laboratory uniaxial compressive strength (UCS) and rock mass deformation modulus determined from back analyses of deformation measurements and normalised to the laboratory intact Young's modulus.*

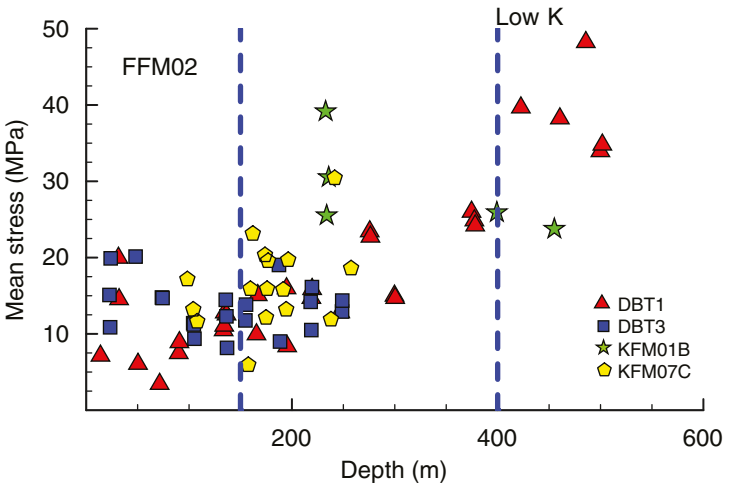

(a) Mean stress data

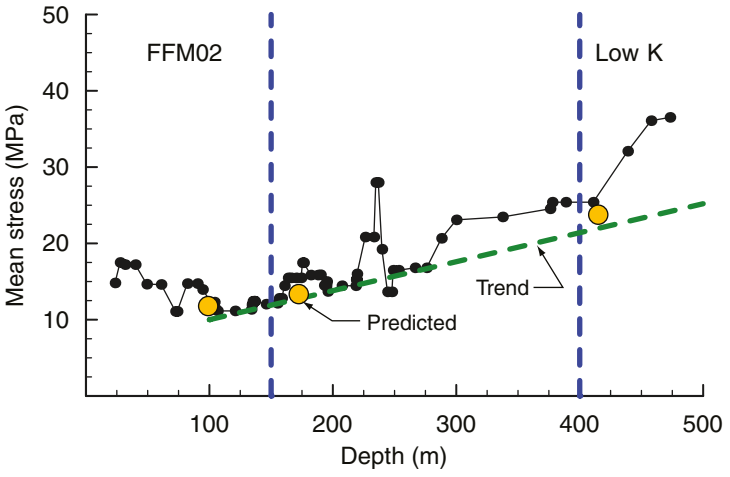

(b) Mean stress using a moving-median data smoothing technique

Figure 6-4. *Summary of mean stress magnitudes with depth from the overcoring campaigns at Forsmark. The predicted mean stress is based on the P-wave velocities and the data in Table 6-1.*

The Site Descriptive Model for Forsmark used the empirical rock mass classification systems RMR and Q to estimate the changes in rock mass properties with depth /SKB 2005a/. This procedure was carried out using a 5-m length in individual boreholes and RMR was found to vary from 73 to 99 for the competent rock in boreholes KFM01A, KFM02A, KFM03A, and KFM04A. The most notable improvement was observed below a depth of 500 m. Estimating the rock mass deformation modulus from empirical classification systems based on borehole data is very challenging, particularly when the rock mass is moderately to sparsely fractured. The seismic profile in Figure 2-9 was determined from large scale regional surveys. The P-wave velocity given in Figure 2-9 was first converted to a dynamic modulus (Ed) and then to a static modulus (Es) using the empirical relationship provided by /King 1983/:

$$E_s = 1.263E_d - 29.5 \text{ (GPa)}. \quad (2)$$

Figure 6-4b shows the predicted mean stress based on the P-wave velocity for the rock mass and data shown in Figure 6-3 compared to the median trend in the overcore data. The agreement between the predicted and measured mean stress suggests that the improvement in mean stress can be explained by an improvement in rock mass quality.

Figure 6-5 shows an alternative interpretation to the data shown in Figure 6-4b. In Figure 6-5 the mean stress is interpreted assuming step-wise increases in the mean stress magnitudes with depth. If the increase in mean stress is related to an improvement in the rock mass quality than the step-wise increases in the mean stress would indicate a significant improvement in rock mass quality. These step-wise like increases occurred at AECL's Underground Research Laboratory (see Figure 6-2). At a depth of 300 m the mean stress in Figure 6-4b appears elevated above the general trend line and at approximately 400 m there is a significant increase in the mean stress above both the trend line and the predicted mean stress. However, at Forsmark, the P-wave velocities suggest that the rapid improvement in rock mass quality occurs in the first 150 m (see Figure 2-9). Below 150 m there is only a modest improvement in P-wave velocity which is also supported by the open fracture frequency shown in Figure 2-8. Hence it appears that the large increase in means stress below 400 m depth at Forsmark may be related to the other factors that may have influenced the overcoring results. At present the thermal effects during overcoring appears to be a major unknown.

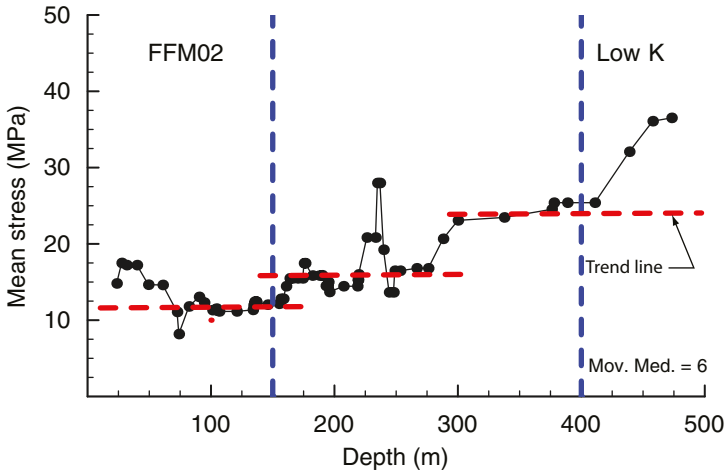

Figure 6-5. *Mean stress showing step-wise trends in mean stress magnitudes with depth.*

6.3 Principal stress ratios

/Hast 1969/ was one of the early researchers to note that both horizontal stresses were consistently greater than the vertical stress. /Brown and Hoek 1978/ compiled stress measurements from various countries and found that the ratio (k) of average horizontal stress $(\sigma_H + \sigma_h)/2$ to vertical stress could be approximated by:

$$100/Z + 0.30 \leq k \leq 1{,}500/Z + 0.50 \quad (3)$$

where Z is the depth. While Equation 3 gives a large range in k, particularly at shallow depths, the authors acknowledged that this range may be reduced by considering only results obtained from the same geological region and environment.

Since the work of /Brown and Hoek 1978/ the number of stress measurements has increased significantly and trends in data can now be compiled for different countries. /Lee et al. 2006/ using stress data from Australia found that the average stress ratios with depth were relatively constant $\sigma_1/\sigma_2 = 1.5$, $\sigma_2/\sigma_3 = 1.5$, and $\sigma_1/\sigma_3 = 2.3$. /Harrison et al. 2007/ compiled the principal stress mean ratios from three other countries and also found that the ratios were quite consistent and similar to those reported by Lee et al. (Table 6-2). /Harrison et al. 2007/ suggested that the consistency in principal stress ratios may imply that the Earth's crust is in a state of limiting equilibrium and that the ratios may be related to limiting friction angles. While the explanation by /Harrison et al. 2007/ was speculation, the consistency in the principal stress average ratios is encouraging. Nonetheless it should be noted that the stress measurements used to establish the data came from different geological environments and stress regimes, and hence the consistency in the ratios may be fortuitous as noted by /Harrison et al. 2007/. For example, at AECL's URL the stress ratios at the 420 m level in massive granite were $\sigma_1/\sigma_2 = 60/48 = 1.25$, $\sigma_2/\sigma_3 = 48/11 = 4.36$, and $\sigma_1/\sigma_3 = 60/11 = 5.45$ which are not consistent with those reported by /Harrison et al. 2007/ (see Table 6-2). Likewise the stress ratios given by /Andersson 2007/ for the Äspö Pillar Stability Experiment (APSE) also differ from those compiled by /Harrison et al. 2007/ (see Table 6-2). These examples illustrate the difficulty of using general regional trends for establishing stress ratios at specific sites.

In Section 2.1 it was shown that the differential stress ratios would be expected to vary, depending on the fault regime. For example assuming a coefficient of friction of 0.75, the differential stress necessary to cause slip on a thrust, strike-slip and normal faults was found to vary from 4:1.6:1, respectively. In addition the coefficient of friction for sedimentary rocks tends to be generally lower than the coefficient of friction for crystalline rocks and hence the rock type would also play a role in the differential stress ratio. Therefore it is not surprising that the σ_1/σ_3 ratios in Table 6-2 show significant variation.

Table 6-2. Summary of average principal stress ratios.

	σ_1/σ_2	σ_2/σ_3	σ_1/σ_3	Fault regime	Reference
Australia	1.5	1.5	2.3		/Lee et al. 2006/
Chile	1.6	1.6	2.6		/Harrison et al. 2007/
United Kingdom	1.6	1.4			/Harrison et al. 2007/
Finland	1.7	1.7	3.0		/Harrison et al. 2007/
Äspö (APSE, 450 m)	2.0	1.5	3	Strike slip	/Andersson 2007/
Canada	1.6	1.8	2.8		/Arjang and Herget 1997/
AECL URL (420 m)	1.25	4.36	5.45	Thrust	/Martin and Read 1996/

6.3.1 Stress ratio σ_1/σ_2

The principal stress ratios of σ_1/σ_2 with depth for the overcore data at Forsmark are shown in Figure 6-6a. The ratios range from approximately 1 to 4 and the trend using the moving median data smoothing technique is shown in Figure 6-6b. The trend in the data in Figure 6-6 suggest a consistent average ratio of approximately 1.7 below a depth of 300 m which is consistent with the σ_1/σ_2 for Finland reported by /Harrison et al. 2007/ (see Table 6-2).

6.3.2 Stress ratio σ_1/σ_3

The principal stress ratios for σ_1/σ_3 are shown versus depth for Forsmark in Figure 6-7a. The data shows considerably more scatter than that observed for the principal stress ratio σ_1/σ_2 with σ_1/σ_3 varying from –4 to 15. This wide scatter reflects the large scatter in the values for σ_3. The trend using the moving median data smoothing technique is shown in Figure 6-7b. Unlike the σ_1/σ_2 ratio in Figure 6-6 the trend in the data in Figure 6-7 also shows considerably more scatter in the trend. Inspection of Figure 6-7b suggest a σ_1/σ_3 ratio of approximately 3.2 provided a reasonable trend to the portions of the data particularly between a depth of 125 m to 275 m. This ratio of 3.2 also appears reasonable for the depth range 0 to 75 m and at the repository depth between 450 and 500 m depth. This ratio of 3.2 is also similar to the σ_1/σ_3 ratio of 3.0 for Finland reported by /Harrison et al. 2007/ (see Table 6-2).

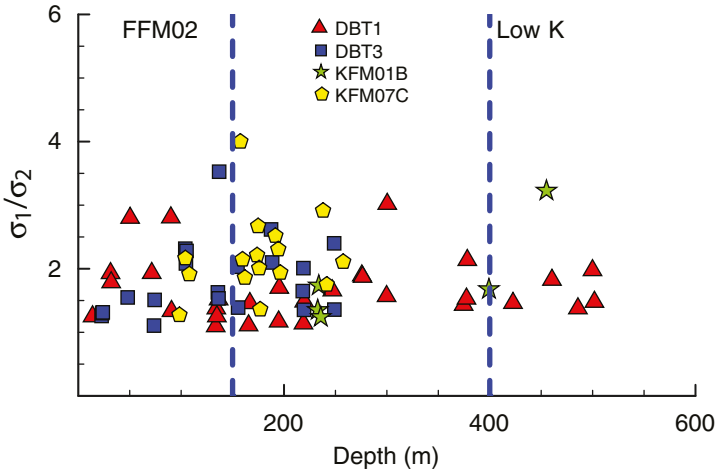

(a) σ1/σ2 data

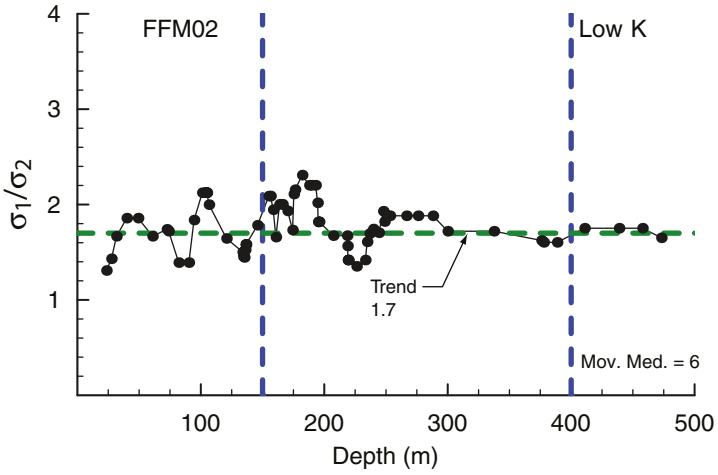

(b) σ1/σ2 trend using a moving-median data smoothing technique

Figure 6-6. *Summary of principal stress ratio of σ_1/σ_2 with depth from the overcoring campaigns.*

6.4 Comparison of σ_2 from overcoring and hydraulic fracturing

When hydraulic fracturing is carried out in vertical or near vertical boreholes the interpreted stress is expected to be the minimum horizontal stress (σ_{hmin}). In low relief areas with geological thrust regimes, the minimum stress is the vertical stress and both horizontal stresses exceed the vertical stress Figure 2-1). In such stress regimes, i.e. Forsmark, the minimum horizontal stress should be approximately equal to the intermediate principal stress ($\sigma_{hmin} \simeq \sigma_2$, see Figure 2-1). As noted by /Doe et al. 2006/ and /Evans and Engelder 1989/ producing a vertical fracture by the hydraulic fracturing method is very challenging in a geological thrust regime, as the fracture propagates normal to the minimum stress and in this geological regime the minimum stress is the vertical stress. Hence despite the orientation of the borehole there is the possibility that the fracture will end in a near horizontal orientation and the interpreted results will reflect the vertical stress. In addition to the traditional hydraulic fracturing measurements, the hydraulic stress required to open pre-existing fractures was also determined using the HTPF method. This opening stress (σ_n) is considered to act normal to the fracture and hence depending on the fracture orientation may also be used to determine the intermediate principal stress σ_2.

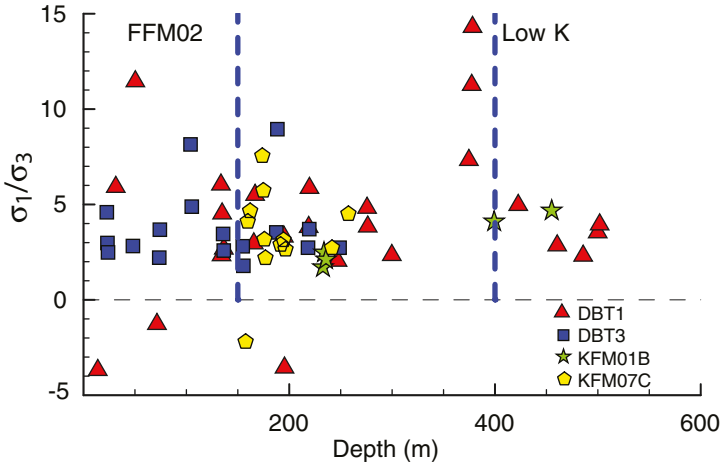

(a) σ1/σ3 data

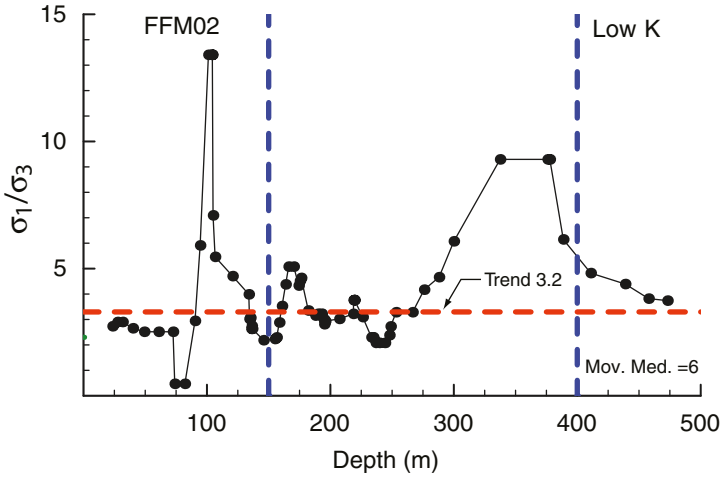

(b) σ1/σ3 trend using a moving-median data smoothing technique

Figure 6-7. *Summary of ratio of σ_1/σ_3 with depth from the overcoring campaigns.*

Figure 6-8a shows the magnitudes of the intermediate principal stresses σ_2 determined from the overcore measurements and Figure 6-8b gives their orientations (trend and plunge) plotted on a lower hemisphere equal area stereonet. The results in Figure 6-8a clearly shows the magnitudes of σ_2 exceeds the calculated vertical stress. The orientations of σ_2 shown in Figure 6-8b displays some scatter but there is a significant grouping of the data in the Northeast-Southwest directions which is consistent with the direction expected based on the orientation of the regional maximum compression (approximately Azimuth 150°).

Figure 6-9a shows all the magnitudes obtained from all hydraulic fracturing measurements, i.e. traditional hydraulic fracturing and HTPF. Unlike Figure 6-8a the magnitudes show strong clustering around the calculated vertical stress. Figure 6-9b shows the orientation of the poles to the fractures obtained from these hydraulic fracturing measurements. In many cases it was not possible to determine the orientation of the hydraulically-induced fracture due to technology limitations and hence there are fewer data points in the orientation dataset. Only data with known fracture Azimuth and dip are included in Figure 6-9b. Because of the use of the HTPF method there is more scatter in the individual orientation data then would be expected from individual traditional hydraulic fracturing data, i.e. individual fractures at different orientation are purposely selected. However, there is a minor clustering of the hydraulic fracturing orientation data in the Southwest-Northeast direction.

To compare the stress magnitudes from the hydraulic fracturing measurements to the overcore results only the fracture poles located in the Northeast-Southwest directions and plunging more than 60°were selected (Figure 6-10). The magnitudes of σ_2 and the σ_{hmin} corresponding to the orientations in Figure 6-10 are shown in Figure 6-11a. The data shows two distinct datasets with little overlap, except at depths between 300 and 350 m. Figure 6-11b shows the trends obtained in those datasets using the moving median data smoothing technique. From Figure 6-11 it appears the stresses from the overcoring and hydraulic fracturing are not measuring the same component of the stress tensor. The correlation of the hydraulic fracturing results with the calculated vertical stress supports the notion by /Doe et al. 2006/ and /Evans and Engelder 1989/ that in this geological regime the application of hydraulic fracturing to measure horizontal stresses is not appropriate.

The trend for the overcore data in Figure 6-11b shows a gradual increase in magnitude to a depth of approximately 400 m. Below 400 m there is a significant increase in σ_2 magnitudes. The data that shows the magnitude increase was obtained from borehole DBT1 (see Figure 6-8). Because of technology limitations at the time of overcoring in DBT1 /see Perman and Sjöberg 2003/) and the thermal concerns during overcoring discussed previously, this increase in magnitudes is suspect.

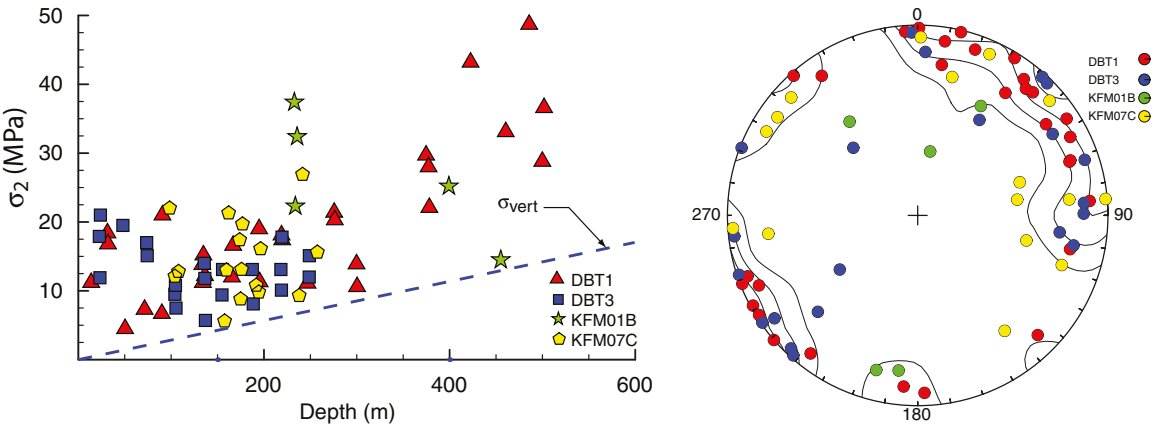

Figure 6-8. *Summary of the overcore intermediate principal stress (σ_2) magnitudes and directions plotted in lower hemisphere equal area stereonet.*

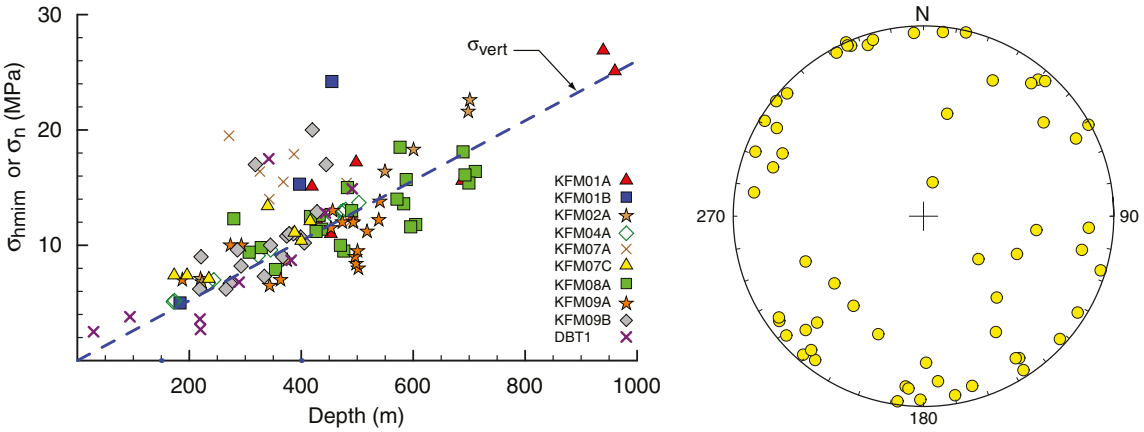

(a) σ_{hmin} or σn magnitudes (b) σ_{hmin} or σn directions

Figure 6-9. *Summary of the hydraulic fracturing stress (σ_{hmin} or σ_n) magnitudes and directions plotted in lower hemisphere equal area stereonet.*

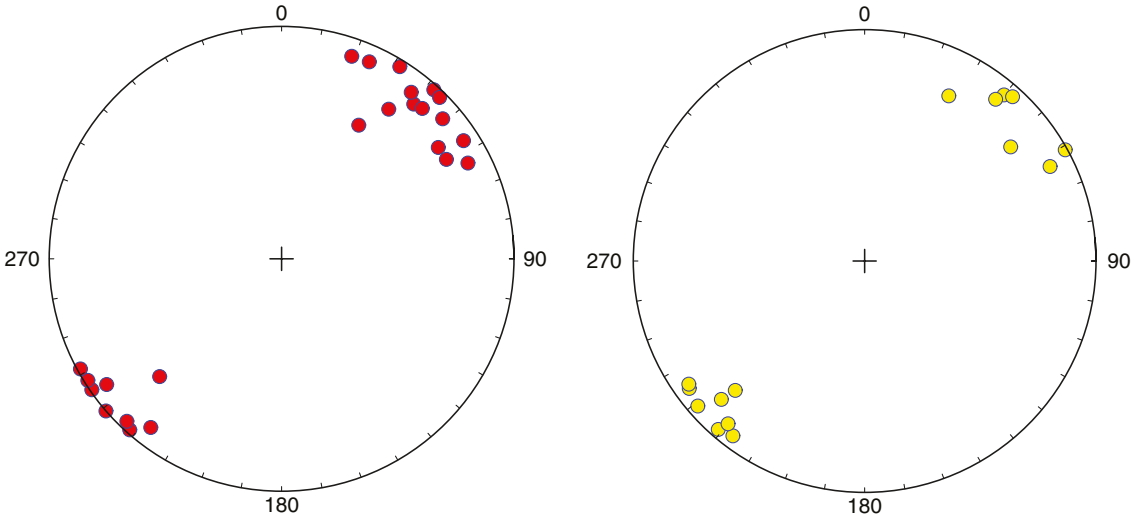

(a) σ_2 overcore orientations (b) σ_{hmin} hydraulic fracturing orientations

Figure 6-10. *Summary of the selected σ_2 and (σ_{hmin}) orientations used for the stress magnitude comparison in Figure 6-11.*

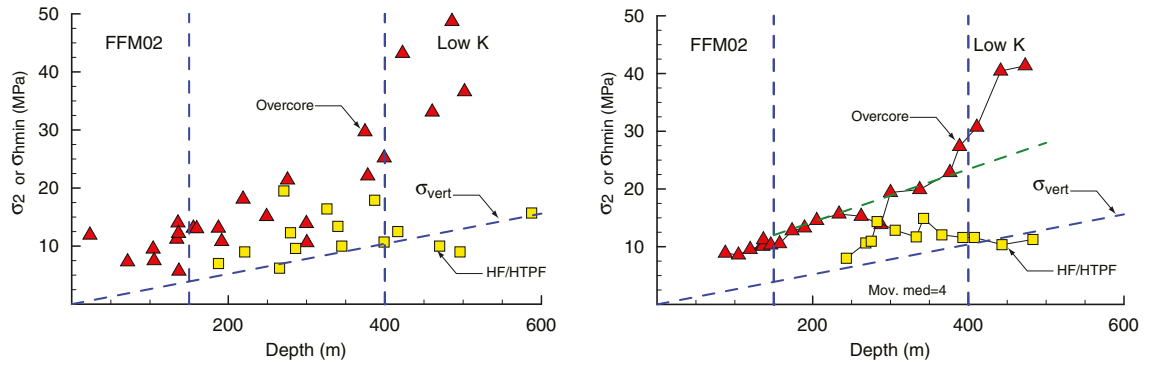

(a) Stress magnitudes (b) Moving median trends applied to stress magnitudes

Figure 6-11. *Summary of the stress magnitudes corresponding to the overcoring (σ_2) and hydraulic fracturing (σ_{hmin}) orientation data in Figure 6-10. The stress magnitudes from overcoring and hydraulic fracturing appear to be measuring different components of the in situ stress tensor.*

Figure 6-12 shows the moving median trend in the magnitudes of all the overcoring σ_2 regardless of orientation and shown in Figure 6-8a. If the stress magnitudes increase as a function of rock mass quality as discussed previously then the increase in σ_2 magnitudes could be interpreted as a step-function with each step reflecting an improvement in rock mass quality. Possible trends in the increase in σ_2 magnitudes are shown in Figure 6-12. These trends suggest that at the target depth of the repository σ_2 is expected to be approximately 25 MPa.

6.5 Stress orientations

The maximum horizontal stress in the Forsmark region, based on the regional seismicity and the borehole breakout data discussed previously, was expected to trend in a Northwest-Southeast direction. Figure 6-13 shows the moving-median trend of the Azimuth of the maximum principal stress from the overcore data base. The moving median technique calculates the mean stress tensor for the data interval selected (6) and the mean value for the maximum principal stress is plotted in Figure 6-13, i.e, the mean is calculated following the rules for 2nd order tensors.

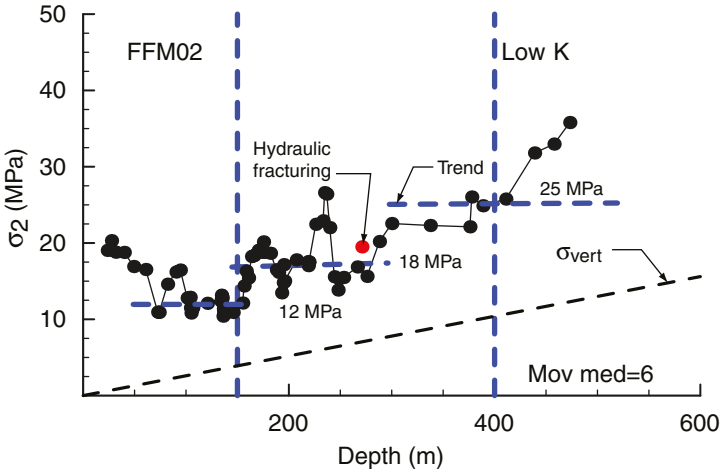

Figure 6-12. *Summary of the moving median for the intermediate principal stress magnitudes (σ_2) and possible step-like trends with depth.*

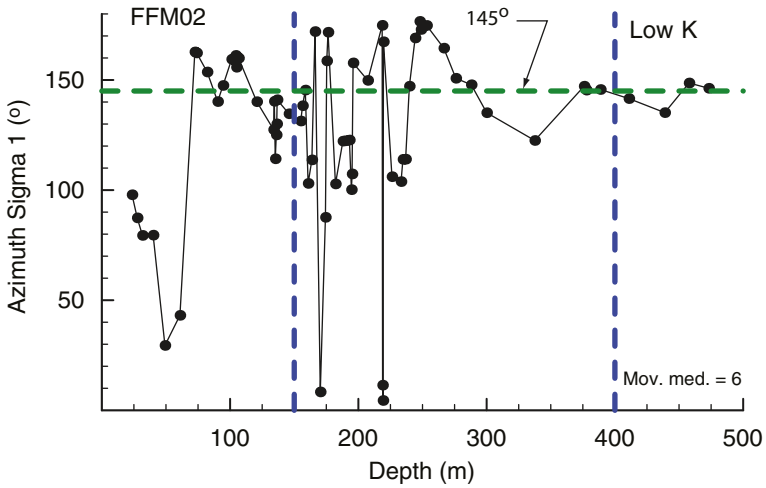

Figure 6-13. *Summary of the Azimuth of the maximum principal stress σ_1 obtained using the moving median data smoothing technique.*

The Azimuths have been adjusted such that they plot between 0 and 180°, i.e. if the actual Azimuth was 270° it is plotted as 90°. While there is some scatter in the overcore data,the results in Figure 6-13 supports the general findings that the trend of maximum horizontal compression is in in a Northwest-Southeast direction.

The data used to develop Figure 6-13 were divided into four depth ranges based on the trends in the data shown in Figure 6-5: 0–150 m, 150–300 m, 300–400 m and > 400 m. The mean stress tensor of the data in each depth range was calculated and the results summarised on the lower hemisphere equalarea stereonets given in Figure 6-14. As shown in Figure 6-14 there is consistency in the orientation of the maximum principal stress for all the depth intervals selected. Below 300 m the Azimuth is approximately 145°.

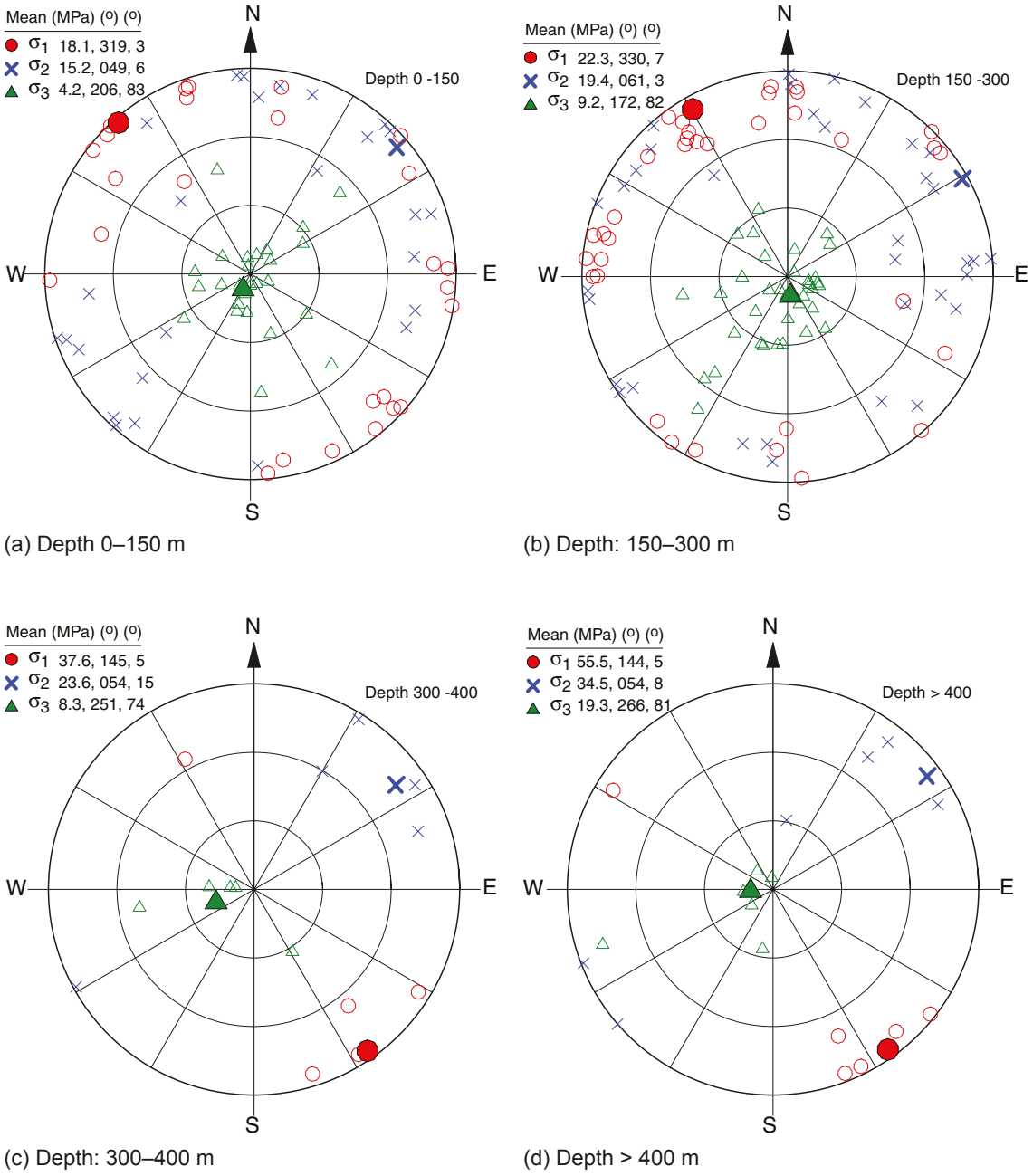

(a) Depth 0–150 m

(b) Depth: 150–300 m

(c) Depth: 300–400 m

(d) Depth > 400 m

Figure 6-14. *Orientation of mean stress tensor from all overcore data in Forsmark target Area. Data plotted on lower hemisphere equal area stereonet.*

6.6 Summary

Both the overcore data and the hydraulic fracturing data shows considerable scatter in the stress magnitudes at Forsmark. In the author's experience this scatter is related more to the measurement technique than the stress variability in situ. The impact of the thermal strains on the overcore results appears to have exaggerated this scatter in the Forsmark data. The application of principal stress ratios and means stress was used in conjunction with a moving median data smoothing technique to establish trends in the data sets.

Despite the scatter in the overcore results, the orientation of the stress tensor shows considerable consistency with depth with σ_1 trending with an Azimuth of approximately 145°and σ_3 plunging approximately vertically.

The stress magnitudes determined from the hydraulic fracturing and the hydraulic testing of pre-existing fractures is consistently lower than the stress magnitudes determined from the overcore data for the minimum horizontal stress. The magnitudes from many of the hydraulic fracturing and the hydraulic testing of pre-existing fractures gave magnitudes that approximate the calculated vertical stress.

7 Estimation of Forsmark stress state

The stress data from the stress measurement campaigns and discussed in Section 6 have shown that at Forsmark the trend of σ_1 is approximately 145°and σ_3 plunges approximately vertically. Hence, the vertical stress at Forsmark is the minimum principal stress (σ_3). Section 6 has also shown that the magnitudes of both the maximum and minimum horizontal stresses are greater than the vertical stress and based on Anderson's fault classification (see Figure 2-1), these stress conditions suggest a thrust fault regime. These findings are consistent with the findings from regional seismicity studies carried out by /Slunga 1991/ and the geological model for the Forsmark tectonic lens given in the Site Descriptive Model /SKB 2006, 2005a/. The uncertainty in the stress state at Forsmark, to be resolved in this section, is related to the magnitude of the maximum and minimum horizontal stresses. The maximum and minimum horizontal stresses are needed to assess the spalling potential in vertical deposition holes.

7.1 Methodology

The data obtained from the Forsmark stress measurement campaigns show considerable scatter. A methodology is proposed for estimating the state of stress that relies not on individual test results but on the trends in the data. The methodology uses the principal stress ratio (R), the mean principal stress (M) and the initiation for spalling expressed as a function of the Spalling Ratio (SR) and the laboratory uniaxial compressive strength (UCS) defined as:

$$\sigma_1/\sigma_2 = R \quad (4)$$

$$(\sigma_1 + \sigma_2 + \sigma_3)/3 = M \quad (5)$$

$$(3\sigma_1 - \sigma_2)/UCS \geq SR \quad (6)$$

where σ_1, σ_2 and σ_3 are the maximum, intermediate and minimum principal stresses, respectively.

The initiation for spalling is not needed to obtain the values for σ_1 and σ_2 from Equations 4 and 5 because the value for σ_3 in Equation 5 is assumed to be a function of depth, i.e. $\sigma_3 = 0.026 \times$ depth in metres, and hence Equations 4 and 5 can be readily solved for σ_1 and σ_2. The initiation for spalling is used as a check to assess if the values for σ_1 and σ_2 determined from Equations 4 and 5 agree with observations, e.g. borehole breakouts from televiewer logs or tunnel spalling observations. A plot of Equations 4, 5 and 6 in σ_1–σ_2 space can be used to assess the if the solution is well constrained.

By using principal stress ratios and the mean principal stress to establish the stress magnitudes, the orientation component of the stress tensor can be ignored. Once the magnitudes are established the orientation must be assessed by some other means, e.g. regional data, borehole breakouts, observations, geology model, etc. The stress tensor that is developed using this methodology is compiled from multiple datasets and hence errors cannot be rigorously assigned using statistical methods but must be established by other means or assessed by engineering judgement.

7.1.1 Application of methodology to AECL URL 420 Level

To illustrate the proposed methodology the stress state for 420 Level of AECL's URL is assessed using the triaxial overcore data and the doorstopper data. The values for R and M were obtained from AECL's overcore stress measurements and and the value (SR) from AECL's Mine-by Experiment. These values were then used to estimate the stress state at the 420 m level and compared to the back-calculated stress state by /Read 1994/. Figure 7-1 shows the possible σ_1 and σ_2 values determined using Equations 4 and 5. Where the equations intersect in Figure 7-1 represents the most likely values for σ_1 and σ_2 and shows that the solution is well constrained.

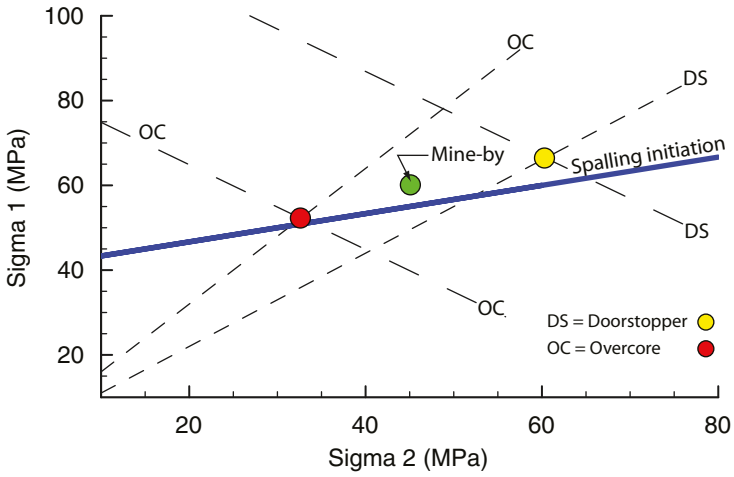

Figure 7-1. *Example of the application of stress ratio and mean stress to determine the magnitudes of σ_1 and σ_2 for 420 Level of AECL'URL using triaxial and Doorstopper test results. The best estimate for the in situ stress magnitudes for the 420 Level were developed by /Read 1994/ using the Mine-by deformation data and a statistically rigorous back-analysis technique.*

The spalling initiation using Equation 6 is also shown in Figure 7-1 using UCS × SR = 120 MPa, given by /Martin et al. 1995/. Despite the problem with the extensive microcracking in the AECL CSIR data producing a highly nonlinear response (/Martin 1990/ suggested not to use the data to estimate the in situ stress state), the data provides a lower bound estimate for the stress magnitudes. The DDGS results provides an upper bound for the data as would be expected based on the findings of /Christiansson and Janson 2002/. A summary of the values from Figure 7-1 that satisfies Equations 4 and 5 for the overcore data and doorstopper are provided in Table 7-1 and compared to the back-calculated best estimate. The values in Table 7-1 illustrate that the error in the predicted value for σ_1 is approximately 10 and 13%, while the error in the predicted value for σ_2 ranges between 26 and 33%. It is clear from Table 7-1 and Figure 7-1 that the magnitude of the error is related to the method and the largest error is associated with the predicted magnitudes for σ_2. Regardless of the errors in the data, both data sets predicted that the in situ stress state would cause stress concentrations on the the boundary of vertical circular excavations to exceed the initiation for spalling and this was observed during construction of the URL circular shaft at the 420 level /Martin 1989/.

Table 7-1. Summary of the principal stress magnitudes predicted using the σ_1/σ_2 ratio and mean stress compared to the best estimate for the AECL's Mine-by Experiment on the 420 m Level of AECL's URL.

Method	σ_1 (MPa)	σ_2 (MPa)	Spalling Ratio	Comments
Mine-by	60	45	0.64	R = 1.25,M = 38.6 MPa
Best Estimate				data from Read /1994/
CSIR Overcore	52	33	0.59	R = 1.6,M = 32 MPa, data from /Martin 1990/
Door Stopper	66	60	0.66	R = 1.1,M = 46 MPa, data from /Thompson and Chandler 2004/

7.2 Target Area stress magnitudes: 0 to 1,000 m

The same methodology used in the example above was applied to the Forsmark overcore data to establish the likely stress state at four depth ranges: 0–150 m, 150–300 m, 300–400 m and 400–1,000 m. These depth ranges were selected based on the trends established in Figure 6–5. The depth range 0–150 m corresponds to fracture domain FFM02 and represents the stresses in the rock mass containing the majority of the open fractures encountered at Forsmark. The three other depth ranges are located in fracture domain FFM01 (150 to 300 m, 300 to 400 m, 400 to 500 m). The changes in the horizontal stress magnitudes from 150 to 400 m are thought to reflect the decreasing open fracture frequency with depth and the increasing rock mass quality.

7.2.1 FFM02: 0 to 150 m depth

The significant number of open highly conductive gently dipping fractures suggests that the stress state in this fracture domain could show the greatest variability in stress magnitude and orientation. While this may be true, the construction of the SFR facility to a depth of 140 m or the water intake tunnels for the nuclear power plant has demonstrated that if this variability existed it did not impact on the construction of the facility.

The horizontal stress magnitudes at 150 m depth were established using:

$$\left.\begin{array}{l} R = 1.7 \\ M = 12 \text{ MPa} \end{array}\right\} \sigma_1 = 20 \text{ MPa, and } \sigma_2 = 12 \text{ MPa} \qquad (7)$$

7.2.2 FFM01: 150 to 300 m depth

At this depth range there is less scatter in the overcore data which is consistent with the notion that the frequency of open fractures is decreasing and the rock mass quality is increasing.

The horizontal stress magnitudes at 300 m depth were established using:

$$\left.\begin{array}{l} R = 1.7 \\ M = 17.5 \text{ MPa} \end{array}\right\} \sigma_1 = 28 \text{ MPa, and } \sigma_2 = 16.5 \text{ MPa} \qquad (8)$$

The predicted σ_2 stress magnitude of 16.5 MPa is only slightly lower than that suggested in Figure 6-12 and also is similar to several of the measured hydraulic fracturing values between 250 and 300 m depth given in Figure 6-11.

7.2.3 FFM01: 300 to 400 m depth

In this depth range the number of overcore measurements is significantly reduced and the scatter in the mean stress magnitudes is significantly reduced (see Figure 6-4b). Whether this is fortuitous or simply a function of the lack of measurements is unknown. Nonetheless the number of open fractures significantly decreases at 400 m depth and this reduction in the range of mean stresses may simply reflect the improved rock mass quality.

The horizontal stress magnitudes at 400 m depth were established using:

$$\left.\begin{array}{l} R = 1.7 \\ M = 24 \text{ MPa} \end{array}\right\} \sigma_1 = 38.6 \text{ MPa, and } \sigma_2 = 22.7 \text{ MPa} \qquad (9)$$

7.2.4 FFM01: 400 to > 500 m depth

In this depth range the number of overcore measurements is significantly reduced and the scatter in the mean stress magnitudes is significantly increased (see Figure 6-4b). The increase in the mean stress is unusually large and there is no significant changes in the rock mass quality or other geological features such as a major deformation zone at this depth to explain the anomalous results. These anomalous mean magnitudes are associate with DBT1 while the mean stress values from KFM01B at approximately 460 m depth give mean stress values between 24.5 and 26 MPa which is consistent with the means stress values from DBT1 at approximately 400 m depth. It appears that the elevated mean stress values in this depth range in DBT1 may be related to other factors, i.e, possibly related to the thermal issues discussed previously, and have not been included in establishing the horizontal stress magnitudes.

While no overcore stress measurement have been conducted at a depth of 1,000 m, an upper bound approach can be used to estimate the stress magnitudes. If we assume that the stress magnitudes at 1,000 m depth are sufficient to initiate borehole breakouts in a vertical borehole, the σ_1 and σ_2 magnitudes can be estimated using the same methodology used above. Assuming that the σ_1/σ_2 ratio will remain constant at 1.7, because of the relatively uniform rock mass conditions below 400 m, and that borehole breakouts initiate when $3\sigma_1 - \sigma_2 = 230 \times 0.56 = 129$ MPa, then $\sigma_1 \approx 53$ MPa and $\sigma_2 \approx 31$ MPa at 1,000 m depth. As discussed previously, there is no evidence from the televiewer surveys that classical stress-induced borehole breakouts (spalling) actually initiate around 1,000 m depth. Therefore these stress magnitudes may represent an upper limit. The assumption in this analysis is that the principal stress ratio R will remain constant at 1.7. While this seems probable from the data set above 400 m it means that σ_2 magnitudes will decrease with depth and at approximately 1,250 m depth σ_2 will equal the vertical stress. While this is possible it implies that the fault regime will change from a thrust to a strike-slip, and there is no evidence from the regional seismicity or the Site Descriptive Model that this condition exists at Forsmark. Hence it is more likely that the horizontal stress ratio will not remain constant but decrease slightly with depth.

The horizontal stress magnitudes at 500 m depth were established by establishing stress gradients between 400 m depth and 1,000 m depth. For these gradients it is assumed that the gradient for σ_2 will be approximately the same as σ_1. Figure 7-2 shows the horizontal stress magnitudes and the estimated spalling strength. Figure 7-2 illustrates that vertical circular excavations should be stable at the depth of the repository, approximately 500 m. These same gradients projected to 1,000 m would suggest the vertical boreholes should also be stable with a safety factor of approximately 10%, which is also consistent with observations from the site investigations.

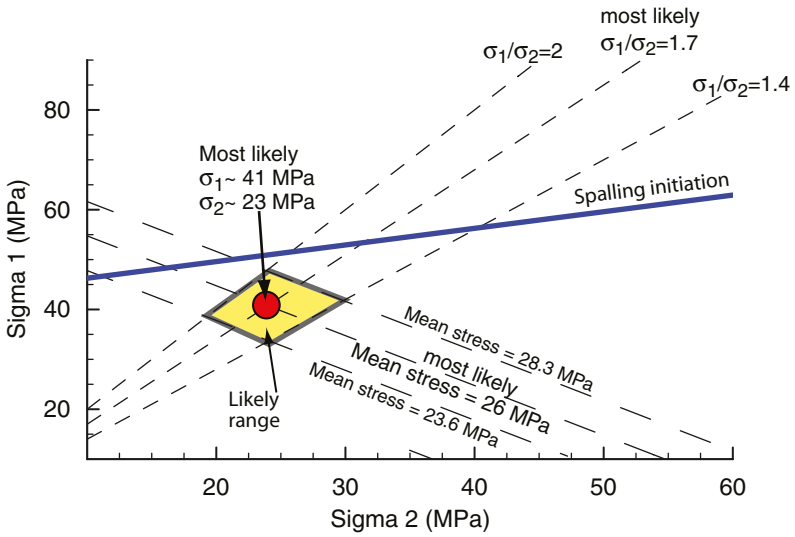

Figure 7-2. *Example of the application of stress ratio and mean stress to determine the magnitudes of σ_1 and σ_2 at a depth of 500 m at Forsmark. The likely range in values are provided as well as the most likely value.*

Figure 7-2 shows the range in horizontal stress magnitudes for different σ_1/σ_2 ratios. Figure 6-6a shows that below 400 m depth this ratio is well constrained and ranges from approximately 1.4 to 2 with a median value of 1.7 (most likely value in Figure 7-2). Figure 7-2 shows that for the measured range in the ratio σ_1/σ_2, the mean stress values are reasonably well constrained and could range from 23.6 to 28.3 MPa. It is clear from Figure 7-2 that if the most likely ratio of σ_1/σ_2 is valid the mean stress cannot be too large since this would imply spalling occurs in vertical boreholes at 500 m depth. As mentioned in Section 4 there is no evidence for spalling in vertical boreholes between 500 and and 1,000 m depth and hence the errors in the ratio of σ_1/σ_2 and the mean stress may not be large.

7.3 Target Area stress gradients: 0 to 600 m

The stress magnitudes at each of the depth ranges discussed above were used to establish the stress gradients for three depth ranges (0–150, 150–400, 400–600 m, Table 7-2). These three gradients have been plotted in Figure 7-3 which also contains the original stress data used to establish these stress gradients. The gradients are expressed as horizontal and vertical stresses because of the less than 5°plunge in the maximum principal stress. Figures 7-3a and 7-3b compares the maximum and intermediate principal stress magnitudes with the predicted stress gradients regardless of the Azimuth of the maximum horizontal stress. Figures 7-3c and 7-3d shows the same stress gradients but with data resolved in the most likely direction of the maximum principal stress (σ_1, Azimuth 145°) and the intermediate principal stress (σ_2, Azimuth 55°). In both cases the trends provide a reasonable fit to the data. Also shown in Figure 7-3 are the mean σ_1 and σ_2 magnitudes for each of the depth ranges shown in Figure 6-14.

Figure 7-3b and 7-3d contains all the overcoring data, as well as the hydraulic fracturing data which was in the same directions as the overcoring σ_2 data, and discussed in Section 6.4. It is evident from Figure 7-3 that the hydraulic fracturing data shows essentially no correlation with the overcoring data at the proposed depth of the repository. The trends in Figure 7-3 also supports the notion that the component of the stress tensor measured by the hydraulic fracturing and HTPF is closer to the weight of the overburden than the minimum horizontal stress.

7.4 Stress modelling of deformation zones

Stress modelling of the Forsmark site was carried out using the three dimensional numerical program 3DEC to assess the impact of the major deformation zones on the spatial distribution of the in situ stress magnitudes and orientations /Mas Ivars and Hakami 2005, Hakami 2006/. The stress models included the near vertical Singö and Forsmark Faults as well as the gently dipping deformation zone ZFMA2. The simulations were carried out by applying displacement boundary conditions to reflect the present day crustal shortening.

Table 7-2. Recommended horizontal and vertical stress gradients for the Forsmark Target Area where the depth below surface is z in metres.

Depth range (m)	σH (MPa)	Trend (°)	σh (MPa)	Trend (°)	σvert (MPa)
0-150	19 + 0.008z	145	11 + 0.006z	055	0.0265z
150-400	9.1 + 0.074z	145	6.8 + 0.034z	055	0.0265z
400-600	29.5 + 0.023z	145	9.2 + 0.028z	055	0.0265z

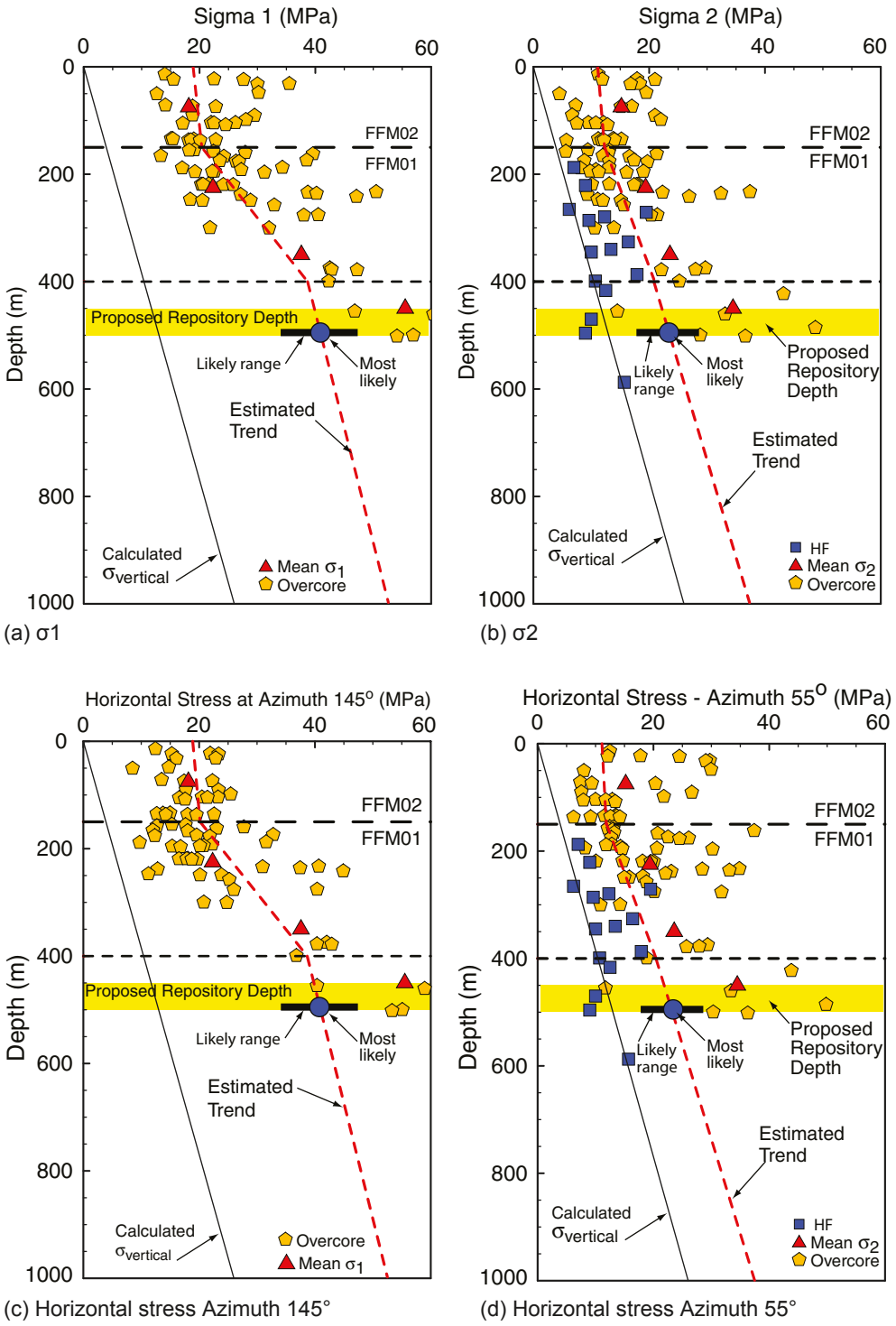

Figure 7-3. *Recommended stress gradients compared to measured overcore and hydraulic fracturing values.*

Based on the regional modelling results, /Hakami 2006/ concluded that the subvertical deformation zones that were slightly inclined to the direction of the maximum horizontal stress (Singö and Forsmark Faults) did not significantly impact either the stress magnitudes or orientations. However, /Hakami 2006/ noted a significant re-distribution of the in situ stress field took place within and around the rock wedge bounded in part by the gently dipping fracture zones, i.e. ZFMA2./ Mas Ivars and Hakami 2005/ concluded that when the gently dipping deformation zone was included in the model, there was a stress release above the deformation zone that significantly reduced the horizontal stress magnitudes. In some cases a stress release of about

18 MPa occurred. This finding is supported by the work of /Martin and Chandler 1993/ who showed that both stress magnitudes and orientations could be significantly affected by major subhorizontal faults. It should be noted that while the results from /Mas Ivars and Hakami 2005/ showed a significant stress release above the gently dipping fracture zone there was no significant affect on the direction of the in situ stresses.

Overcore measurements were conducted in borehole KFM02B located at Drill Site 2. This borehole penetrated fracture domain FFM03 and the gently dipping deformation zone ZFMA2 (see Figure 2-5). Thirteen overcore measurements were carried out between a depth of approximately 110 m and 312 m. These measurements gave approximately the same average Azimuth (137°) for the maximum horizontal stress as the other overcore stress data in the Target Area. However, the average horizontal stress magnitude (≈ 11 MPa) was approximately 50% lower compared to the horizontal stress magnitude (≈ 24 MPa) at comparable depths in the Target Area. No successful stress measurements were carried out below ZFMA2 and the borehole was terminated at approximately 500 m depth. Hence it is not known if the lower horizontal stress magnitudes exist below ZFMA2. Nonetheless, the results do support the findings from the stress modelling that stress release, resulting in lower horizontal stress magnitudes, has occurred above ZFMA2.

7.5 Variability and uncertainty in recommended stress gradients

The results from the stress measurement campaigns show significant scatter. This scatter can be attributed to two sources: (1) scatter associated with systematic errors and (2) scatter associated with spatial variability. The former are caused by biases within the instrumentation and measurement procedures, e.g. orientation of the instrument or fracture, temperature changes, etc. These types of errors are handled by first identifying them and then improving the instrumentation or testing procedure. The attempts to identify these errors during the stress campaigns are discussed in this report. Minimising these errors in future stress measurement campaigns will require additional instrumentation development and/or modifications.

The natural spatial variability of in situ stress cannot be avoided but can normally be handled statistically during data analysis. /Martin et al. 1990/ showed that the scatter in small-scale measurements in relatively good quality rock tended to be larger then the scatter observed in large scale measurements. More importantly they showed that one large scale measurement provided approximately the mean value of many small scale measurements. Figure 7-4 shows the data provided in /Martin et al. 1990/ but converted to the mean stress. It is clear in Figure 7-4

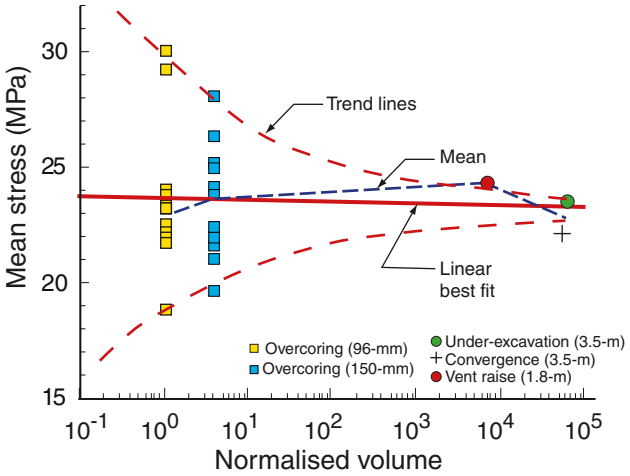

Figure 7-4. *Effect of scale on the mean stress, data from /Martin et al. 1990/.*

that spatial variability of the mean stress magnitude at the scale of a tunnel excavation is considerably less than the spatial variability of the mean stress magnitude from overcore tests. While the trends in Figure 7-4 are encouraging, it was not possible to establish the scatter associated with the large scale measurements for the data used by /Martin et al. 1990/ since only a single data-point could be determined for each of the large-scale tests.

/Read 1994/ using deformation measurements from 8 radial extensometers installed ahead of a 3.5-m-diameter circular tunnel was able to show, using rigourous statistical treatment of the data, that the stress tensor determined from large scale measurements supported the findings reported by /Martin et al. 1990/. /Read 1994/ showed that the range in the large-scale measurement was in fact much smaller than that obtained from small scale measurements. The range in stress magnitudes and orientations reported by /Read 1994/ for each of the principal stresses are given in Table 7-3.

The mean stress magnitude for the stress tensor given in Table 7-3 is (60 + 45 + 11)/3 = 38.7 MPa. The possible variability in the mean stress was determined by assigning a triangular distribution to each of the principal stresses with the errors given in Table 7-3 as the minimum and maximum values. Figure 7-5 gives the error in the mean stress and shows for this particular case that the mean stress could range from 35.7 to 41.6 MPa. While the range in the maximum principal stress varied from ±5% the mean stress varied approximately ±7.6%. Surprisingly, the orientations determined by /Read 1994/ were very robust and consistent. /Read et al. 1995/ later confirmed the stress orientations using a completely different approach. It is likely that these results may represent the minimum uncertainty achievable in determining stress magnitudes, as the tunnel was excavated using non-destructive techniques in a homogeneous massive rock where the environmental boundary conditions (humidity and temperature) were controlled.

Table 7-3. Summary of the in situ stress tensor determined by /Read 1994/ using 8 radial extensometers for a 3.5-diameter circular tunnel.

	σ1	σ2	σ3
Magnitudes (MPa)	60 ± 3	45 ± 4	11 ± 4
Trend/Plunge (°)	145/11	054/08	290/77

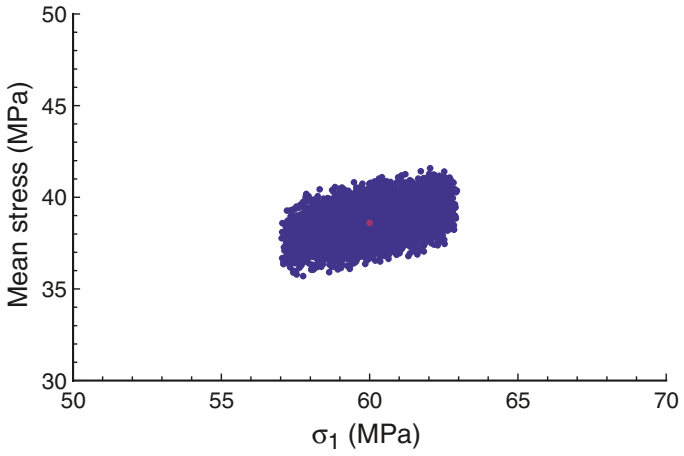

Figure 7-5. *Error in the mean stress for the stress tensor given in Table 7-3.*

The scatter in the stress magnitudes from the Forsmark stress measurement campaigns are clearly much larger than those given by /Read 1994/. This scatter can be attributed to stress measurement method uncertainty and stress spatial variability. However, as indicated throughout this report it is practically impossible to separate method uncertainty from spatial variability, and as shown by /Read 1994/ regardless of the methods used there will always be uncertainty associated with the results. The stress gradients given in Table 7-2 were provided as the best estimate based on an overall evaluation of all the results from the stress measurement campaigns, indirect observations and geological setting, following the integration/consistency steps outlined in the flow chart given in Figure 1-1. Table 7-4 gives the most likely value and and the likely range in the stress gradients for the Target Area. The likely range decreases slightly with depth reflecting the notion that the rock mass is more uniform with depth, which is in keeping with the geological model for the site.

Table 7-4. Recommended most likely value and likely range in horizontal and vertical stress gradients for the Forsmark Target Area where the depth below surface is z in metres. The range in vertical stress gradient is related to the variability in rock mass density.

Depth range (m)	σ_H (MPa)	Trend (°)	σ_h (MPa)	Trend (°)	σ_{vert} (MPa)
0–150	19 + 0.008z, ± 20%	145 ± 20	11 + 0.006z, ± 25%	055	0.0265z, ± 0.0005
150–400	9.1 + 0.074z, ± 15%	145 ± 15	6.8 + 0.034z, ± 25%	055	0.0265z, ± 0.0005
400–600	29.5 + 0.023z, ± 15%	145 ± 15	9.2 + 0.028z, ± 20%	055	0.0265z, ± 0.0005

8 Discussions and conclusions

/Stephansson et al. 1991/ concluded from approximately 500 stress measurements that in the Fennoscandia shield: (1) there is a large horizontal stress component in the uppermost 1,000 m of bedrock, and (2) the maximum and minimum horizontal stresses exceed the vertical stress assuming the vertical stress is estimated from the weight of the overburden. In addition, based on the findings from the World Stress Map the orientation of the maximum horizontal stress in Scandinavia was expected to be in the SE-NW direction, i.e. Azimuth approximately 130–140 degrees. Hence prior to the investigations at Forsmark, the in situ stress magnitudes and orientations were expected to be constrained by these findings.

The in situ stress state in a rock mass is a consequence of its geological history and the current tectonic boundary conditions. The approximately 50 km thick crust of this portion of the Scandinavian Shield formed approximately 1.8 billion years ago and since then has undergone several periods of deformation. Despite these deformation periods the rock mass within the Target Area is considered relatively uniform being bounded by two major deformation zones: the Singö and Forsmark Faults. According to /Hakami 2006/ these major deformation zones appear to have little influence on the current stress state at Forsmark. Within the Target Area, the rock mass has two significant fracture domains: FFM01 and FFM02. FFM02 is considered a blocky rock mass with several fracture sets while FFM01 contains few open fractures and can be considered as sparsely fractured to massive.

Several stress campaigns involving both overcoring and hydraulic fracturing, including hydraulic testing of pre-existing fractures, have been carried out at Forsmark to establish the in situ stress state. The results from the initial campaigns, which supported the 1991 findings by /Stephansson et al. 1991/, were summarised by /Sjöberg et al. 2005/ and formed the bases for the stresses provided in the Site Descriptive Model version 1.2 /SKB 2005a/. Since then additional stress measurement campaigns have been completed and have confirmed the earlier findings. In addition to these measurements the following additional studies were undertaken to aid in assessing the stress state at Forsmark.

1. A detailed televiewer survey of approximately 6,900 m of borehole walls was carried out to assess borehole wall damage, i.e, borehole breakouts, to depths of 1,000 m.

   Findings: The study concluded that less than 16% of the boreholes surveyed had some form of breakout but only 3% of the survey length displayed stress-induced breakouts. Of these 68% were associated with geological structure/fractures. The Azimuth of the horizontal stress inducing these breakouts not associated with structure was 135°.

2. Evaluation of nonlinear strains in laboratory samples to depths of approximately 800 m to assess if stress magnitudes were sufficient to create stress-induced microcracking.

   Findings: There was no evidence from the stress-strain behaviour of laboratory samples to depths of 700 m that the in situ stress magnitudes were sufficient to create significant stress-induced microcracking. Based on empirical experience this suggest that σ_1/σ_c is less than 0.2, i.e, less than approximately $\sigma_1 < 50$ MPa.

3. Assessment of the magnitudes required to cause core disking and survey of core disking observed at Forsmark.

   Findings: Solid core disking appears as a random occurrence in a few short sections (< 0.5 m length) in the boreholes drilled to 100 m depth and were frequently associated with pegmatite and the end of the core-run. There is no evidence to suggest that the frequency of core disking increases with depth and hence supports the notion that the horizontal stress magnitudes are not significantly increasing with depth. Ring core disking is commonly observed during the overcoring process, caused in part by the thin (≈ 12 mm) overcore cylinder and possibly the drill bit temperature. Numerical analyses of solid core disking suggests that the maximum horizontal stress at 500 m depth could range between 35 and 55 MPa, while the minimum horizontal stress would range between 20 and 30 MPa.

The extensive effort to measure the stress state at Forsmark, while confirming the expected regional trends, have identified several keys issues that may be unique to Forsmark site and have impacted the results from the overcoring and hydraulic fracturing stress measurement campaigns. These are summarised below.

Hydraulic fracturing

1. When hydraulic fracturing is carried out in vertical or near vertical boreholes the interpreted stress is expected to be the minimum horizontal stress (σ_{hmin}). The stress magnitudes from the hydraulic fracturing campaigns provided stress magnitudes that were consistently lower than the minimum horizontal stress magnitudes obtained from the overcoring campaigns at comparable depths.
2. The majority of the stress magnitudes determined from the hydraulic fracturing campaigns were close to the calculated weight of the overburden and many of the measurements below 400 m depth were less than the calculated weight of the overburden. This was especially noticeable in the second hydraulic fracturing campaign when the amount of water injected during the first cycle was controlled to a relatively small volume.
3. The stress magnitudes acting normal to pre-existing fractures that were identified as suitably oriented to provide the minimum horizontal stress still provided stress magnitudes considerably lower than the corresponding overcore stress magnitudes.
4. The correlation of the hydraulic fracturing results with the calculated vertical stress supports the notion by /Doe et al. 2006/ that in a geological thrust regime the application of hydraulic fracturing in vertical boreholes to measure horizontal stresses is not appropriate. The Forsmark results indicates the hydraulic fracturing method in vertical and near vertical boreholes measures some component of the stress tensor that is significantly less than the minimum horizontal stress.

Overcoring

Despite the extensive quality control procedures and development of the technique that was carried out during the Forsmark Site Investigation Phase, the success rate of acceptable test results using the Borre Probe was only 30%. The low success rate may be a related to the Forsmark geology (20–40% quartz content) which required significantly more energy to drill than the rock mass at Oskarshamn, likely causing elevated temperatures at the drill bit.

1. Unstable strain readings during biaxial testing resulted in many low quality biaxial test results that showed significant hysteresis, making it difficult to determine the Young's modulus and Poisson's ratio of the overcored hollow cylinder.
2. Nearly all the overcore results showed an unusual rapid reduction in the measured strain response immediately after the overcoring bit passed the strain cell.
3. An extensive investigation into the effect of microcracking on the overcore and biaxial results from KFM07C showed that the effect of microcracking is minor and and cannot be used to explain the unusual strain response during overcoring and biaxial testing.
4. Preliminary numerical analyses of simulated overcoring indicates the unusual strain response is likely thermally-induced. The full impact of this thermal response on the overcore results is unknown at the time of this report. However, this thermal response will effect the calculated stress magnitudes and may be the source of the hysteresis observed in the biaxial tests. These affects are currently under investigation.
5. The thin-wall overcore cylinder produced by the Borre Probe makes it very susceptible to thermally-induced effects. The elevated stresses resulting from these thermal-affects may be the main reason for the significant occurrence of ring-disking encountered at Forsmark.

6. The manufacturer of the Borre Probe should consider modifying the probe from its current configuration such that the temperature is recorded at the strain gauges and not the data logger. The data logger temperature only changed a few degrees but the thermally-induced strains suggest much higher temperatures were occurring in the vicinity of the strain gauges. Modification of the flushing procedures and flushing gap should also be considered but only measuring the temperature at the strain gauge location will show if the temperature was adequately controlled during overcoring.

Data analysis

The magnitudes and orientations from the stress measurement campaigns were analysed to establish the best estimate of the stress magnitudes and orientations within the Target Area and at the proposed repository depth. The overcore data were first analysed in terms of the principal stresses (σ_1, σ_2, σ_3) and the horizontal maximum (σ_H) and minimum (σ_h) stress. An attempt was made to resolve the stress magnitudes from the overcoring and hydraulic fracturing for the minimum horizontal stress. However, the data suggests that the overcoring and hydraulic fracturing techniques are not measuring the same component of the tress tensor despite taking the magnitudes in approximately the same orientation. The hydraulic fracturing stress magnitudes were significantly less than the overcore magnitudes.

The mean stress expressed as $(\sigma_1 + \sigma_2 + \sigma_3)/3$ and the stress ratios (σ_1/σ_2, σ_2/σ_3, σ_1/σ_3) were used in establishing trends in the data set. The trends were assessed using a moving-median data smoothing technique. The stress magnitudes were determined by constraining the mean stress and the ratio of σ_1/σ_2. It is suggested that the mean stress and stress ratios are less sensitive to the errors in the overcore data if the errors were thermally induced.

Recommended stress gradients and orientations

The magnitudes and orientations have been separated into four depth ranges: 0 to 150 m corresponding to fracture domain FFM02, and the three other depth ranges occurring in fracture domain FFM01 (150 to 300 m, 300 to 400 m, 400 to 1,000 m). The changes in the horizontal stress magnitudes from 150 to 400 m reflect the decreasing open fracture frequency with depth and the increasing rock mass quality. Below 400 m depth the rock mass is characterised as sparsely fractured and massive, and the stress gradients below 400 m are expected to continue to greater depths. The recommended stress magnitudes (stress gradients) and orientations with depth are given in Table 7-2 with the anticipated range in these values given in Table 7-4. The gradients are expressed as maximum and minimum horizontal stress because the maximum principal stress appears to have a plunge of approximately 5°.

The orientations for the maximum horizontal stress are based primarily on the overcoring measurements. The mean stress tensor was compiled from 26, 35, 5, and 6 overcore measurements in each of the 4 depth ranges, 0–150 m, 150–300 m, 300–400 m, and > 400 m, respectively. These measurements gave a mean orientation for σ_1 of 139, 150, 145 and 144° and agreed with the orientations from the borehole breakout survey and the regional direction of maximum compression.

Stress data and design

Despite the extensive efforts made during the Forsmark Complete Site Investigation Phase, measuring the state of stress in the Forsmark Target Area to depths of 1,000 m has been challenging and has demonstrated the difficulty of measuring stress in deep 76-mm-diameter surface-drilled boreholes. It is very doubtful if additional efforts using surface based boreholes will provide more reliable information at the proposed depths of the repository (400 to 500 m).

At the proposed repository depth, it is adequate for Design Step D2 to assume that the recommended stress gradients are relatively uniform across site. This assumption is consistent with the relatively uniform geological conditions for the site at the repository depth and the stress modelling results by /Hakami 2006/ and /Mas Ivars and Hakami 2005/.

The Observation Method is a major component of the underground design strategy outlined in SKB's Design Premises /SKB 2004/. The stress data provided in this report is adequate for design step D2. However, in keeping with the Observation Method, the impact of underestimating the stress magnitudes should be considered during this design step. In preparation for construction and the verification of the design assumptions, this Design Step should prepare a plan for stress measurements during construction. Many of the issues encountered in the overcoring campaigns to date can be readily managed or eliminated when applying the overcoring technique from underground openings. In addition, as demonstrated by /Andersson 2007/ routine convergence monitoring of large scale excavations can be readily used to determine the in situ stress magnitudes and orientations.

References

Anderson E M, 1951. The dynamics of faulting. Oliver & Boyd, Edinburgh.

Andersson C J, 2007. Äspö Hard Rock Laboratory. Äspö pillar stability experiment, Final report. Rock mass response to coupled mechanical thermal loading. SKB TR 07-01, Svensk Kärnbränslehantering AB.

Arjang B, Herget G, 1997. In situ ground stresses in the Canadian hardrock mines: an update. International Journal Rock Mechanics And Mining Science, 34(3/4):652, paper No. 015.

Ask M V S, Ask D, Christiansson R, 2006. Detection of borehole breakouts at the Forsmark Site, Sweden. In Proceedings of International Symposium on In-situ Rock Stress, Trondheim (Eds. Lu M, Li CC, Kjorholt H, Dahle H), pp. 79–86, A.A. Balkema, Rotterdam.

Bartlett W L, Friedman M, Logan J M, 1981. Experimental folding and faulting of rocks under confining pressure. part ix. wrench faults in limestone layers. Tectonophysics, 79:255–277.

Barton N, 1988. Discontinuum modelling of URL Shaft excavation response. Tech. rep. Atomic Energy of Canada Limited.

Barton N, By T L, Chryssanthakis P, Tunbridge L, Kristiansen J, Løset F, Bhasin R K, Westerdahl H, Vik G, 1994. Predicted and measured performance of the 62 m span Norwegian Olympic Ice Hockey Cavern at Gjøvik. International Journal Rock Mechanics Mining Science & Geomechanics Abstracts, 31(6):617–641.

Bell J S, Gough D I, 1979. Northeast-southwest compressive stress in Alberta: Evidence from oil wells. Earth Planet. Sci. Lett. 45:475–482.

Brown E T, Hoek E, 1978. Trends in relationships between measured and in situ stresses and depth. International Journal Rock Mechanics Mining Science & Geomechanics Abstracts, 15:211–215.

Carlsson A, Christiansson R, 1986. Rock stress and geological structures in the Forsmark area. In Proc. Int. Symp. on Rock Stress and Rock Stress Measurements, Stockholm (Ed. Stephansson O), pp. 457–465, Centek Publishers, Lulea.

Carlsson A, Christiansson R, 1987. Geology and tectonics at Forsmark, Sweden. Tech. Rep. U(B) 1987/42, Vattenfall – Swedish State Power Poard.

Carlsson A, Christiansson R, 2007. Construction experiences from underground works at Forsmark. SKB R-07-10, Svensk Kärnbränslehantering AB.

Carlsson A, Olsson T, 1982. Rock stresses as a consequence of glaciation. Nature, 298:739–742.

Cartwright P B, 1997. A review of recent in-situ stress measurements in United Kingdom coal measures strata. In Proc. Int. Symp. on Rock Stress, Kumamoto (Eds. Sugawara K, Obara Y), pp. 469–474, A. A. Balkema, Rotterdam.

Castro L A M, 1996. Analysis of Stress-induced Damage Initiation around Deep Openings Excavated in a Moderately Jointed Brittle Rock Mass. Ph.D. thesis, Civil Engineering Department, University of Toronto, Toronto, Ontario, Canada.

Chernis P J, 1984. Comparison of the pore-microstructure of shallow and deep samples of the Lac du Bonnet granite. Technical Record 223, Atomic Energy of Canada Limited.

Christiansson R, Hudson J A, 2003. ISRM Suggested Methods for rock stress estimation – Part 4: Quality control of rock stress estimation. International Journal Rock Mechanics And Mining Science, 40(7–8):1021–1026.

Christiansson R, Janson T, 2002. Test with three different stress measurement methods in two orthogonal bore holes. In Proceedings Fifth North American Rock Mechanics Symposium and the 17th Tunnelling Association of Canada Conference, Toronto (Eds. Hammah R, Baden W, Curran J, Telesnicki M), vol. 2, p. 1429–1436, University of Toronto Press, Toronto.

Cloos E, 1955. Experimental analysis of fracture patterns. Bull. Geol. Soc. of Am. 66:241–256.

Corkum A, Martin C D, 2007. The mechanical behaviour of weak mudstone (Opalinus Clay) at low stresses. International Journal Rock Mechanics And Mining Science, 44(2):196–209.

Doe TW, Zieger M, Enachescu C, Böhner J, 2006. In-situ stress measurements in exploratory boreholes. Felsbau, 24(4):39–47.

Evans K, Engelder T, 1989. Some problems in estimating horizontal stress magnitude in thurst regimes. International Journal Rock Mechanics Mining Science & Geomechanics Abstracts, 26(6):647–660.

Everitt R A, Lajtai E Z, 2004. The influence of rock fabric on excavation damage in the Lac du Bonnet granite. International Journal Rock Mechanics And Mining Science, 41(8):1277–1303.

Fredriksson A, Hässler L, Söderberg L, 2001. Extension of CLAB – Numerical modelling, deformation mesaurements and comparison of forecast with outcome. In Proc. ISRM Regional Symposium EUROCK2001, Espoo, Finland (Eds. Särkkä P, Eloranta P), pp. 743–747, A.A. Balkema, Rotterdam.

Haimson B C, Cornet F H, 2003. ISRM Suggested Methods for rock stress estimation – Part 3: hydraulic fracturing (HF) and/or hydraulic testing of pre-existing fracture (HTPF). International Journal Rock Mechanics And Mining Science, 40(7–8):1011–1020.

Hakala M, 1999. Numerical study on core damage and interpretation of in-situ state of stress. Tech. Rep. POSIVA-99-25, Posiva Oy, Helsinki, Finland.

Hakala M, Hudson J A, Christiansson R, 2003. Quality control of overcoring stress measurement data. International Journal Rock Mechanics And Mining Science, 40(7–8):1141–1159.

Hakami H, 2006. Numerical studies on spatial variation of the in situ stress filed at Forsmark – A further step. Site descriptive modelling Forsmark – stage 2.1. SKB R-06-124, Svensk Kärnbränslehantering AB.

Harrison J P, Hudson J A, Carter J N, 2007. Is there a relation between the in situ principal stress magnitudes in rock masses? In Proceedings 1st Canada-U.S. Rock Mechanics Symposium, Vancouver.

Hast N, 1969. The state of stress in the upper part of the earth's crust. Tectonophysics, 8(3):169–211.

Hast N, 1973. Global measurements of absolute stress. Philosophical Transactions of the Royal Society of London. Series A, Mathematical and Physical Sciences, 274(1239):409–419.

Herget G, Arjang B, 1990. Update on ground stresses in the Canadian Shield. In Proc. Stresses in Underground Structures, Ottawa (Eds. Herget G, Arjang B, Bétournay M, Gyenge M, Vongpaisal S, Yu Y), pp. 33–47, Canadian Government Publishing Centre, Ottawa, Canada.

Hicks E C, Bungum H, Lindholm C D, 2000. Stress inversion of earthquake focal mechanism solutions from onshore and offshore Norway. Norsk Geologisk Tidsskrift, 80:235–250.

Hoek E, Brown E T, 1980. Underground Excavations in Rock. The Institution of Mining and Metallurgy, London.

Hudson J A, Cornet F H, Christiansson R, 2003. ISRM Suggested Methods for rock stress estimation – Part 1: Strategy for rock stress estimation. International Journal Rock Mechanics And Mining Science, 40(7–8):991–998.

Jacobsson L, Flansbjer M, Christiansson R, Jansson T, 2007. Measurement of micro crack volume in low porosity crystalline rock. In Proceedings 11th Congress of the International Society for Rock Mechanics, Lisbon (Eds. e Sousa LR, Olalla C, Grossmann N), vol. 1, pp. 55–58, Taylor & Francis Group, London.

Jaeger J C, Cook N G W, 1963. Pinching-off and disking of rocks. Journal Geophysical Research, 888(6):1759–1765.

Jaeger J C, Cook N G W, 1979. Fundamentals of Rock Mechanics. Chapman and Hall, London, third edn.

Juhlin C, Bergman B, Palm H, 2002. Reflection seismic studies in the Forsmark area – stage 1. SKB R-02-43, Svensk Kärnbränslehantering AB.

Juhlin C, Stephens M B, 2006. Gently dipping fracture zones in Paleoproterozoic metagranite, Sweden: Evidence from reflection seismic and cored borehole data and implications for the disposal of nuclear waste. Journal Geophysical Research, 111(B09302).

Kinck J J, Husebye E S, Larsson F R, 1993. The Moho depth distribution in Fennoscandia and the regional tectonic evolution from Archean to Permian times. Precambrian Research, 64:23–51.

King MS, 1983. Static and dynamic elastic properties of rocks from the canadian shield. International Journal Rock Mechanics Mining Science & Geomechanics Abstracts, 20(5):237–241.

Klee G, Rummel F, 2004. Forsmark site investigation – rock stress measurements with hydraulic fracturing and hydraulic testing of pre-existing fractures in borehole kfm01a, kfm01b, kfm02a and kfm04a results of in-situ tests. SKB P-04-311, Svensk Kärnbränslehantering AB.

Lee MF, Mollison LJ, Mikula P, Pascoe M, 2006. In-situ rock stress measurements in Western Australia's Yilgarn Craton. In Proceedings of International Symposium on In-situ Rock Stress, Trondheim (Eds. Lu M, Li CC, Kjorholt H, Dahle H), pp. 35–42, A.A. Balkema, Rotterdam.

Lim S S, In Progress. In-situ stress magnitudes from core damage processes. Ph.D. thesis, Dept. Civil & Environmental Engineering, University of Alberta, Edmonton, Alberta, Canada.

Lim S S, Martin C D, Christiansson R, 2006. Estimating in-situ stress magnitudes from core disking. In Proceedings of International Symposium on In-situ Rock Stress, Trondheim (Eds. Lu M, Li CC, Kjorholt H, Dahle H), pp. 159–166, A.A. Balkema, Rotterdam.

Lim S S, Martin C D, Christiansson R, 2007. In-situ stress estimation using crack closure energy in crystalline rock. In Proceedings 1st Canada-U.S. Rock Mechanics Symposium, Vancouver (Eds. Eberhardt E, Stead D, Morrison T), vol. 1, pp. 683–689, Taylor & Francis Group, London.

Lindfors U, Perman F, Ask M, 2007. Forsmark site investigation, Overcoring rock stress measurements in borehole KFM07C. SKB P-07-130, Svensk Kärnbränslehantering AB.

Lindfors U, Perman F, Sjöberg, 2005. Forsmark site investigation: Evaluation of the over-coring results from borehole KFM01B. SKB P-05-66, Svensk Kärnbränslehantering AB.

Ljunggren C, Changa Y, Janson T, Christiansson R, 2003. An overview of rock stress measurement methods. International Journal Rock Mechanics And Mining Science, 40(7–8):975–989.

Lund C E, Gorbatschev R, Smirnov A, 2001. A seismic model of the Precambrian crust along the coast of southeastern Sweden: the Coast Profile wide-angle airgun experiment and the southern part of FENNOLORA revisted. Tectonophysics, 339:93–111.

Marotta A M, Mitrovica J X, Sabadini R, Milne G, 2004. Combined effects of tectonics and glacial isostatic adjustment on intraplate deformation in central and northern europe: Applications to geodetic baseline analyses. Journal Geophysical Research, 109(B01413).

Martin C D, 1989. Failure observations and in situ stress domains at the Underground Research Laboratory. In Proc. Conf. on Rock Mech. and Rock Physics at Great Depth, Pau, France (Eds. Maury V, Fourmaintraux D), vol. 2, pp. 719–726, A.A. Balkema, Rottterdam.

Martin C D, 1990. Characterizing in situ stress domains at the AECL Underground Research Laboratory. Canadian Geotechnical Journal, 27:631–646.

Martin CD, Chandler NA, 1993. Stress heterogeneity and geological structures. International Journal Rock Mechanics Mining Science & Geomechanics Abstracts, 30(7):993–999.

Martin C D, Christainsson R, Söderhäll J, 2001. Rock stability considerations for siting and constructing a KBS3 repository: Based on experiences from Äspö HRL, AECL's URL, tunnelling and mining. SKB TR-01-38, Svensk Kärnbränslehantering AB.

Martin C D, Christiansson R, 1991a. Overcoring in highly stressed granite – Comparison of the the USBM and Modified CSIR devices. Rock Mechanics and Rock Engineering, 24(4):207–235.

Martin C D, Christiansson R, 1991b. Overcoring in highly stressed granite – The influence of microcracking. International Journal Rock Mechanics Mining Science & Geomechanics Abstracts, 28(1):53–70.

Martin C D, Kaiser P K, Christiansson R, 2003. Stress, instability and the design of underground excavations. International Journal Rock Mechanics And Mining Science, 40(7–8):1027–1047.

Martin C D, Martino J B, Dzik E J, 1994. Comparison of borehole breakouts from laboratory and field tests. In Proc. EUROCK'94, SPE/ISRM Rock Mechanics in Petroleum Engineering, Delft, pp. 183–190, A.A. Balkema, Rotterdam.

Martin CD, Read RS, 1996. AECL's Mine-by Experiment: A test tunnel in brittle rock. In Proc. 2nd North American Rock Mechanics Symposium, Montreal (Eds. Aubertin M, Hassani F, Mitri H), vol. 1, pp. 13–24, A.A. Balkema, Rotterdam.

Martin C D, Read R S, Chandler N A, 1990. Does scale influence in situ stress measurements?– Some findings at the Underground Research Laboratory. In Proc. First Int. Workshop on Scale Effects in Rock Masses, Loen, Norway (Ed. da Cunha AP), pp. 307–316, A.A. Balkema, Rotterdam.

Martin C D, Read RS, Dzik EJ, 1995. Near-face cracking and strength around underground openings. In Proc. 2nd Int. Conf. on Mechanics of Jointed and Faulted Rock, Vienna (Ed. Rossmanith HP), pp. 765–770, A.A. Balkema, Rotterdam.

Martin C D, Stimpson B, 1994. The effect of sample disturbance on laboratory properties of Lac du Bonnet granite. Canadian Geotechnical Journal, 31(5):692–702.

Mas Ivars D, Hakami H, 2005. Effect of a sub-horizontal fracture zone and rock mass heterogeneity on the stress field in Forsmark area – A numerical study using 3DEC Preliminary site description Forsmark area – version 1.2. SKB R-05-59, Svensk Kärnbränslehantering AB.

Morgenstern N R, Tchalenko J S, 1967. Microstructural observations on shear zones from slips in natural clays. In Proceedings of the Geotechnical Conference on Shear Strength of Natural Soils and Rocks, Oslo, vol. 1, pp. 147–152, Norwegian Geotechnical Institute, Oslo.

Müller B, Zoback M L, Fuchs K, Mastin L, Gregersen S, Pavoni N, Stephansson O, Ljunggren C, 1992. Regional patterns of tectonic stress in Europe. Journal of Geophysical Research, 97(B8):11783–11803.

Nocquet J M, Calais E, Parsons B, 2005. Geodetic constraints on glacial isostatic adjustment in Europe. Geophysical Research Letters, 32(L06308).

Obert L, Stephenson D E, 1965. Stress conditions under which core discing occurs. Transactions of the Society of Mining Engineers of the American Institute of Mining Engineers, 232(3):227–235.

Ojala V J, Kuivamäki A, Vuorela P, 2004. Postglacial deformation of bedrock in Finland. Report YST-120, Geological Survey of Finland, Nuclear Waste Disposal Research.

Olofsson I, Simeonov A, Stigsson M, Stephens M, Follin S, Nilsson A C, Röshoff K, Lindberg U, Lanaro F, Fredriksson L, Persson L, 2007. Site descriptive modelling Forsmark, stage 2.2, a fracture domain concept as a basis for the statistical modelling of fractures and minor deformation zones, and interdisciplinary coordination. SKB R-07-15, Svensk Kärnbränslehantering AB.

Perman F, Sjöberg J, 2003. Transient strain analysis of overcoring measurements in boreholes DBT-1 and DBT-3. SKB P-03-119, Svensk Kärnbränslehantering AB.

Read R S, 1994. Interpreting excavation-induced displacements around a tunnel in highly stressed granite. Ph.D. thesis, Department of Civil & Geological Engineering, University of Manitoba, Winnipeg, Manitoba, Canada.

Read R S, Martin C D, Dzik E J, 1995. Asymmetric borehole breakouts at the URL. In Proc. 35th U.S. Symp. on Rock Mechanics, Lake Tahoe (Eds. Daemen J, Schultz R), pp. 879–884, A.A. Balkema, Rotterdam.

Riedel W, 1929. Zur mechanik geologischer brucherscheinungen. Centralbl. f. Mineral. Geol. u. pal. B:354–368.

Ringgaard J, 2007a. Forsmark site investigation, mapping of borehole breakouts, processing of acoustical televiewerdata from KFM08A, KFM08C, KFM09A, KFM09AB and KFM90B. SKB P-07-166, Svensk Kärnbränslehantering AB.

Ringgaard J, 2007b. Mapping of borehole breakouts. processing of acoustical televiewer data from KFM01A, KFM01B, KFM02A, KFM03A, KFM03B, KFM04A, KFM05A, KFM06A and KFM07C. SKB P-07-07, Svensk Kärnbränslehantering AB.

Rothenburg L, Berlin A A, Bathurst R J, 1991. Microstructure of isotropic materials with negative Poisson's ratio. Nature, 354:470–472.

Rummel F, Weber U, 2004. Rock stress measurements with hydraulic fracturing and hydraulic testing of pre-existing fractures in borehole kfm01a, kfm01b, kfm02a and kfm04a. laboratory core investigations. forsmark site investigation. SKB P-04-312, Svensk Kärnbränslehantering AB.

Sibson R H, 1974. Frictional constraints on thrust, wrench and normal faults. Nature, 249:542–544.

Sjöberg J, Christiansson R, Hudson J A, 2003. ISRM Suggested Methods for rock stress estimation – Part 2: Overcoring methods. International Journal Rock Mechanics And Mining Science, 40(7–8):999–1010.

Sjöberg J, Klasson H, 2003. Stress determinations using the Borre (SSPB) probe. International Journal Rock Mechanics And Mining Science, 40:1205–1224.

Sjöberg J, Lindfors U, Perman F, Ask D, 2005. Evaluation of the state of stress at the forsmark site. preliminary site investigation forsmark area – version 1.2. SKB R-05-35, Svensk Kärnbränslehantering AB.

SKB, 2004. Deep repository. Underground design premises. Edition d1/1. SKB R-04-60, Svensk kärnbränslehantering AB.

SKB, 2005a. Preliminary site description, Forsmark area – version 1.2. SKB R-05-18, Svensk Kärnbränslehantering AB.

SKB, 2005b. Programme for further investigations of geosphere and biosphere. Forsmark site investigation. SKB R-05-14, Svensk Kärnbränslehantering AB.

SKB, 2006. Site descriptive modelling Forsmark stage 2.1 – feedback for completion of the site investigation including input from safety assessment and repository engineering. SKB R-06-38, Svensk Kärnbränslehantering AB.

Skempton A W, 1966. Some observations on tectonic shear zones. In Proc. First Congress of the International Society for Rock Mechanics, Lisbon, vol. 1, pp. 329–335.

Slunga R, 1991. The Baltic Shield earthquakes,. Tectonophysics, 189:323–331.

Stephansson O, Ljunggren C, Jing L, 1991. Stress measurements and tectonic implications for Fennoscandia. Tectonophysics, 189:317–322.

Tchalenko J S, 1970. Similarities between shear zones of different magnitudes. Geological Society of America Bulletin, 81:1625–1640.

Thompson P, Chandler N, 2004. In situ rock stress determinations in deep boreholes at the Underground Research Laboratory. International Journal Rock Mechanics And Mining Science, 41(8):1305–1316.

Thompson P M, Lang P A, Snider G R, 1986. Recent improvements to in situ stress measurements using the overcoring method. In Proc. 39th Canadian Geotechnical Conference, Ottawa, pp. 143–150.

Appendix A

Overcore test results

Table A–1: Summary of the overcore results used in this report and available from SICADA. Note that in SICADA, the names of DBT1 and DBT3 are labelled KFK001 and KFK003, respectively.

BH Name	BH Length (m)	σ_1 (MPa)	Trend (°)	Dip (°)	σ_2 (MPa)	Trend (°)	Dip (°)	σ_3 (MPa)	Trend (°)	Dip (°)
DBT1	13.87	14.0	99	1	11.2	9	8	–3.8	196	82
DBT1	31.36	35.5	87	12	18.4	356	4	6	249	78
DBT1	31.96	30.0	58	10	16.8	326	12	–3.2	185	75
DBT1	50.37	12.6	9	9	4.5	103	19	1.1	256	69
DBT1	71.40	14.1	308	3	7.3	218	9	–11.1	57	81
DBT1	90.00	18.8	341	5	6.7	250	6	–3.1	114	82
DBT1	90.62	29.5	268	3	21	178	7	–3.8	18	82
DBT1	133.61	15.1	155	6	13.8	246	10	2.5	35	79
DBT1	134.18	15.4	305	21	11.2	41	14	6.6	161	65
DBT1	134.74	19.0	324	44	15.2	70	16	4.2	175	42
DBT1	136.41	18.5	285	26	12.2	19	9	6.9	126	63
DBT1	165.54	13.3	49	6	12	318	2	4.5	208	84
DBT1	166.80	24.2	275	10	16.6	9	21	4.4	162	67
DBT1	194.77	22.2	275	2	19.0	185	11	6.7	15	79
DBT1	195.39	19.2	283	9	11.3	13	1	–5.4	111	81
DBT1	218.90	20.6	329	26	18.1	238	2	5.4	144	64
DBT1	219.63	25.8	181	27	17.4	85	10	4.4	336	61
DBT1	246.94	18.4	45	1	11.1	135	12	9.0	311	78
DBT1	275.65	40.5	323	4	21.4	55	18	8.4	222	71
DBT1	276.31	38.0	270	8	20.3	0	2	9.9	102	82
DBT1	299.71	21.8	311	11	13.9	43	12	9.3	180	73
DBT3	105.23	17.1	133	5	7.5	224	4	3.5	350	84
DBT3	135.70	22.8	317	1	14	226	28	6.6	49	62
DBT3	136.31	18.1	141	4	11.8	235	49	7.0	48	41
DBT3	136.93	20.1	314	3	5.7	44	3	–1.3	179	85
DBT3	154.78	19.1	3	9	9.4	97	26	6.8	256	63
DBT3	155.38	18.2	326	16	13.1	235	1	10.2	142	74
DBT3	187.40	34.3	322	20	13.1	59	18	9.7	188	63
DBT3	188.45	17.0	22	29	8.1	291	1	1.9	199	61
DBT3	218.24	21.6	3	22	13.1	101	18	7.9	223	59
DBT3	218.85	20.3	349	25	10.1	86	13	1.1	201	61
DBT3	219.45	24.1	184	17	17.8	89	14	6.5	322	68
DBT3	248.73	28.8	354	11	12	264	3	–2	157	78
DBT3	248.92	20.5	326	10	15.1	234	8	7.5	106	77
KFM01B	238.94	50.5	102	42	37.4	324	39	29.6	214	23
KFM01B	240.01	38.7	282	12	22.3	187	19	15.6	43	67
KFM01B	242.05	40.2	289	12	32.4	195	17	19	53	69
KFM01B	412.79	42.3	141	28	25.2	30	34	10.3	261	43
KFM01B	471.69	46.8	156	23	14.5	11	62	10	252	14
KFM02B	113.74	10.8	114	6	4.8	21	26	–1	216	63
KFM02B	135.80	8.8	167	20	–0.4	73	13	–6.9	312	66
KFM02B	144.17	15.1	126	15	4.9	219	11	2.3	343	72
KFM02B	156.72	13.7	138	59	11.9	358	25	3.4	260	17
KFM02B	164.10	8.3	132	26	5.1	226	9	–0.2	333	62
KFM02B	178.03	10.4	155	14	4.3	263	50	–3.3	54	36
KFM02B	179.87	20.0	153	12	9.5	247	19	4.9	33	67
KFM02B	252.83	21.3	128	5	11.8	220	30	5.4	30	60
KFM02B	253.77	15.9	139	10	11.7	232	14	1.1	15	72
KFM02B	256.13	16.6	130	10	8.7	224	18	1.0	12	69

Appendix B

Hydraulic fracturing data

Table B-1: Summary of the hydraulic fracturing data used in this report.

BH name	BH Length (m)	Depth (m)	Azimuth (°)	Dip (°)	σ_n (bar)	σ_{vert} (bar)	Comments
KFM08A	942.7	719.5	223	88	160	187	
KFM08A	928.4	711	–	–	164	185	Pre-existing fractures
KFM08A	910.7	699.5	323	49	154	182	Sub-horizontal fracture
KFM08A	901	692.5	–	–	161	180	Multiple sub-horizontal fracture
KFM08A	893.7	689	18	72	181	17	No
KFM08A	766.8	604.5	339	56	118	157	Sub-horizontal fracture
KFM08A	753.7	595.5	24	70	116	155	Pre-existing fractures
KFM08A	741.9	587.5	307	84	157	153	Sub-horizontal fracture
KFM08A	735.7	583	–	–	136	152	Two pre-existing fractures
KFM08A	725.9	576.5	–	–	185	150	Pre-existing fracture
KFM08A	717.9	571	278	88	140	149	No
KFM08A	606	490	96	87	130	127	Sub-horizontal fracture
KFM08A	595.4	482.5			150	216	Sub-horizontal fracture
KFM08A	586.7	476	184	76	95	124	Sub-horizontal fracture
KFM08A	578.5	470	142	69	100	122	Multiple sub-horizontal fracture
KFM08A	534.2	436.5	197	87	114	114	No
KFM08A	527.8	432	308	50	126	112	No
KFM08A	520.6	426.5	222	86	112	111	No
KFM08A	508	416.5	316	75	125	108	No
KFM08A	427.2	354	291	56	79	92	Sub-horizontal fracture
KFM08A	395.1	328.5	238	61	98	85	No
KFM08A	365.8	307	260	85	94	80	Another inclined fracture
KFM08A	333.5	279.5	311	86	123	73	No
KFM09A	672.6	540.5	21	84	138	141	Two sub-horizontal fractures
KFM09A	669.7	538.5	103	46	122	140	Sub-horizontal fractures
KFM09A	640.6	517.5	67	87	112	135	No
KFM09A	619.8	502	66	90	80	131	Two sub-horizontal fractures
KFM09A	613.9	498	–	–	84	130	Multiple sub-horizontal fractures
KFM09A	611	496	153	79	90	129	No
KFM09A	617	500.5	–	–	95	130	Sub-horizontal fracture
KFM09A	606.5	493	276	79	120	128	Sub-horizontal fracture
KFM09A	580.8	473.5	72	84	120	123	No
KFM09A	557.9	456	212	85	130	119	Two sub-horizontal fractures
KFM09A	553.7	453	31	79	115	118	Sub-horizontal fracture
KFM09A	437	363	0	74	70	94	Two sub-horizontal fractures
KFM09A	412.6	343.5	265	76	65	89	No
KFM09A	348.9	293	62	87	100	76	Two sub-horizontal fractures
KFM09A	325.2	273.5	269	66	100	71	Sub-horizontal fracture
KFM09A	222.5	187.5	117	69	70	49	Sub-horizontal fracture
KFM09B	555.5	428.2	66	88	129	100	Multiple inclined fracture
KFM09B	542.8	419.8	87	86	200	107	Multiple inclined fracture

BH name	BH Length (m)	Depth (m)	Azimuth (°)	Dip (°)	σ_n (bar)	σ_{vert} (bar)	Comments
KFM09B	523	405.5	105	15	102	103	Two sub-horizontal fractures
KFM09B	514.9	399	310	81	107	102	Multiple inclined fracture
KFM09B	477.9	374	42	86	108	95	Sub-horizontal fracture
KFM09B	469	367	236	79	90	94	Multiple inclined fracture
KFM09B	439.2	345	324	83	100	88	Multiple inclined fracture
KFM09B	424.5	334	74	86	73	85	Multiple inclined fracture
KFM09B	403.3	318	275	80	170	81	Multiple inclined fracture
KFM09B	368.6	292.5	192	74	82	75	Sub-horizontal fracture
KFM09B	359.7	286	130	83	96	73	Sub-horizontal fracture
KFM09B	342.7	273	8	79	67	70	Sub-horizontal fracture
KFM09B	333.2	265.5	325	82	62	68	Sub-horizontal fracture
KFM09B	579.2	444.5	–	–	170	113	Sub-horizontal fracture
KFM09B	495.6	386	–	–	110	98	Sub-horizontal fractures
KFM09B	484.7	378.5	–	–	110	96	Sub-horizontal fractures
KFM09B	276.2	221	132	85	90	56	Sub-horizontal fractures
KFM09B	272.2	218.5	103	89	62	56	Sub-horizontal fractures
KFM07A	–	493	237	86	120	128	Table 1, Cornet report Mar 2007 Draft
KFM07A	–	487	237	78	120	127	Table 1, Cornet report Mar 2007 Draft
KFM07A	–	481	254	82	154	125	Table 1, Cornet report Mar 2007 Draft
KFM07A	–	387	319	85	179	100	Table 1, Cornet report Mar 2007 Draft
KFM07A	–	368	271	86	155	96	Table 1, Cornet report Mar 2007 Draft
KFM07A	–	343	33	82	140	89	Table 1, Cornet report Mar 2007 Draft
KFM07A	–	326	151	89	164	85	Table 1, Cornet report Mar 2007 Draft
KFM07A	–	271	129	79	195	70	Table 1, Cornet report Mar 2007 Draft
KFM07C	–	416	202	44	121	108	Table 2, Cornet report Mar 2007 Draft
KFM07C	–	400	187	50	104	104	Table 2, Cornet report Mar 2007 Draft
KFM07C	–	388	228	48	111	101	Table 2, Cornet report Mar 2007 Draft
KFM07C	–	340	315	68	134	86	Table 2, Cornet report Mar 2007 Draft
KFM07C	–	235	218	30	71	61	Table 2, Cornet report Mar 2007 Draft
KFM07C	–	196	38	88	74	51	Table 2, Cornet report Mar 2007 Draft
KFM07C	–	173	31	87	74	45	Table 2, Cornet report Mar 2007 Draft

Table B-2: Summary of the hydraulic fracturing data from /Rummel and Weber 2004/ used in this report.

Borehole name	Test no.	BH Length (m)	True depth (m)	σ_{hmin} (MPa)	σ_{Hmax} (MPa)	Azimuth σ_{Hmax} (°)
KFM01A	24	422.00	419.00	15.1	29.9	105
KFM01A	17	433.41	430.28	12.0	18.2	71
KFM01A	8	456.26	452.87	11.0	21.0	121
KFM01A	3	496.00	492.11	12.4	24.1	140
KFM01A	2	502.00	498.03	17.2	33.7	86
KFM01A	13	695.00	687.51	15.6	30.5	108
KFM01A	11	954.00	939.52	26.9	54.9	87
KFM01A	10	975.50	960.32	25.1	51.8	102
KFM01B	2	187.90	183.46	5.0	8.1	77
KFM01B	8	410.50	397.00	15.3	31.6	3
KFM01B	6	471.20	454.68	24.2	52.3	144
KFM02A	35	220.70	220.09	7.1	11.8	110
KFM02A	34	223.50	222.88	6.8	10.7	125
KFM02A	32	376.00	374.78	8.7	15.9	24
KFM02A	20	551.60	549.53	16.4	32.9	128
KFM02A	12	603.00	600.58	18.3	37.5	137
KFM02A	4	701.50	698.30	21.6	44.5	142
KFM02A	3	704.30	701.08	22.6	47.5	136
KFM04A	11	194.58	171.43	5.1	13.6	172
KFM04A	10	196.91	173.47	5.2	13.6	125
KFM04A	9	266.33	233.61	6.7	14.4	59
KFM04A	8	277.99	243.63	7.0	14.5	131
KFM04A	7	371.20	322.95	9.1	15.4	140
KFM04A	6	398.00	345.30	9.6	15.7	120
KFM04A	5	535.88	457.03	12.5	17.0	21
KFM04A	4	553.90	471.33	12.9	17.2	99
KFM04A	3	558.33	474.84	13.0	17.2	46
KFM04A	2	564.02	479.34	13.1	17.3	114
KFM04A	1	593.63	502.91	13.7	17.6	77